Master thesis in Physical Oceanography

Tides and shallow water dynamics near Tromsø

Håvard Espenes

May 31, 2018

Geophysical Institute (University of Bergen) and Akvaplan-niva

Forord

Denne oppgaven ville ikke blitt slik den er nå uten veilederne mine, Ole Anders Nøst og Knut Barthel. Tusen takk for all tiden dere satt av for å diskutere de ulike fenomenene, og ikke minst for å hjelpe meg med skriveprosessen. Jeg er svært takknemlig for at dere lot meg få dure på med det jeg til enhver tid fant interessant, selv om det tok litt tid før jeg presenterte utkast til teoridelen og den slags. Uten den friheten til å gjøre det jeg følte for ville det sikkert ikke vært like artig å skrive oppgaven - takk for tilliten, rett og slett. Videre vil jeg takke Knut for at jeg ble interessert i numerisk modellering (et fag jeg til å begynne med var skeptisk til, pc-greier var skumle greier!). Uten den gnisten jeg fikk i GEOF211 tror jeg det ville blitt veldig tungt å skrive denne oppgaven.

Takk til alle dere i Fagutvalget som deltok på FIFA kvelder, fuktige badstuhelger i utkanten av Voss, samt for vaffelsøndagene når eksamensperioden sto på som verst. Jeg savner de jeg har feira 17. mai med de siste årene, de som ble med på håpløse turer i snøstorm over Vidden (gjerne dagen før eksamen) og ikke minst for hverdagen - jeg savner kaffepausene (og frokostpausene, lunsjpausene, middagspausene - egentlig for pausene)! Det var artig å bli (litt mer) voksen i Bergen!

De sniker seg kanskje ikke forbi forsiden, men det få så være: Mamma og Pappa, jeg tror ikke jeg kan takke dere nok for alt dere gjør for meg - tusen ganger holder i hvert fall ikke!

Håvard Espenes
Tromsø, 31 Mai 2018

Abstract

I have investigated the tidal dynamics near Tromsø using data from some observations and from a numerical model. These data show that currents relating to the shallow water tides are very pronounced at the Tromsøysund and Sandnessund constrictions. This is due to two tidal waves - one of them force the northern, while the other force the southern side of those constrictions - being differently influenced by the shallow water tides. The pressure gradient along the channels is therefore significantly influenced by the difference in shallow water tides on either side. Furthermore, the data suggest that high frequency oscillations superimposed on the tidal signal create strong velocities at some stations. The numerical model suggests that these high frequency oscillations can be attributed to dipoles forming at the constrictions. They build up strong low-pressure zones, and propagate downstream after some time. The streamwise momentum balance indicate that dipoles first start moving away from the constriction after making conditions unfavourable for flow-separation close to the constrictions. My results suggest that such dipoles can force a faster flow far downstream of- than at constrictions, and that they do so frequently in Rystraumen.

Contents

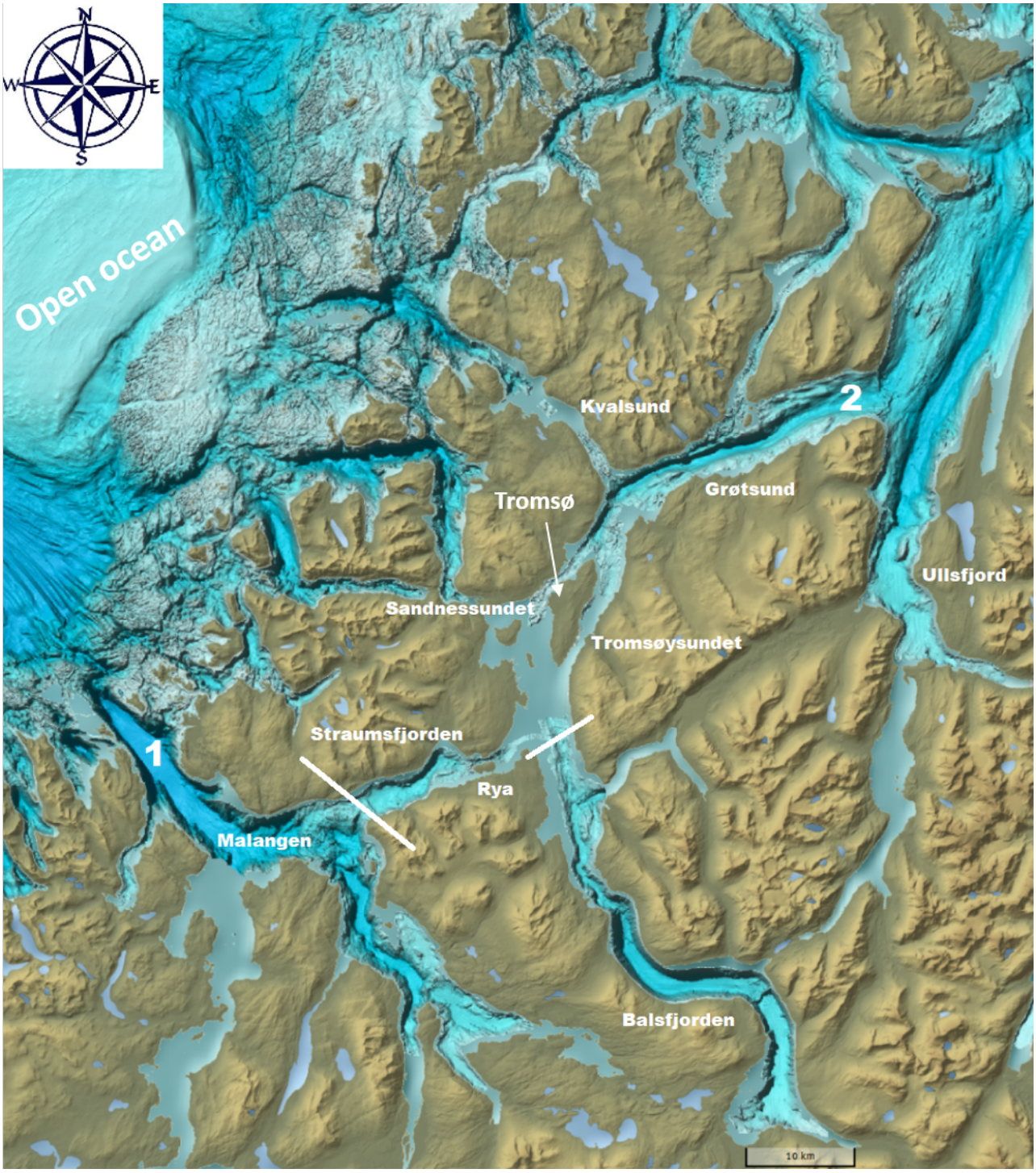

Figure 1: Map of the sounds and fjords connecting Tromsø to the open ocean. The grey zones are shallower than 10m. The white line to the left indicates where Straumsfjorden begins, and Malangen ends. The other white line indicates the mouth of Balsfjorden. Screenshot from Norgeskart.no, Kartverket 2017

Chapter 1

Introduction

The purpose of this thesis is to explain the tidally forced flow (stream) in Tromsø using a combination of observations and results from a numerical model. The tidally forced streams near Tromsø have not been studied before, but the oceanographers at Akvaplan have for some time wanted to understand the dynamics of the system better. Tromsø and its surroundings is shown in Figure 1. The domain is fairly large, and a thorough investigation of all straits, fjords and bays is too ambitious for one thesis. My goal is to understand what occurs near the Rystraumen and Tromsøysund constrictions.

Data from the observations and a numerical model suggest that the tidally forced stream in this region is significantly influenced by shallow water harmonics and tidal vortices formed close to the constrictions. In fact, the numerical results suggest that the strongest streams in the region occur far downstream of the constrictions, as I will present in Chapter 6. In this chapter, however, I present the region and some relevant established knowledge.

There are two channels in Rya, on either side of an island - Ryøya, connecting Straumsfjorden/Malangen on its western side to Balsfjorden on the eastern side, see Figure 1.1a. Rystraumen has the biggest cross section (about $500m$ wide and $55m$ deep at the constriction). "Litjestraumen" is a smaller supplementary channel on the other side of the island (roughly $160m$ wide and $5m$ deep at the constriction). I will focus on the biggest channel. The Norwegian Mapping Authority and their pilot guide claim that the strongest stream in Rystraumen can reach about $3m/s$, and that the stream create eddies downstream which can cause significant shear. They report that the stream is still ($Speed = 0$) roughly $25min$ before and strongest $2h45min$ after high/low tide. Droniou (2012) measured the stream in Rystraumen using an ADCP device and found that the stream peaked at $2.5m/s$. It should, according to his estimates, be able to reach $3.6m/s$ on spring tide.

Tromsøysundet is roughly $500m$ wide and about $7m$ deep at the constriction and it is one of two channels close to the Tromsø island, see Figure 1 and 1.1b. The channel on the other side is called Sandnessund. I will, too keep it short, only look at Tromsøysundet. It is connected to Balsfjorden on the southern side, and to Grøtsundet on the northern side. The pilot guide claim that the current in Tromsøysundet normally is about $1m/s$ strong, but that it can exceed $2.5m/s$ in extreme situations - without specifying which type of

extreme events. They report that the stream is strongest at high/low tide. The stream is, in strong contrast to Rystraumen, still between high/low tide which imply that the maximum volume transport in Tromsøysund is at high/low tide. That is an odd feature for a channel connecting a fjord to the open ocean. Tromsøysundet is adjacent to the city centre, which is an area with marine traffic and emissions of water-borne materials. Akvaplan has therefore gathered data in Tromsøysundet several times over the years. I will study data from those surveys in this thesis.

I will - for convenience - define the Tromsø fjord system to be the region bounded by the mouth of Malangen, in the south (indicated "1" on Figure 1), Kvalsund and the mouth of Grøtsund (2 on Figure 1). The inner fjord system is the region bounded by Rystraumen, Sandnessundet and Tromsøysundet which has a surface area of $280 km^2$.

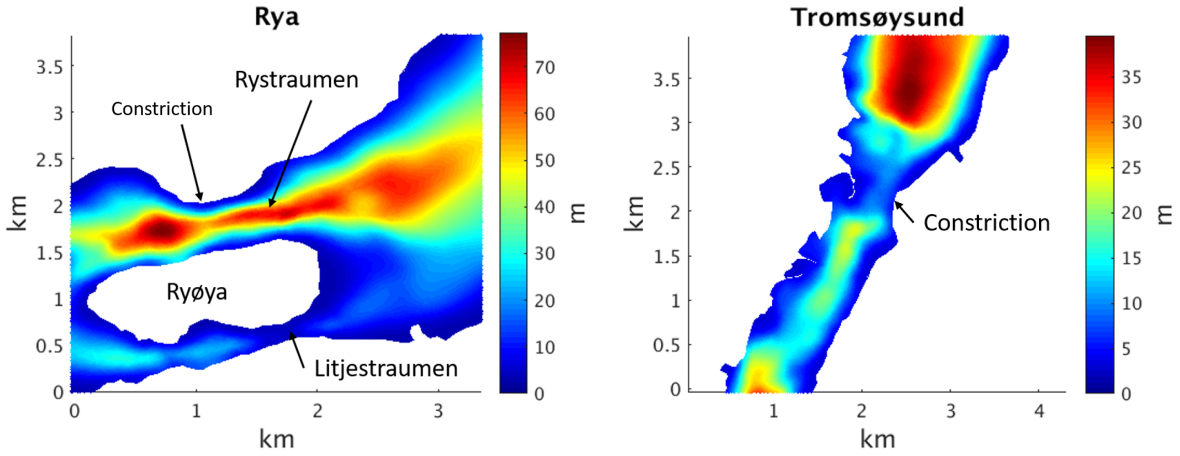

(a) (b)

Figure 1.1: *Detailed bathymetry of the channels in the studied domain, extracted from the model. Note that each figure has its own colorscale.*

The thesis is divided into 9 chapters. Chapter 2 explain the relevant theory, such as why there is a tide and some phenomena one has to take into consideration when studying it in shallow and coastal waters. Chapter 3 explain how the measurements were obtained, how the numerical model work and introduce the methods I used to analyse the data. The results are divided into two chapters, Chapter 4 and Chapter 6. Chapter 4 describe the observations, Chapter 5 compares the observed- to the modelled tide to see if the model creates features which look like the observed ones, and Chapter 6 has a closer look at the features I found in the observations using the results from the numerical model. I present my interpretation of the results in Chapter 7. Chapter 8 summarize the thesis and Chapter 9 proposes how future studies can build on my results to improve the knowledge of the Tromsø tidal system specifically, and of similar oceanic environments in general.

Chapter 2

Theory

This chapter explain why there is a tide and how it is altered by complex coastal geometries. I thereafter present a process creating vortices downstream of headlands and give a brief introduction to the spectral analysis methods I used in this thesis.

2.1 The tide

2.1.1 Forcing

Two large scale forces due to celestial objects acting on the earth are sufficient to understand why there is a tide: Gravitation and the centrifugal force. Gravitation from the moon and sun pulls on water parcels on the earth. I have used the moon as an example since it is the most important contributor to the tide near Tromsø, but the mechanism is similar for the tides relating to the sun.
Gravity is explained by Newton's law of universal gravitation;

$$F_G = \frac{GMm}{r^2} \tag{2.1}$$

where "r" is the distance from the moon centre of mass to a body experiencing its gravitational field. M & m are masses of the moon and parcel, respectively. G is the universal gravitational constant. Moving a body away from the moon (increase r) reduces the force F so that the moon pull stronger on parcels closest to it.
The centrifugal force experienced by earth at its centre of mass as it revolve around the common centre of mass must equal the gravitational attraction since the moon stay at a (so to say) fixed distance from earth, l.

$$m\omega^2 l = F_G \tag{2.2}$$

$\omega = 2\pi/28d$ is the angular frequency of one month. The earth move around the joint centre of mass in a motion known as "revolution without rotation", meaning that every point on earth move around a rotational axis with a radius equal to l, Drange (2016). Thus the centrifugal force on earth point in the same direction with the same magnitude everywhere. The sum of gravitation and the centrifugal force is in balance at the centre of earth, but is directed *toward* the moon at locations facing it (Equation 2.3) and away

from it on the other side of earth (Equation 2.4).

$$m\omega^2 l < F_G \tag{2.3}$$

$$m\omega^2 l > F_G \tag{2.4}$$

The vertical momentum balance (relative to a coordinate system at the earth surface) at the sea surface is dominated by earth gravity. The moon therefore does not "pull" the water up toward it to create the tides. The sea surface elevation is instead created by a *horizontal* imbalance which generate a sea surface gradient - we know it as the tide. Water converges at the side facing the moon, and on the other side of earth - resulting in two "bulges" of water. Locations 90° to the moon-earth axis experience low tide. Earth rotate around itself once a day. Observers fixed to the earth move through the force balance and experience two high and low tides each day, and they will say that the tide rose and sunk twice. The direct forcing from the moon results in a 12.42h periodic tide, M2. Similarly, the S2-tide (12h) is due to the sun, Pugh and Woodworth (2014). M2 and S2 tides are known as semi-diurnal tides since they occur twice a day, in contrast to diurnal tides which occur once a day. Spring tides occur when the peak elevation from the S2 and M2 tides coincide, at neap tide they oppose each other. Many other tidal frequencies exist, each of them have a name - for example the already introduced M2, S2 tides. Such names are called *tidal constituents*. Each constituent force a sea surface deviation following that frequency travelling the global ocean as gravity waves.

2.1.2 Gravity waves

A gravity wave is the result of a sea surface perturbation displacing fluid parcels from rest. Parcels will attempt to move back to rest, but overshoot and instead move in an infinite up/down movement (in absence of friction). Gravity waves where the particle motion has a much longer horizontal extent than vertical are called shallow water waves, and in such waves one can neglect the vertical particle acceleration. Long gravity waves are significantly influenced by the coriolis force, short waves are not.

Kelvin wave

Kelvin waves exist due to a balance between the pressure gradient and a local acceleration in the direction they propagate, and between the pressure gradient and the Coriolis force in the perpendicular direction. The Coriolis force must be directed toward a solid boundary and propagate with land on the "right hand side" to their direction of propagation on the northern hemisphere. Hence they propagate from south toward north along the European continent. They excite waves propagating into a fjord as they move pass its mouth.

Waves in fjords

The force balances in such waves is between local acceleration and the pressure gradient in the horizontal dimension - if they exist on small enough scales for the Coriolis force to be negligible - and a hydrostatic balance in the vertical.

$$\frac{\partial u}{\partial t} = -g\frac{\partial \eta}{\partial x} \tag{2.5}$$

$$\frac{\partial p}{\partial z} = -g\rho \tag{2.6}$$

$$\frac{\partial \eta}{\partial t} + \frac{\partial uD}{\partial x} = 0 \tag{2.7}$$

The phase velocity of shallow water waves is $c_p = \sqrt{gD}$. A gravity wave in a fjord will follow the same frequency as the Kelvin wave forcing it (Drange, 2016). The sea surface elevation excited by waves can, at a given fixed location, be expressed $\eta(t) = Acos(\omega t + \phi_\eta)$. The associated particle motion (tidal stream) can be expressed $u = Ucos(\omega + \phi_U)$. A is the wave amplitude, ϕ_η is the sea surface phase shift. U is the tidal stream peak speed and ϕ_U is the stream phase shift. The difference between ϕ_U and ϕ_η tell us whether the wave is progressive or not.

Progressive and standing waves

Progressive waves propagate in a direction without another wave of the same frequency propagating in the opposite direction. The tidal stream in open waters behave as such waves. The current associated with such waves is strongest at maximum/minimum sea surface perturbation (η). Standing waves are the superposition of two opposite-propagating waves. The tidal stream in such waves is weakest at high/low tide, and strongest when $\eta(t)$ is zero. Thus the stream in standing waves are 90° out of phase from the sea surface elevation, while progressive waves are in phase ($\phi_U - \phi_\eta = 0°$) with it. One will measure a phase difference somewhere in between $0 - 90°$ if one of the progressive waves is weaker than the other. I will for convenience call waves with phase differences $\leq 45°$ progressive. The phases and amplitudes at a location are (in general) not known a priori but can be determined by a harmonic analysis based on a time series of the sea surface elevation and stream.

2.1.3 Harmonic analysis

We do not know the tidal surface elevation or stream associated with each constituent a priori, but we know their frequencies, ω. In harmonic analysis, one use these to identify how much of the surface elevation or current that can be attributed to each constituent. The total tidally forced sea surface elevation or current at a specific time and place is then simply a sum of the contribution from each single constituent, as shown in Equation 2.8. One finds these amplitudes through the least squares method given a time series of the sea surface elevation and/or currents at a location. The measured sea surface elevation at a specific time can be expressed:

$$\eta(t) = \eta'(t) + \overline{\eta} + \sum_{m=1}^{M} C_m cos(\omega_m t - \phi_m) \tag{2.8}$$

$$\eta(t) = \underbrace{\eta'(t)}_{1} + \underbrace{\overline{\eta}}_{2} + \underbrace{\sum_{m=1}^{M} A_m cos(\omega_m t) + B_m sin(\omega_m t)}_{3} \tag{2.9}$$

where M is the total number of tidal constituents. The terms in Equation 2.9 are: (1)

Noise in the dataset (due to wind generated surface waves, ships and other activities close to the sensor etc.), (2) is the mean water level and term (3) is the total surface elevation caused by the tide. We can, using the least square method, solve for A and B by minimizing the square of the error (1)

$$e^2 = \sum_{n=1}^{N} \eta'^2(t_m) \tag{2.10}$$

by finding the minima of the derivative of e^2 with respect to the amplitude of the tides

$$(\frac{\partial}{\partial A_m}, \frac{\partial}{\partial B_m})e^2 = (0, 0) \tag{2.11}$$

this method give more accurate estimates as the time-series length increase - ergo as we measure more tidal cycles (Thomson and Emery, 2014). Once having determined the coefficients A_m and B_m one can find the amplitude and phase of each constituent and reconstruct the tide for any given time.

2.1.4 Shallow water effects

Astronomic tides are derived by neglecting the non-linear terms in the momentum and continuity equation. The assumption is invalid where velocities are strong, and the tidally forced sea surface elevation is not much smaller than the mean water depth. Non-linear terms in the continuity and momentum equation will alter the shape of the tide. The effect can be modelled as an introduction of higher harmonics to the original signal, known as *shallow water constituents*.

The non-linear continuity effect
Crests move faster than troughs in waters where the sea surface elevation caused by the tide, η, is not significantly smaller than the mean fluid depth $\overline{D}$. Shallow water waves will then propagate with $c_p(t) = \sqrt{g(\overline{D} + \frac{3\eta(t)}{2})}$, Pugh and Woodworth (2014). Crests catch up with troughs, resulting in shorter ebb to flood- than flood to ebb periods. The sea surface forced by the tide will be asymmetric, see Figure 2.1b, and the tidal stream loose its sinusoidal shape in the process.

Effect of advection of momentum
The tidal stream u create a convergence-divergence pattern forcing the sea surface elevations but it can also transport them which alter the phase speeds. The altered - or "effective" - phase speed is $c_p \approx \sqrt{g\overline{D}} + u$ at flood and $c_p \approx \sqrt{g\overline{D}} - u$ at ebb (Parker, 1991).

How friction alter the tide
Friction can be expressed by the quadratic relation $\mathcal{F} = \frac{C_d u|u|}{\overline{D}+\eta}$, simplified $\mathcal{F} \approx \frac{C_d u|u|}{\overline{D}} - \frac{C_d \eta u|u|}{\overline{D}^2}$. These terms influence the tide differently. $u|u|$ attenuate the tide most when the stream is strong and is independent of the instantaneous water depth. The second

term, $\eta u|u|$, express that the flow is more attenuated during ebb than at flood - and the tidal wave is therefore more delayed at low tide than at high tide. High tide will be less attenuated, and catch up with low tide (Kabbaj and Provost, 1980).

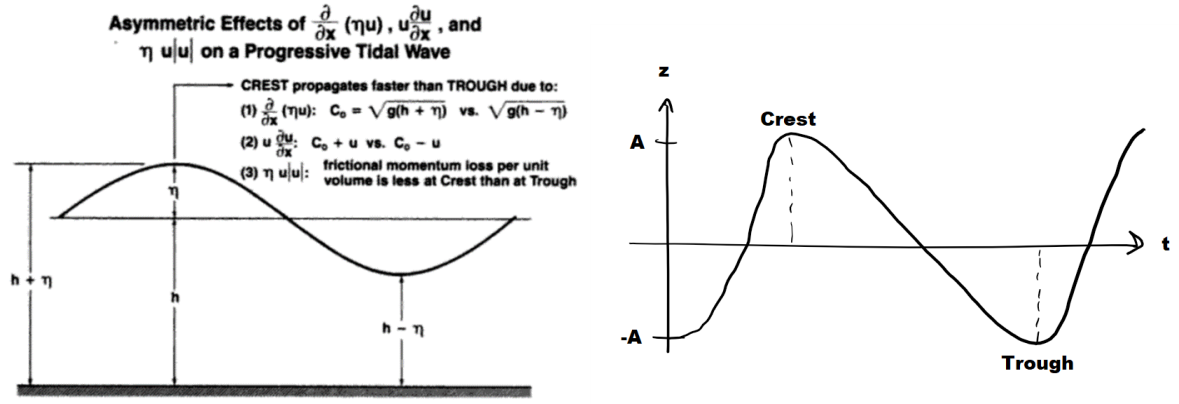

(a) *Terms distorting the wave, Parker (1991).* (b) *Resulting sea surface*

Figure 2.1: *A shallow water wave distorted by non-linear effects. The (b)-figure show the sea surface elevation one would measure over after the wave is modified. Time on x-axis and sea surface displacement on the z-axis.*

The altered wave is not a sine-wave but it is periodic and can be expressed by introducing new higher frequency waves superimposed on the original tidal wave. One can derive these new frequencies. The list beneath show how one constituent, whose sea surface elevation is given by $\eta = Hcos(\omega t + \phi_H)$ and current is $u = Ucos(\omega t + \phi_U)$, interact with itself in the non-linear continuity equation (1.) and in the momentum equation (2.-4.) to create shallow water tides.

1. Substituting the velocity and sea surface elevation into the non-linear continuity equation gives $\nabla \eta u = \nabla HU(cos(\omega + \phi_H)cos(\omega + \phi_U))$, which oscillates as $\nabla \eta u = \nabla \frac{HU}{2}(cos(2\omega + \phi_U + \phi_H) + cos(\phi_H - \phi_U))$. It introduce even-harmonics.

2. The advection term $u\nabla u$ oscillates as $cos(\omega)cos(\omega) = \frac{1}{2}(cos(2\omega) + 1)$, hence it too introduce even harmonics.

3. Friction through $u|u|$ can be represented by the fourier series $u|u| = Acos(\omega) + Bcos(2\omega) + Ccos(3\omega) + Dcos(5\omega) + ...$ for a two dimensional flow, see Kabbaj and Provost (1980). Notice that this is the only term introducing odd harmonics.

4. Friction through the term $\eta u|u|$ generate even-harmonics, which one can derive by multiplying the harmonics in (3.) by $\eta = Hcos(\omega + \phi)$.

The example show how *one* constituent interact with itself and introduced new harmonics to a system originally just forced by a wave of frequency ω. The true tidal stream and sea surface at any given location is never given by one single constituent but by many;

$$u_{tot} = U_{M2}cos(\omega_{M2} + \phi_{M2}) + U_{S2}cos(\omega_{S2} + \phi_{S2}) + U_{M4}cos(\omega_{M4} + \phi_{M4}) + ... \qquad (2.12)$$

All constituents interact with themselves and each other, and introduce a wealth of new harmonics which are divided in categories. Andersen et al. (2006) explain that interactions of a tidal constituent with it self (or its higher harmonics) result in "overtides", for example the M4 ($2\omega_{M2}$), M6 ($3\omega_{M2}$) constituents. Interactions between constituents from different sources result in "compound tides", for example interaction between M2 with S2 which result in the MS4 ($\omega_{M2} + \omega_{S2}$) and 2MS6 ($2\omega_{M2} + \omega_{S2}$) constituents. Non-linearities in the governing equations are therefore important since they modify the large scale shape of the tide.
Non-linear processes will also alter the stream and sea surface elevation on smaller scales. Friction, for example, does not just attenuate the flow. It can also distort the direction of the stream by generating vorticity, which it does best where the stream is strong - for example near choked constrictions.

Choking

A channel where pressure and advection of momentum dominate the other terms is said to be "choked", and the associated stream is called a tidal jet. The phenomena develop in channels where the cross-section is small due to a section (constriction) being narrow, shallow or a combination of both. Two effects force the speed (Stigebrandt, 2012).

1. Sea surface elevations on the fjord side of the constriction lag that of the open ocean side during rising tide which lead to an along-channel pressure gradient, it will accelerate the flow.

2. The stream must be fastest in regions with narrow cross-sections to conserve the volume transport.

It gain the momentum to drive process 2 by transferring potential- to kinetic energy, in other words by lowering the sea surface. The velocity due to this process is maximum where the sea surface is minimum, which is at the narrowest section (the constriction). A pressure gradient is therefore directed toward the constriction centre from both sides, accelerating the upstream region, and decelerating it downstream. Friction and diffusion are not negligible in areas of strong streams, even if their magnitudes do not compare to the other terms in the force balance since they produce vorticity and therefore eddies - sometimes referred to as tidal vortices.

Tidal vortices

Vortices form downstream near headlands due to flow separation, an effect caused by the adverse pressure gradient behind the obstacle. Pressure oppose friction and diffusion upstream of the constriction but work together to attenuate it on the downstream side. The point where pressure, friction and diffusion has worked together against the inertial force to the force flow back toward the constriction is known as the point of flow separation (Cohen and Kundu, 2007). An eddy will form behind the point - headland eddies. Such eddies form if the force balance is significantly influenced by advection and the pressure gradient, but may not do so if the environment is unsteady (strong local acceleration) and/or are strongly influenced by friction, Signell and Geyer (1991). They also say that it is important to resolve the shape of the coastal geometry to accurately model flow

separation. The generation process for headlands is equivalent for channels, but the latter create two counter rotating eddies - one on each side of the jet flowing through the channel which will move away from the constriction when they are sufficiently big (Wells and van Heijst (2003), Afanasyev (2006)) as dipoles. Some dipoles may propagate away from the constriction even as the tide turns and transport water-borne particles efficiently, but it still remain to be answered how important such dipoles are for estuarine environments.

2.2 Spectral analysis

Spectral analysis studies the frequency distribution of energy for time series where a large portion of the action in it is related to periodic oscillations. We want to study a time series $S(t)$ where the series is controlled by a dynamic forcing and noise superimposed on it.

$$S_{observed}(t) = D_{dynamic}(t) + N_{noise}(t) \tag{2.13}$$

The dynamic term can contain a non-periodic term - a trend - in addition to a periodic oscillation. The latter is of course of great interest for me when studying the tide.

$$D_{dynamic}(t) = D_{trend}(t) + D_{oscillation}(t) \tag{2.14}$$

One transforms the entire time series to frequency space to identify the energy contained in the oscillatory part from the trend. We obtain such an estimate of a time series in frequency space by a fourier transformation. Time series of sea surface elevation may contain rather large and non-uniformly spaced noise due to surface stress by winds. The noise act to decrease the reliability of spectral estimates (Thomson and Emery, 2014).

Confidence intervals

Confidence intervals are used to give a measure on how reliable the estimate of the energy-distribution in a spectrum is. We must remember that even though we measured something, we might not have captured the true distribution of the parameter we are interested in. Confidence intervals tell us where we can expect to find the true population for a given probability.

Separating constituents in the energy spectrum

In a time record consisting of several waves it is important to know how long time record one need to distinguish the waves from each other. The Rayleigh criterion is a measure of the frequency difference required to distinguish the spectral peaks between two waves. It require that the difference in frequency between the waves is longer than $\Delta f = \frac{1}{T}$ where T is the length of the recorded time series. (Thomson and Emery, 2014).

Chapter 3

Methods

I have used data gathered in the field by Akvaplan-niva and results from FVCOM, their preferred numerical model. This chapter describe how the instruments sample data, how I identify the tide based on the observations and how the numerical model work. I will also describe a method to look at the forces driving the fluid motion based on the numerical results.

3.1 Instrumentation

Data of sea surface elevation and current at a location is gathered using two types of instruments, point measurements (Aanderaa RCM) and profiling instruments (Aanderaa seaguard 2 and Nortec profiler).

Aanderaa RCM

Figure 3.1 illustrate the RCM instrument in action. It record velocity in a horizontal plane surrounding the sensor (Figure 3.1a) as well as pressure. Pressure measurements are used to estimate water depth with the hydrostatic approximation, $z = \frac{p}{\rho g}$. Pressure measurements are, according to Aanderaa, $\pm 0.02\% FSO$ (Full Scale Output) accurate and current measurements are approximately $\pm 0.15 \frac{cm}{s}$ accurate. The device record data over 2.5min intervals which are averaged and thereafter stored in bins representing 10 minutes. This procedure smooths the measurements, reduce the influence of instrument noise and save energy since the device does not have to record data continuously.

Figure 3.1b illustrate how the device is deployed in the water column. A line is fixed to the bottom by an anchor and kept strict by a buoyant device higher up in the water column. The instrument is typically positioned close to the anchor. This set-up is called "the rig". Some rigs are deployed with two separate anchors, where the second anchor is connected to a surface buoy - the retrieval float. Some of Akvaplans rigs are not deployed with two anchors, and the retrieval float at such rigs is connected to the buoyant device instead. Akvaplan processed the raw data following routines suggested by Aanderaa before I got my hands on it. Measurements where the instrument had a tilt of more than 35 degrees relative to the vertical were removed. Data where the signal strength was less than -65 and/or the single pin standard deviation was more than $15 cm/s$ were removed.

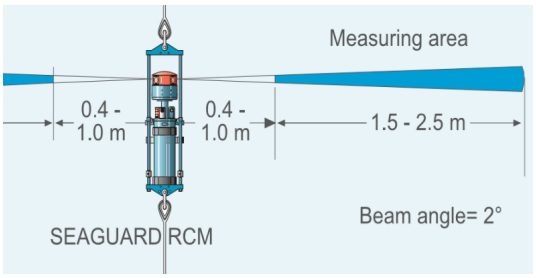

(a) Measuring currents

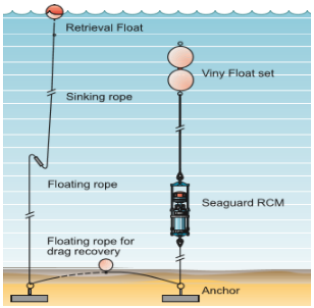

(b) Position in water column

Figure 3.1: Seaguard RCM

Profiling instruments

Profiling instruments send sound waves through the water column at specific frequencies, which are reflected back to the instrument throughout the entire water column. The instruments record the frequency of the reflected waves. By measuring how long time the wave travelled one can find the depth where it was reflected, and by measuring the change in frequency one can find the velocity of the parcel that reflected the wave. I used data sampled by Nortek Profiler and Anderaa Seaguard 2 instruments which store measurements in vertical bins spaced 2m apart. I averaged the currents between the bins h = -8m below the sea surface to the 3rd lowest bin by advice from the technical staff at Akvaplan since the uppermost cells are known to be very noisy and the lowermost are too close to the sensor for accurate sampling. It is not ideal to ignore the upper $8m$ since the sill of Tromsøysundet is very shallow, approximately 7m. I estimated the tidal stream based on the observed stream with UTide.

3.2 Utide - Tidal analysis

UTide is a set of MATLAB scripts developed by Daniel L. Codiga (Codiga, 2011) performing a harmonic analysis on time-series of sea surface elevation and current. I let UTide choose which constituents to look for automatically, which it does based on a noise modified variant of the Rayleigh criteria. UTide returns the amplitude and phase of each constituent, the 95% confidence intervals of the estimates, and the kinetic and potential energy associated by each constituent in percent of the total energy contained by tidal waves. Users can use the ordinary least squares method described in Section 2.1.3 or a modified version of it, the robust iteratively-reweighed least squares (IRLS) technique. I chose IRLS since Codiga say that it should give greatly reduced confidence intervals. Confidence intervals are estimated using a coloured noise technique, in contrast to the more common white noise techniques found in competing tidal analysis toolboxes. The coloured technique discard noise at high frequencies, only assessing the energy spectrum close to that of the tidal frequencies, which should result in greatly reduced confidence intervals. I used UTide to extract amplitudes and phases of time series, and to make charts showing spatial patterns of amplitude and phases based on data from FVCOM. UTide estimates the phase of the stream relative to when the strongest tidal stream had a northerly component in Greenwich Mean Time (GMT), so the phase of the stream (and

the relation $\phi_\eta - \phi_U$) may vary significantly over short distances. I will subtract 180° when the difference is bigger than 90° and add 180° when it is smaller than −90° and give the absolute value of the difference when I investigate whether the wave is progressive or standing.

3.3 FVCOM

The Finite Volume Community Ocean Model (FVCOM) is a numerical model estimating oceanic flows using a finite volume technique on an unstructured mesh with small triangles close to solid boundaries and shallow and/or narrow sections and big triangles in areas where one does not expect interesting physics to occur. FVCOM was developed by Chen et al. (2003) in a collaboration between Woods Hole Oceanographic Institution and the University of Massachusetts. I ran FVCOM on the supercomputers "Stallo" and "Vilje". My thesis is based on a version of FVCOM using the vertically integrated governing equations, hence just modelling the 2D flow field. Data from FVCOM is stored representing an instantaneous value, in contrast to the observations which are averaged values. A 2D model lets me evaluate the most basic features of the flow, and hopefully revealing the physics governing it. Hench and Luettich Jr (2003) and Wan et al. (2015) mention that a more sophisticated effort including vertical variation, stratification and non-hydrostatic effects will typically benefit from having a "first guess" of the barotropic state and characteristics of the system to compare with.

3.3.1 Formulation

This section shows how FVCOM solves the set of equations. All information herein is based on the FVCOM manual, see Chen et al. (2013). My numerical experiments were performed without wind forcing, so I will not introduce those terms.

Governing equations

$\bar{u}$ and $\bar{v}$ are the vertically averaged velocities in x- and y-directions. $D(x, y, t)$ is the depth at any given location and time. The equations for conservation of vertically averaged momentum in the x- and y-directions are

$$\frac{\partial \bar{u}D}{\partial t} + \frac{\partial \bar{u}^2 D}{\partial x} + \frac{\partial \bar{u}\bar{v}D}{\partial y} - f\bar{v}D = -gD\frac{\partial \eta}{\partial x} - C_d\sqrt{\bar{u}^2 + \bar{v}^2}\bar{u} + DF_u \tag{3.1}$$

$$\frac{\partial \bar{v}D}{\partial t} + \frac{\partial \bar{u}\bar{v}D}{\partial x} + \frac{\partial \bar{v}^2 D}{\partial y} + f\bar{u}D = -gD\frac{\partial \eta}{\partial y} - C_d\sqrt{\bar{u}^2 + \bar{v}^2}\bar{v} + DF_v \tag{3.2}$$

C_d is a depth dependent drag coefficient. It is constant and equal to $C_d = 0.0027$ for water shallower than 3m and varies with depth according to Equation 3.3 elsewhere.

$$C_d = g(\frac{N^2}{D^{\frac{1}{3}}}) \tag{3.3}$$

where $N = 1/50$. The continuity equation for an incompressible fluid $\nabla \cdot \vec{u} = 0$ integrated over the instantaneous depth $D(x, y, t)$ is;

$$\frac{\partial \eta}{\partial t} = -(\frac{\partial \bar{u} D}{\partial x} + \frac{\partial \bar{v} D}{\partial y}) \tag{3.4}$$

Symbols	Meaning
x, y	East, North
$\bar{u}, \bar{v}$	Depth averaged velocity components in the x and y directions
η	Sea surface elevation. Measure of pressure.
f	Coriolis parameter, which redistributes momentum between the x and y directions.
$F_{u,v}$	Horizontal momentum diffusion
g	Gravitational acceleration

Discretization procedure

The governing equations are integrated over a fixed volume and the integrals are thereafter discretized - known as the Finite Volume (FV) technique. Forces are expressed as fluxes through the walls bounding the volume. Applied on the continuity equation;

$$\iint_S \frac{\partial \eta}{\partial t} dxdy = -\iint_S (\frac{\partial uD}{\partial x} + \frac{\partial vD}{\partial y}) dxdy = -\int_{s'} (\vec{u}D) \cdot \vec{n} ds' \tag{3.5}$$

$$\iint_S \frac{\partial \eta}{\partial t} dxdy = -\int_{s'} v_n D ds \tag{3.6}$$

s' is a trajectory bounding the beige area (S) in Figure 3.2a, and v_n is the velocity component normal to s'. Similarly, we can integrate the conservation of momentum equation in the x-direction over a volume V

$$\iint_A \frac{\partial \bar{u} D}{\partial t} dxdy + \oint_{a'} \bar{u} D \bar{v_n} da' - \iint_A f \bar{v} D dxdy = -\iint_A gD \frac{\partial \eta}{\partial x} dxdy - \iint_A \frac{\tau_x}{\rho_0} dxdy + \iiint_V F_u dV \tag{3.7}$$

where A is the red area in Figure 3.2b and a' is the path bounding it. We can, for example, integrate the advection of momentum equation in the x-direction and use the divergence theorem to arrive at a line integral which can be discretized.

$$u\frac{\partial u}{\partial x} + v\frac{\partial u}{\partial y} = \nabla \cdot (u\vec{u}) \tag{3.8}$$

$$\iiint_V \nabla(u\vec{u}) dV = \oint_{a'} \bar{u}\bar{v_n} D da' \approx \sum_{m=1}^{3} D_m \bar{u}_m \bar{v}_{n,m} a'_m \tag{3.9}$$

$m = 1:3$ is a index for the side walls, a'_m is the length of cell wall m, $v_{n,m}$ is the velocity component normal to a'_m. The pressure gradient - for example in the x direction, can be discretized after using Stokes theorem to get the line integral. If $G = (0, \eta)$ one gets

$$F_{press,x} = -gD_{cell} \iint_A \frac{\partial \eta}{\partial x} dA = -gD_{cell} \iint_A \nabla \times G dA = -gD_{cell} \oint_{a'} \eta dy \tag{3.10}$$

$$F_{press,x} \approx -gD_{cell} \sum_{m=1}^{M} \eta_m \delta y_m \tag{3.11}$$

Similarly for y-component of the pressure gradient, redefining $G = (-\eta, 0)$ we get

$$F_{press,y} \approx gD_{cell} \sum_{m=1}^{M} \eta_m \delta x_m \tag{3.12}$$

Horizontal momentum diffusion

FVCOM use the Smagorinsky eddy parametrization method to determine the eddy diffusivity parameter (A). This parametrization use diffusion parameters which depend on the area of the triangle, and of the velocity gradients, see Equation 3.13.

$$A_N = 0.5C\Omega_N \sqrt{(\frac{\partial u}{\partial x})^2 + 0.5(\frac{\partial v}{\partial x} + \frac{\partial u}{\partial y})^2 + (\frac{\partial v}{\partial y})^2} \tag{3.13}$$

Where N is the number of triangles, C is the Smagorinsky coefficient which is equal to 0.1 in my experiments, and Ω_N is the surface area of each mesh triangle.

Model mesh

FVCOM uses a triangular and unstructured mesh. Velocity is stored at the centre of mass of each cell (element), all other variables (bathymetry, η and diffusion coefficients) are stored at the corners (nodes), see Figure 3.2.

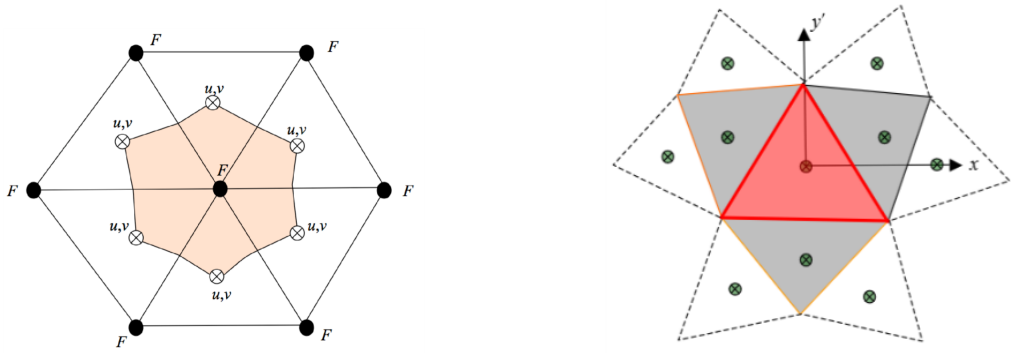

(a) Continuity equation control volume in beige

(b) Control volume for forces shaded in red

Figure 3.2: *Illustrations of the integration volumes, Chen et al. (2013)*

These meshes can be designed such that they cover land areas flooded by tides, but my experiments did not include this wetting/drying effect. The surface area of my domain is therefore independent of time. Figure 3.3a shows the mesh of the computed domain. The studied area is indicated by the red box. Figure 3.3b shows a zoomed in picture of the mesh in Rystraumen to illustrate how it increases the resolution near narrow constrictions. The resolution (distance between elements) of this mesh varies from $\mathcal{O}(5000m)$ near the

open boundaries, to $\mathcal{O}(30-40m)$ in coastal areas. The shape and size of islands and constrictions in the domain are well resolved by the mesh, and is one of the reasons that Akvaplan use a FV model rather than a Finite Difference (FD) model.

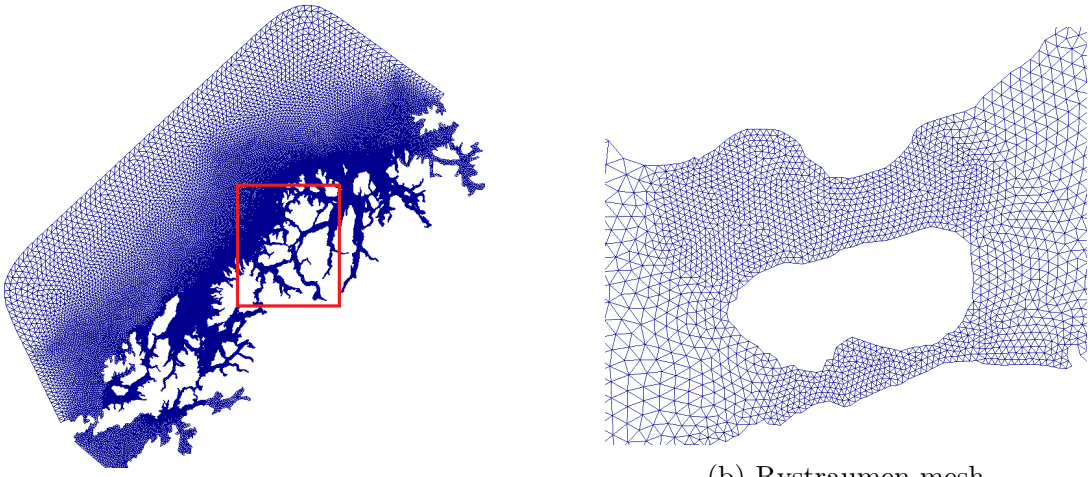

(a) Total mesh, study area in red box

(b) Rystraumen mesh

Figure 3.3: *The grid in my numeric experiments.*

Benefits and disadvantages of using a triangular mesh

Coastal regions are known to have geometries changing rapidly over short length scales. An irregular triangular mesh reproduce coastal geometries better than conventional FD models would since coastlines are smooth instead of the "staircase" shape found in FD models. Jones and Davies (2007) used a finite element model (FEM) and found that a triangular grid had two benefits over FD models for studies of tidally generated vorticity.

1. An increased resolution in areas with strong streams and rapid variation, without needing to resolve the entire domain which such fine a resolution, gave accurate results in shallow areas at a low computational cost.

2. The triangular grid of the finite element model they used seemed not to produce much artificial vorticity. The FD model, in contrast, generated much artificial vorticity - which they attributed to its staircase-coastline.

Dupont et al. (2003) investigated the vorticity production and -transport in an FD model where he aligned the grid along the coastline and at angles to it. The results were strongly dependent on the angles, and increasing the resolution did not eliminate the problem. There are not just advantages using the FV method and unstructured grids. FVCOM use a second order accurate fourth order Runga-Kutta time stepping scheme and a second order accurate upwind scheme in space (Huang et al., 2008), which is worse than for example the popular ROMS model and its structured Arakawa C-grid, which can use fourth-order accurate flux calculations. The triangular mesh accuracy is influenced by the shape, size and organization of the triangles. It is most accurate for equilateral triangles. They are in general not equilateral, as the angles must change when the mesh expand/contract. Adjacent cells should therefore not expand/contract too fast, and have

similar cell areas. FVCOM experiments with the same number of sea surface elevation locations as a finite difference model will have roughly twice as many (u,v) locations. FVCOM thus require more storage for a mesh with the same number of surface nodes. Huang et al. (2008) show that FVCOM can give similarly accurate result as ROMS when using a grid which resolves vivid regions better than still regions indicating that expansion/contraction might be less crucial than the resolution problem. Chen et al. (2007) compared FVCOM to two popular FD models, POM and ECOM-si, at a domain with curved coastlines for problems which are common in estuarine environments. The results were in favour of FVCOM, partly due to the more accurate vorticity production.

3.3.2 Boundary forcing and initial conditions

My experiments are started from rest. In an attempt to identify which suits Tromsø best, the open boundary amplitude and phase of each constituent (M2, S2, N2, K2, K1, P1, O1 and Q1) are interpolated to the open boundary nodes from the Arctic Ocean Tidal Inverse Model (AOTIM, Padman and Erofeeva (2004)) database in one experiment and from the TOPEX/Poseidon (TPXO, Egbert and Erofeeva (2002)) database in another. Velocity information at the open boundary is not needed in FVCOM, since no cells are located there, velocities are instead determined by conservation of volume at the boundary triangles. The only kinematic boundary condition is one that require no velocity (volume transport) normal to the solid boundaries ($v_n = 0$).

3.4 Streamwise momentum balance

Textbooks in fluid mechanics often assume the flow to follow one of the lateral coordinate axes for ease of interpretation. Following the same philosophy one can rotate the coordinate system such that one axes follow the flow at any point in the domain (streamwise) and one is normal to it (crosswise), see Hench and Luettich Jr (2003). Let U_s be the speed of a parcel, and α be the angle U_s makes with the x-axis;
Streamwise

$$\frac{\partial U_s}{\partial t} + U_s(cos\alpha\frac{\partial U_s}{\partial x} + sin\alpha\frac{\partial U_s}{\partial y}) + g(cos\alpha\frac{\partial \eta}{\partial x} + sin\alpha\frac{\partial \eta}{\partial y}) + \frac{C_d U_s^2}{D} = 0 \tag{3.14}$$

The first and second terms are accelerations. The first term, local acceleration, express the change in speed at a location. The second term, streamwise advection is the change of speed in the direction of movement. The third and fourth terms are negative forces, namely streamwise pressure gradient and bottom friction.
Crosswise

$$U_s\frac{\partial \alpha}{\partial t} + U_s^2(cos\alpha\frac{\partial \alpha}{\partial x} + sin\alpha\frac{\partial \alpha}{\partial y}) + fU_s + g(cos\alpha\frac{\partial \eta}{\partial y} - sin\alpha\frac{\partial \eta}{\partial x}) = 0 \tag{3.15}$$

The first term is the crosswise acceleration showing how fast the currents change direction, the second is the centripetal acceleration. The third term is the Coriolis force, and the last one is the crosswise (normal) pressure gradient. I will only use the streamwise balance (Equation 3.14) in this thesis, since I wish to investigate where the forces providing momentum to the fluid are strongest.

Momentum balances in coastal areas

By looking at the depth integrated momentum balance, Hench and Luettich Jr (2003) investigated the shallow Beaufort Inlet and compared it to an idealized and comparable inlet with straight walls and two identical headlands forming a channel connecting the inlet and the open ocean. They found that patterns in the ideal and in the real geometries were similar. The streamwise balance oscillated between two distinct regimes. The first regime (strong stream) was dominated by the pressure gradient and advection upstream of the constriction and by advection and friction downstream. The balance near slack, however, was dominated by the pressure gradient and local acceleration - which is the force balance in a tidal wave. The stream was in general strong, so the flow was normally dominated by friction, advection and the pressure gradient. Local acceleration was therefore only important as the tide turned. Zhao et al. (2006) looked at momentum balances in a strait, but had a different approach. They studied the temporal evolution of the Cartesian coordinate balances for some channels in a system close to Massachusetts and Rhode Island rather than looking at representative snapshots of the momentum balance for the entire domain. Their channels are much deeper than the Beaufort Inlet. They found that the dominating terms in the momentum equations were local acceleration, pressure gradient and advection. Friction was comparable to the other terms when the tide turned, but otherwise negligible in comparison.

Momentum balance routine

The momentum balance I present in this thesis is estimated based on the velocity- and sea surface field outputted by the model every $60 second$. I interpolated the data to a regular grid with a resolution comparable to the smallest cells using the built-in function "griddata" and its linear interpolation algorithm. Gradients are estimated with the Matlab function "gradient" with a single sided difference along boundaries and centered differences in the interior. I estimated time derivatives using a centred scheme, $\frac{\partial u}{\partial t}_n = \frac{u(t_{n+1})-u(t_{n-1})}{2\delta t}$, and thereafter interpolated it to the fixed grid. The forces are therefore not estimated by the same procedure as the model, which solves time-derivatives every $5s$ and use the finite volume method to estimate the forces. The balances I present in this thesis are therefore estimates of the modelled balance - not a perfect reconstruction.

3.5 Data processing and visualization

All figures in this thesis showing spatial data are plotted with north point up the page, and east in the positive x-direction (toward readers right). I used Matlab R2014a and R2016b for post-processing the observations and model results and to visualize the data. The only non-native Matlab package I used was "panel", since it make better subplots than the built-in matlab "subplot". I plotted streamlines using the built-in matlab function "streamslice", which show the path a massless parcel would travel if the flow field was steady state. I had to interpolate the data to a fixed grid to use streamslice, which I did using griddata - again using the linear interpolation algorithm.

Chapter 4

Observations

This chapter presents the observed data. The data was sampled at different locations which I will divide into sections. I will show that the stream in Grøtsundet is strongest near high/low tide. That is not the case in Balsfjord where it is stronger in between high and low tide. I will show that high frequency oscillating streams with strong amplitudes are important in Tromsøysund, and that streams there are influenced by shallow water constituents as well.

4.1 Locations

Tromsøysundet is represented by six stations (see Figure 4.1a). TR1, TR2 and TR3 measured data with the Aanderaa RCM instrument. Data from TRdin1,2 and 3 were sampled with profiling instruments fixed to the bottom. All stations except TR1 are located north of the Tromsøysundet constriction.
Balsfjorden has three stations, BL1, BL2 and BL3 (see Figure 4.1b). They were positioned far away from the Tromsøysund, Sandnessund and Rya constrictions, roughly 15km into the fjord.
The TRN section consists of three stations (TRN1,2 and 3) near and north of Tromsøya (see Figure 4.2a). TRN1 is located close to Sandnessund, TRN2 is near the northern end of Tromsøya and TRN3 is north of where Kvalsundet connects to Grøtsundet.
Section OU consists of four stations from the outer boundary of the system and all of them are located close to the straits connecting the fjord system to the open ocean (see Figure 4.2b). Stations OU1 and 2 are located on the southern side of the domain, Stations OU3 and 4 are located on the northern side.

I have collected information about the depth, position and time of measurement for all stations in Table 4.1. It lists the distance between each vertical cell where the profiling instruments measured the current, and the depth where the point measurements were taken. The data I got from Akvaplan did not include the instrument depth above the sea floor, but comparisons with "www.norgeskart.no" suggest that all instruments except for BL1 and BL2 were positioned close to the bottom.

Table 4.1: Instruments and details about them. "Depth" gives the depth of the instrument. Start and end date are given in Day:Month:Year format.

Station	Lat	Lon	Depth [m]	Start	End
Tromsøysund					
TR1	69.6430	18.9638	7.48	05-02-2014	01-04-2014
TR2	69.6628	19.0064	20.53	05-02-2014	19-03-2014
TR3	69.6633	18.9951	19.56	05-02-2014	19-03-2014
TRdin1 (Seaguard)	69.6595	18.9888	34 : 1.8 : 7	30-03-2017	05-05-2017
TRdin2 (Nortek)	69.6642	18.9996	24.5 : 2 : 8.5	30-03-2017	05-05-2017
TRdin3 (Nortek)	69.6668	19.0018	26 : 2 : 8	31-03-2017	05-05-2017
Balsfjorden					
BL1	69.3660	19.0699	82.72	11-07-2014	25-08-2014
BL2	69.4236	19.0395	93.79	11-07-2014	25-08-2014
BL3	69.4234	19.0018	19.95	05-02-2014	21-03-2014
North					
TRN1 (Nortek)	69.6829	18.8847	25.23 : 2 : 8	31-03-2017	05-05-2017
TRN2	69.7265	19.0216	50.92	19-09-2013	11-11-2013
TRN3	69.7951	19.2431	16.68	05-02-2014	21-03-2014
Entrances					
OU1	69.5690	17.9078	87.11	17-07-2015	13-08-2015
OU2 (Nortek)	69.8479	18.8260	35 : 2 : 8	26-03-2015	01-05-2015
OU3	69.8494	19.6731	67.49	04-02-2015	06-03-2015
OU4	70.0409	19.9157	57.70	25-03-2015	05-05-2015

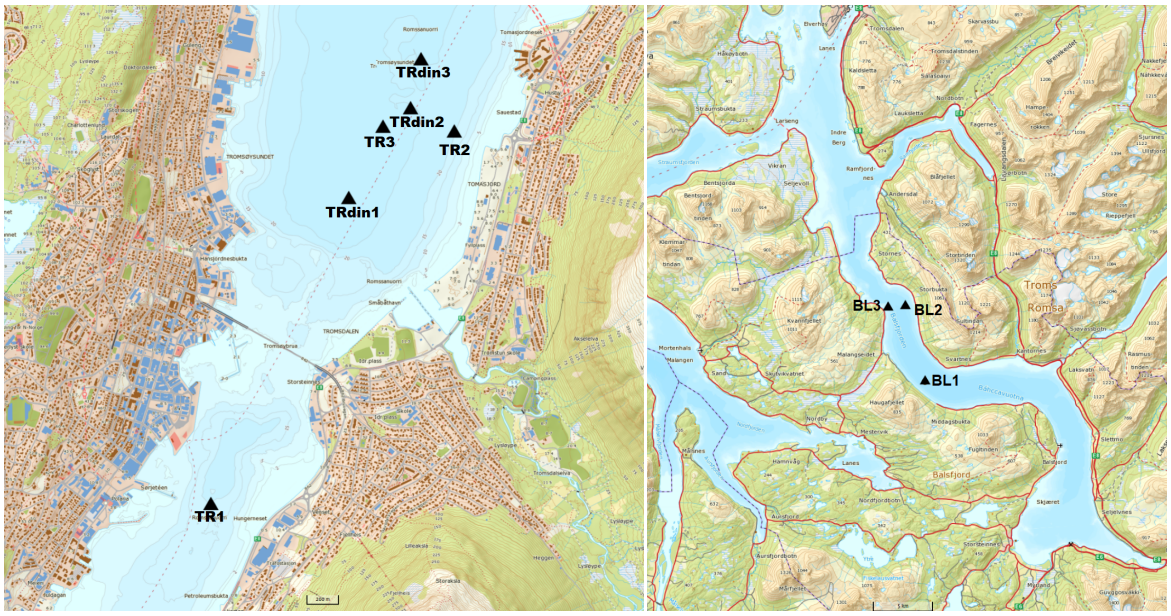

(a) Stations in Tromsøysundet (b) Stations in Balsfjorden

Figure 4.1: *Screenshot from "www.norgeskart.no", Kartverket 2018*

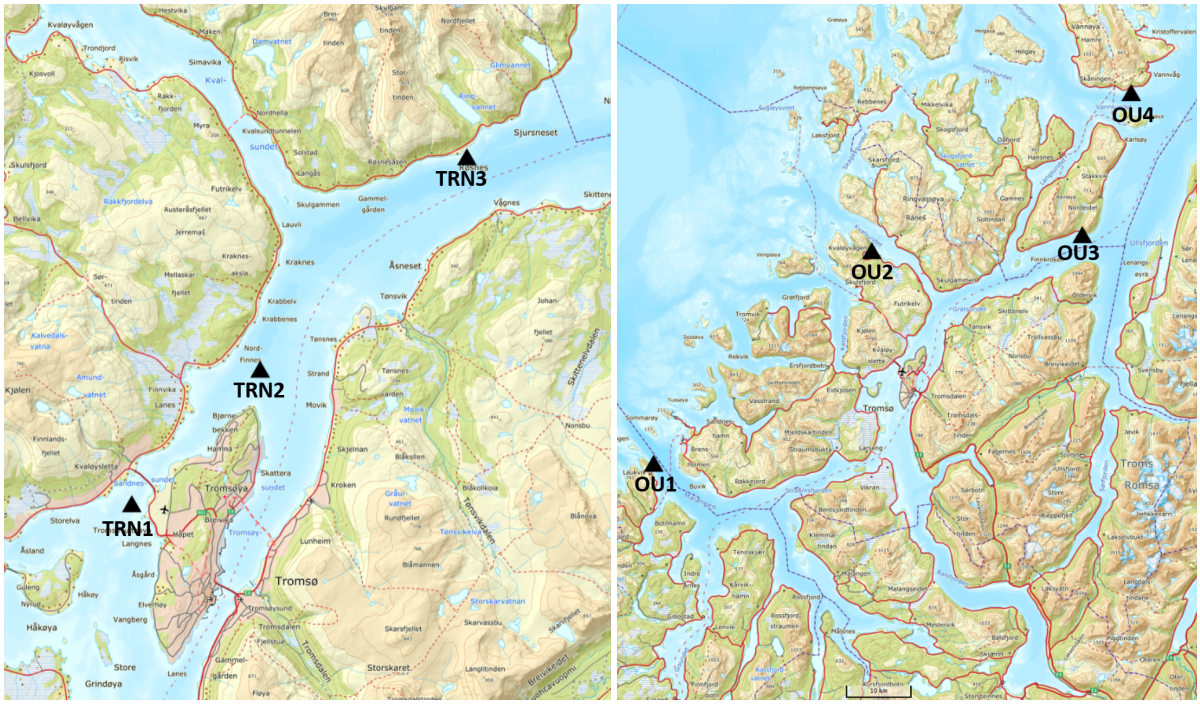

(a) Stations north of Tromsø (b) Stations at the outer boundary

Figure 4.2: *Screenshot from "www.norgeskart.no", Kartverket 2018*

4.2 Data

The ratio of the K1 and O1 to the M2 and S2 sea surface amplitudes, known as the form factor (Pugh and Woodworth, 2014), is very close to or less than 0.1 at all stations (not shown) - semi-diurnal tides dominate this region. I will therefore restrict my study to the M2, S2 and N2 constituents. I will show three measures of tide at each section.

1. The sea surface elevation.
2. The phase of the tidal sea surface elevation - since it is tells us where the sea surface maximum occurs first.
3. Whether the tidal constituent behaves as a progressive or standing wave, to see when the strongest tidal stream (tidal current) occurs relative to the sea surface.

I chose to have a closer look at the Tromsøysund data since that is where I have the densest dataset, and data from both sides of the constriction. I primarily use data from the other regions of the domain to gain an overview of the tidal motion in the fjord system and, later on in Chapter 5, to validate that the model reproduce similar features.

4.2.1 Outer boundary, OU

Table 4.2 and 4.3 show the sea surface elevation and tidal stream constants.

South: The OU1 and OU2 M2 amplitudes are roughly $74cm$. The tide arrive approximately simultaneously at OU1 and OU2 (Greenwich phase ≈ 342). One may argue that OU2 lead OU1 - which suggest that the M2 tidal wave propagate southward. I believe the phase difference is either related to that OU1 is located on the fjordward side of the Malangen mouth (fjords lag the open ocean) or instrument related inaccuracies. The S2 amplitude is about $20cm$ at OU1 and $30cm$ at OU2. The OU2 S2 wave lag OU1 by 8°.

North: The M2 amplitude is $110cm$ at OU4 and $90cm$ at OU3, both are taller than the southern stations - but the difference between OU3 and OU4 is remarkably big, again possibly due to inaccurate measurements. The amplification north of Tromsø is nevertheless a known phenomenon, and was mentioned by Gjevik et al. (1994) as due to co-oscillations over the shelves north of Tromsø. The M2 wave arrive about 10° later than at the southern stations. S2 phase estimates are very different from station to station and they are uncertain, but it is clear that the northern side lag the southern. The data is therefore consistent with northward propagating M2 and S2 kelvin waves. Furthermore the observations suggest that the M2 wave is progressive at OU3, just 14° out of phase.

Table 4.2: Surface elevation constituents on the outer border of the fjord-system

Station	Const.	% PE	Amp. [cm]	95% amp. [cm]	Greenwich phase	95% phase
OU1	M2	79	73	1	343.6	1.0
OU2	M2	83	75	0	341.4	0.1
OU3	M2	81	92	3	356.1	1.8
OU4	M2	76	107	2	349.8	1.2
OU1	S2	6	18	1	9.3	4.2
OU2	S2	12	28	1	17.6	0.3
OU3	S2	12	35	2	46.7	3.9
OU4	S2	8	35	2	30.6	3.2

Table 4.3: Currents at the outer boundaries

Station	Const.	% KE	Major axis [cm/s]	Greenwich phase	95% phase
OU1	M2	68	7	122.9	4.0
OU2	M2	40	1	66.0	5.0
OU3	M2	38	2	190.7	22.6
OU4	M2	84	21	317.3	1.6
OU1	S2	10	3	193.5	10.3
OU2	S2	11	0	109.6	11.0
OU3	S2	15	2	191.7	36.1
OU4	S2	8	6	350.7	5.7

4.2.2 North of Tromsøya, TRN

Table 4.4 summarize the sea surface harmonics, Table 4.5 show the tidal stream constants.

M2: The TRN2 and TRN3 stations (the Grøtsundet stations) suggests that the M2 tide is 92cm tall, which is comparable to what OU3 found. TRN1 is slightly smaller, 85cm. The phases at TRN1,2, and 3 are so to say identical, 359° and they lag OU3 by about 3°. The currents at station TRN1,2 and 3 are roughly $34°, 90°$ and 18° out of phase from the sea surface. The tide behave as a standing wave at TRN2, and as a progressive one at TRN1 and 3. TRN1 and TRN3 agree with OU3, hence most stations near Grøtsundet suggest that the strongest M2 stream occur close to high/low tide.

S2: The S2 amplitudes are slightly different. It is 34cm at TRN2, 37cm at TRN3 and is 32cm at TRN1. All of them are therefore roughly the same as at OU3 (35cm). The phase is identical at TRN2 and TRN3, but the phase at TRN1 lag the others by about 10°. The S2 tide is roughly $6°, 43°$ and 5° out of phase at the TRN1,2 and 3 stations.

In short, the tidal stream caused by the M2 and S2 tides near Grøtsundet is strongest near high/low tide. The amplitudes are bigger than at the OU1 and OU2 stations suggesting that the tide moving into Grøtsundet from the north determine the amplitudes. S2 estimates are less reliable than M2 estimates.

Table 4.4: Tidal amplitude constituents TRN

Station	Const.	PE [% of tot]	Amp. [cm]	95% amp [cm]	Gr. phase	95% phase
TRN1	M2	82	85	0.2	359.2	0.2
TRN2	M2	85	92	0.5	359.6	0.3
TRN3	M2	82	92	0.5	359.1	0.3
TRN1	S2	12	32	0.3	37.4	0.4
TRN2	S2	11	34	0.6	27.5	0.9
TRN3	S2	13	37	0.5	27.5	0.7

Table 4.5: TRN section currents

Station	Const.	% KE	Major axis [cm/s]	Greenwich phase	95% phase
TRN1	M2	69	29	213.0	1.5
TRN2	M2	59	7	88.4	4.4
TRN3	M2	77	15	196.6	1.8
TRN1	S2	13	13	211.2	3.6
TRN2	S2	5	2	251.4	28.0
TRN3	S2	4	3	212.4	6.6

4.2.3 Balsfjorden, BL

Table 4.6 show the sea surface related constants, Table 4.7 show the constants related to the tidal stream.

M2: The amplitude at the BL stations is about $88cm$. The Malangen measurement (OU1) is roughly $15cm$ smaller than Balsfjorden (BL), while the BL amplitudes are $4cm$ smaller than at TRN stations - the communication between BL and Grøtsundet must be essential for the BL M2 amplitude. The BL phases differ significantly from station to station, and I can not - based on these observations - tell if the BL tide lead or lag Grøtsundet. It is, however, clear that the BL tide lag the Malangen tide significantly since OU1 lead the BL section by about 15°. The stream and sea surface behave as a standing wave.

S2: The measured amplitude is about $30cm$. The S2 tide lag Grøtsundet and Malangen significantly. It lag OU1 more than it lags the stations in Grøtsundet. The amplitude in Balsfjorden is closer to Grøtsundet- than Malangen values. Balsfjorden S2 phases lag the TRN station, but are comparable to the TR section (next subsection). The Balsfjorden S2 tide behave as standing wave. I suspect that the differences in the S2 estimates may originate from inaccurate measurements rather than physical processes.

Table 4.6: Tidal amplitude constituents in Balsfjorden.

Station	Const.	PE [% of tot]	Amp. [cm]	95% amp [cm]	Gr. phase	95% phase
BL1	M2	84	87	0.7	358.3	0.5
BL2	M2	81	88	0.6	354.3	0.4
BL3	M2	82	88	0.8	2.3	0.5
BL1	S2	8	28	0.7	52.9	1.1
BL2	S2	9	29	0.7	50.3	1.1
BL3	S2	12	34	0.8	55.6	1.6

Table 4.7: Tidal current constituents in Balsfjorden.

Station	Const.	KE [% of tot]	Major axis. [cm/s]	Gr. phase	95% phase
BL1	M2	76	4	78.8	2.1
BL2	M2	72	5	100.4	2.4
BL3	M2	70	16	74.5	1.2
BL1	S2	10	1	149.3	5.5
BL2	S2	8	2	166.5	5.6
BL3	S2	14	7	131.8	2.9

4.2.4 Tromsøysundet, TR

Table 4.8 show the sea surface harmonic constants, Table 4.9 show the tidal stream constants.

Tidal elevations north of the constriction:
The M2 amplitudes at the northern stations are about $90cm$ tall. All stations agree that the M2 phase is roughly $358 - 359°$. Point- and profiling instrument estimates of the S2 amplitudes are comparable ($35cm$) but data from point instrument lag the profiling instruments by about 12°. Phases from the point instruments are comparable to the BL section but the TRdin-stations lead BL by about $15° - 20°$. Both the S2 and M2 waves are progressive regardless of which type of instrument I looked at.

Tidal elevation at TR1 (south of the constriction):
The M2 amplitude is about $13cm$ smaller than at stations north of the constriction and roughly $10cm$ smaller than the stations in Balsfjord. TR1 lead all stations in its direct vicinity, but only slightly ($1° - 2°$). The M2 wave is 15° out of phase thus the progressive wave dominate. The S2 amplitude is is slightly smaller than at the northern stations, $31cm$. The S2 phase is similar to the one measured in Balsfjorden, roughly 48°. It lags the northern side of the constriction slightly when compared to other point measurement stations (TR) and it lags significantly behind the profiling stations (TRdin). The S2 wave is progressive, 20° out of phase.

The S2 phase estimates is very dependent of whether the observation was done with a profiling or point instrument. The M2 and S2 waves are progressive, and the amplitudes are comparable to both the TRN and BL sections.

Table 4.8: Surface elevation constituents in Tromsøysundet

Station	Const.	PE [% of tot]	Amp. [cm]	95% amp. [cm]	GMT phase	95% phase
TR1	M2	81	76	0.8	357.8	0.6
TR2	M2	82	89	0.4	359.4	0.3
TR3	M2	81	91	0.4	358.2	0.2
TRdin1	M2	82	91	0.4	359.4	0.2
TRdin2	M2	82	89	0.3	358.6	0.2
TRdin3	M2	81	91	0.2	358.0	0.1
TR1	S2	13	31	1.0	48.3	1.6
TR2	S2	13	35	0.4	47.0	0.6
TR3	S2	13	37	0.3	46.0	0.5
TRdin1	S2	12	35	0.3	35.1	0.5
TRdin2	S2	12	34	0.3	34.8	0.5
TRdin3	S2	13	36	0.2	34.5	0.3

Table 4.9: Tidal stream constituents in Tromsøysund

Station	Const.	KE [% of tot]	Major axis. [cm/s]	Gr. phase	95% phase
TR1	M2	67	33	192.8	1.8
TR2	M2	56	8	188.9	3.7
TR3	M2	62	9	219.8	4.2
TRdin1	M2	65	14	199.6	1.4
TRdin2	M2	69	9	216.3	1.3
TRdin3	M2	64	7	170.0	2.6
TR1	S2	7	10	208.6	5.8
TR2	S2	5	2	217.4	10.6
TR3	S2	4	2	220.5	15.6
TRdin1	S2	7	4	227.1	5.5
TRdin2	S2	9	3	213.6	3.8
TRdin3	S2	7	2	204.5	9.7

Currents: The observed current at some of the stations are well approximated by the harmonic analysis, while others are not. Measurements on the northern side of the constriction, for example, do not fit the harmonic analysis as well as at TR1 (Figure 4.3). The tidal stream from the UTide harmonic analysis fits the observed stream at TRdin1 well until the strongest northerly-flowing currents when high frequency oscillations influence the stream significantly, see Figure 4.3a. Maximum currents are different from high tide to the next (positive meridional component). Such maxima can be seen at other stations on the northern side of the constriction as well (see Appendix C), suggesting that high frequency oscillations is a common feature of the northern side of Tromsøysund.

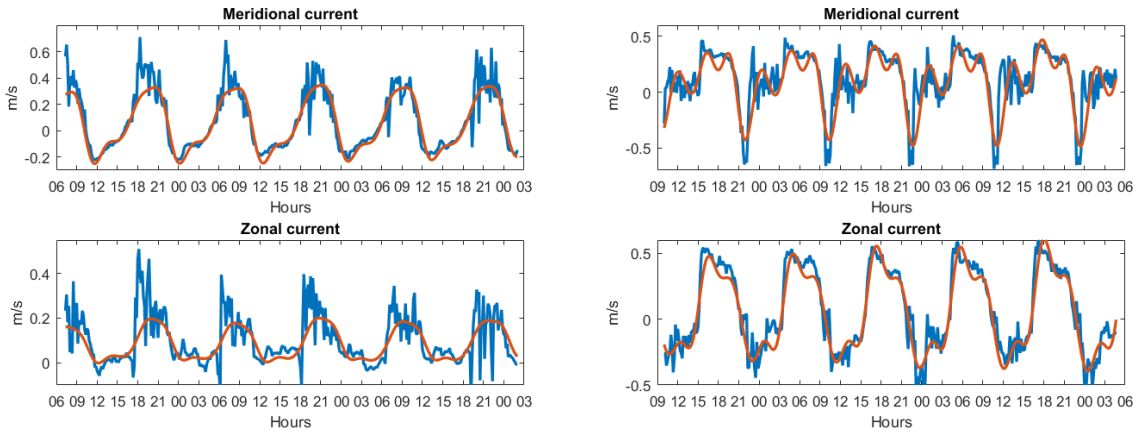

(a) Velocity components at TRdin1

(b) Velocity components at TR1

Figure 4.3: *Measured current (blue curve). Harmonic analysis (UTide) estimate of tidal stream (orange curve). Positive meridional component mean that the flow is northerly, and positive zonal component indicate easterly currents.*

The TR1 tidal stream is, in contrast, well reproduced by the harmonic analysis. Only the strongest Balsfjorden-flowing stream (southward) is systematically lost (Figure 4.3b). Some noise is superimposed on the TR1 tidal stream, but not by the same amounts as at TRdin1. All Tromsøysund measurements, both on the northern and southern sides, are influenced by the shallow water constituents (see Appendic C).

Figure 4.4 show how the different higher harmonics modify the flow. I reconstructed the tidal stream at TR1 using different combinations of the shallow water harmonics. The stream is well reproduced when adding the three leading M2 overtones, M4 ($2\omega_{M2}$), M6 ($3\omega_{M2}$) and M8 ($4\omega_{M2}$) to the leading constituents M2, S2 and N2 (top panel). The stream is better reproduced when I add the neap-spring cycle harmonics MS4 ($\omega_{M2} + \omega_{S2}$), 2MS6 ($2\omega_{M2} + \omega_{S2}$) and the elliptic orbit related constituent 2MN6 constituent to the mix (middle panel). Thus UTide shows that the stream is dominated by the M2 related over- and compound tides. The bottom panel compare the stream constituted of 35 harmonics to the leading 19 harmonics. The orange line (35 harmonics) is so to say indistinguishable from the blue line (19 harmonics). In short, shallow water constitutes are responsible for the interesting tidally forced flow patterns at TR1. These shallow water harmonics create flow patterns one normally would not expect, such as how the flow can turn direction from down-channel to up-channel for brief periods of time before turning back again. I have not seen these features other places in the domain.

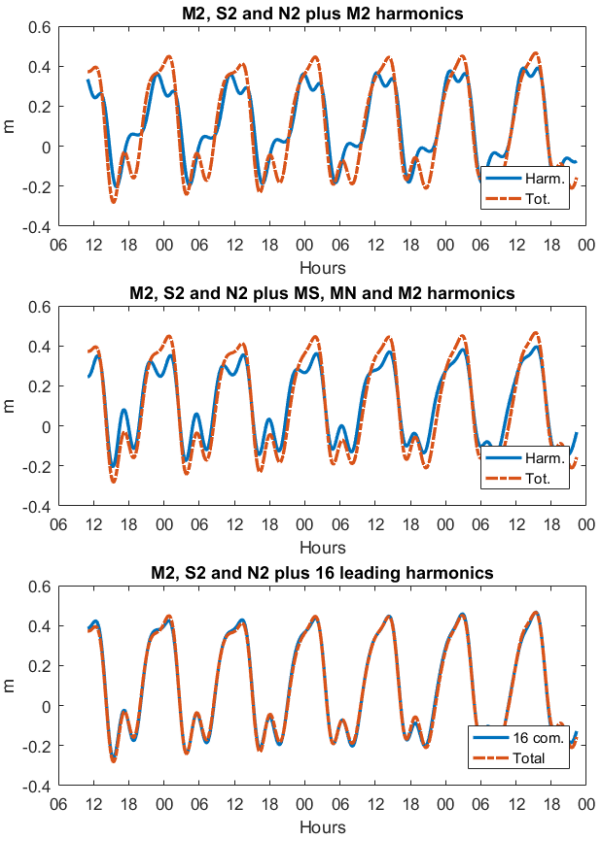

Figure 4.4: *Reconstructed v-component illustrating non-linear constituents*

Tromsøysund compared to the TRN and BL sections

So shallow water constituents are very pronounced in Tromsøysund. Similar (but less pronounced) features can be found in other areas of the fjord system, as I have illustrated in Figure 4.5 & 4.6. Figure 4.5 show TR1 and TR2 are plotted for the same time interval, and TRdin1 for a similar spring tide. All of them agree that the stream should weaken after peak southward flow. The feature is not equally strong at station BL1, even though it too is influenced by higher harmonics - albeit not as much as TR1 and TR2. TRN3 is so to say unaffected by shallow water harmonics, at least compared to the other stations.

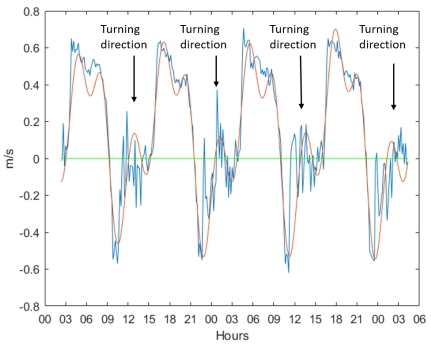

(a) TR1, along channel flow

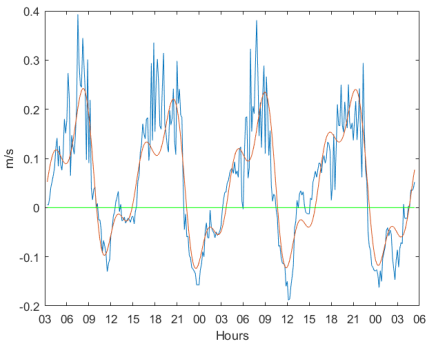

(b) TR2, along channel flow

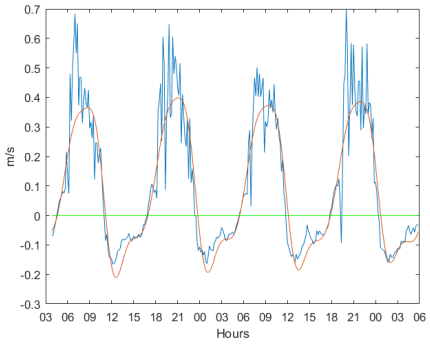

(c) TRdin1, along

Figure 4.5: *Measured stream (blue line), and UTide estimated tidally forced stream (orange line) for TR1, TR2 and TRdin1. TR1 and TR2 are plotted at the same time interval during a spring tide. The TRdin1 stream is plotted for another spring-tide.*

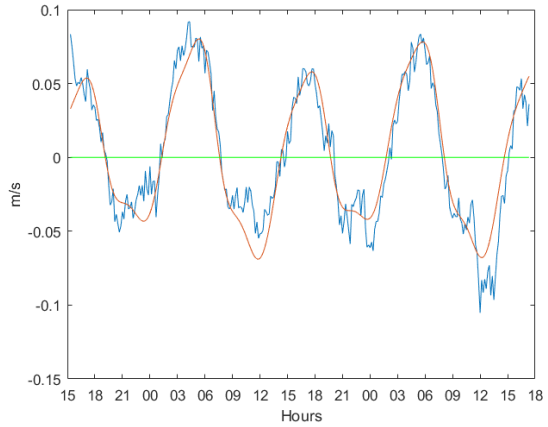

(a) BL1 v-component

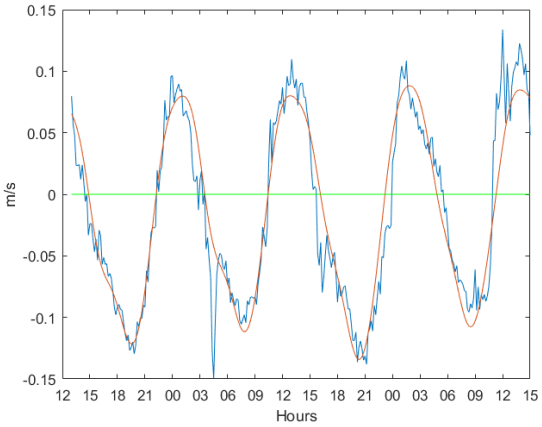

(b) TRN3 v-component

Figure 4.6: *Measured stream (blue line), and UTide estimated tidally forced stream (orange line) for some selected stations. The time intervals do not correspond to each other.*

4.3 Tromsø constrictions: Stream and sea surface

Having a very progressive tide mean that the volume transport is directed toward Balsfjorden when the tide rise in the fjord and also when it fall. Being affected by the shallow water constituents result in a flow with "wobbly", or "bumpy" features. Figure 4.7 show how the flow relate to the sea surface elevation at TRN1 and TRdin1. The maximum flow into Balsfjorden occur near high tide, and the maximum flow out near low tide. There is not a significant neap-spring variability to the progressive flow, one should always expect strong streams near high/low tide.

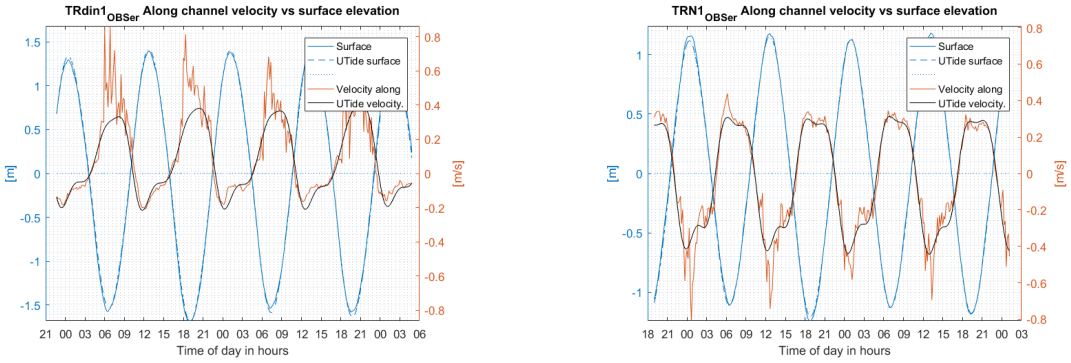

Figure 4.7: *The flow along Tromsøysund (left panel) and Sandnessund (right panel). Positive velocities indicate a flow away from Balsfjord. The figures apply for the same time interval, showing the measured- and UTide interpretation of the sea surface (blue colors) and current (red and black).*

4.4 Important features

This data is consistent with Gjevik et al. (1994) who mentioned a co-oscillating tide north of Tromsø causing bigger amplitudes than on the southern side of the domain. The M2 and S2 waves are progressive in Grøtsund, Sandnessund and Tromsøysund - hence the stream there is strongest near high/low tide. Tidal amplitudes in Balsfjorden are bigger than in Malangen, which must be the reason why the stream in Rystraumen turns *before* high tide. Shallow water harmonics are important for the stream in Tromsøysund and Sandnessund even though the sea surface is dominated by the linear frequencies. The nearby sections report streams dominated by the linear constituents. The stream on the northern and southern side of the Tromsøysund constriction behave differently, the southern side (TR1) is well described by the harmonic analysis while the northern side (TRdin1) is significantly affected by high-frequency oscillations. The harmonic analysis can describe southerly and weak northerly flow well but not once it exceed a threshold. There are uncertainties associated with the estimates of the harmonic constants. M2 tide estimates are independent of what instrument is used to sampled the data, but the S2 constituent is not. Profiling instrument estimates of the S2 phase consistently lead those measured by point-instruments. These discrepancies must be kept in mind when comparing the observations to model results.

Chapter 5

Model vs Observations

This chapter compares two different model experiments to the observations. The first experiment is forced by the AOTIM database, and the second was done using TPXO. It is structured as follows; I first compare the modelled sea surface to the observations and thereafter compare $\phi_\eta - \phi_U$ for the M2 constituent at each station to get an impression of how well the stream-to-sea-surface relation is modelled. I will show how well the model reproduce the S2 and N2 tides at some locations as well. I seek to understand the mechanisms governing the flow in this thesis, not creating a forecast of the tidal stream in the region and I will therefore look for a stream which *behave* like the observed one.

5.1 Sea surface

Table 5.1 and 5.2 show how much the FVCOM modelled sea surface elevations deviate from the observations. $\delta A = A_{FVCOM} - A_{Observed}$ and likewise $\delta\phi = \phi_{FVCOM} - \phi_{Observed}$ are the differences between modelled and observed tidal amplitude and phase at each station. Negative values show that the model underestimate, positive show that it overestimate. Both tables show the differences for the three leading constituents (M2, S2, and N2).

AOTIM forcing

Table 5.1 compare TPXO and AOTIM amplitudes to the observations, Table 5.2 compare the phases.

Amplitude: M2 amplitudes are underestimated by about $3 - 6cm$ at most stations. Station OU4 stand out, being the only station where the M2 deviate more than 7cm. S2 amplitudes are more underestimated than the M2 constituent. The N2 tide is, in contrast, overestimated at all station. S2 and N2 amplitudes are almost equally large, but that is not supported by the observations.

Greenwich phase: The M2 tide is very well reproduced, typically deviating by less than $2°$, in a mix of over- and underestimations. The S2 phase is consistently overestimated, typically by $20°$, and the N2 phase is consistently underestimated by $70 - 90°$. OU4 deviates the most relative to the observations. The M2 tide is very well reproduced, but the S2 and N2 constituents are consistently misrepresented both with respect to phase and amplitude.

TPXO forcing

Amplitude: The M2 amplitude is underestimated by about $5 - 7cm$ at most locations. TPXO results typically deviate roughly $2cm$ more than the AOTIM experiment. S2 and N2 amplitudes are underestimated, often deviating by similar amounts.
Greenwich phase: The M2 phase deviates more with TPXO at OU1 and OU2 than with AOTIM, but TPXO is closer to the observations at OU3 and 4. In Tromsoysundet, where I had access to a much denser set of observations than elsewhere in the domain, we see that TPXO perform similar as AOTIM for the M2 constituent, but significantly better with respect to the S2 and N2 constituents.

Table 5.1: Observed vs FVCOM surface amplitudes given in cm

	Observed			FVCOM$_{AOTIM}$			FVCOM$_{TPXO}$		
	A	A	A	δA	δA	δA	δA	δA	δA
Station	M2	S2	N2	M2	S2	N2	M2	S2	N2
OU1	72.5	18.3	9.8	-2.9	1.7	9.4	-5.6	3.0	4.3
OU2	74.7	28.4	16.1	0.1	-7.2	4.4	-5.7	-5.6	-0.8
OU3	92.2	35.4	24.3	-4.4	-10.8	1.5	-8.3	-8.6	-6.7
OU4	107.1	34.6	22.2	-20.9	-10.6	3.0	-24.9	-8.4	-4.9
BL1	87.0	27.5	21.4	-2.4	-3.2	2.1	-4.7	-1.4	-4.6
BL2	87.1	29.2	21.4	-2.8	-5.0	1.9	-5.0	-3.2	-4.7
BL3	88.0	33.7	18.9	-3.8	-9.5	4.0	-6.0	-7.8	-2.2
TR1	76.4	30.6	15.7	6.8	-6.8	7.2	3.3	-5.1	0.8
TR2	89.3	35.3	19.6	-3.2	-10.9	5.7	-5.9	-8.9	-2.4
TR3	90.6	36.5	20.4	-4.6	-12.4	5.0	-7.0	-10.1	-3.2
TRdin1	91.2	34.7	20.4	-5.3	-10.4	5.0	-7.7	-8.2	-3.2
TRdin2	89.3	34.2	19.6	-3.3	-9.8	5.7	-5.7	-7.8	-2.4
TRdin3	91.0	36.4	19.9	-5.1	-11.7	5.2	-7.6	-10.0	-2.7
TRN1	84.5	32.2	18.5	-0.4	-8.3	4.9	-3.9	-6.5	-1.8
TRN2	92.0	33.6	16.2	-5.6	-9.1	9.1	-8.7	-7.2	1.1
TRN3	92.3	36.6	20.9	-5.5	-12.0	4.5	-8.8	-10.0	-3.6

Similar features

Both the TPXO and AOTIM forced experiments underestimate the M2 and S2 constituents at most stations. The observations suggested that the M2 phase had strong local differences in Balsfjord, but FVCOM suggest that all areas in Balsfjorden are in phase. Balsfjorden lags Malangen in these experiments, just as the observations suggests. OU stations (except for OU4) deviate by similar magnitudes as the BL section, which I interpret as a sign that FVCOM choke the tide sufficiently at the constrictions.

Table 5.2: Observed vs FVCOM surface phases, units in day degrees relative to GMT

	Observed			FVCOM$_{AOTIM}$			FVCOM$_{TPXO}$		
	ϕ	ϕ	ϕ	$\delta\phi$	$\delta\phi$	$\delta\phi$	$\delta\phi$	$\delta\phi$	$\delta\phi$
Station	M2	S2	N2	M2	S2	N2	M2	S2	N2
OU1	343.6	9.3	327.6	-0.5	33.8	-88.1	7.5	15.7	-17.0
OU2	341.4	17.6	308.1	3.2	26.6	-68.9	9.5	8.1	3.9
OU3	356.1	46.7	333.2	1.7	11.1	-80.8	0.4	-6.3	-5.5
OU4	349.8	30.6	315.5	7.8	26.9	-63.4	6.5	9.4	11.7
BL1	358.3	52.9	336.0	-2.6	5.5	-82.1	0.8	-13.8	-10.8
BL2	356.3	51.6	335.5	-0.5	7.0	-81.5	2.8	-12.4	-10.3
BL3	2.3	55.6	331.3	6.6	2.9	-77.4	3.2	-16.5	-6.2
TR1	357.8	48.3	324.6	-2.4	8.9	-72.4	0.4	-9.3	0.3
TR2	359.4	47.0	325.1	-1.6	10.9	-71.9	-1.9	-6.4	2.7
TR3	358.2	46.0	322.6	-0.4	11.6	-69.8	-0.6	-5.5	5.0
TRdin1	359.4	35.1	344.1	-1.4	22.4	-90.8	-1.8	5.5	-16.3
TRdin2	358.6	34.8	343.0	-0.8	23.1	-89.6	-1.0	5.6	-15.4
TRdin3	358.0	34.5	339.1	-0.1	23.5	-85.3	-0.4	6.0	-11.5
TRN1	359.2	37.4	345.2	-3.2	20.4	-92.7	-0.9	1.6	-20.1
TRN2	359.6	27.5	336.4	-2.0	30.2	-83.3	-2.4	12.9	-8.8
TRN3	359.1	47.5	323.1	-1.2	10.6	-69.8	-2.1	-6.8	4.9

5.2 Tidal stream

Figure 5.1 to 5.3 plot the observed and modelled sea surface elevation and stream together. The figures are plotted for half a month, covering neap and spring tides. The FVCOM figures are plotted for the same time-interval, but they do not correspond to the same time interval as the observed stream. The observation show double-peak stream at both spring and neap tide and the stream is progressive the entire neap spring period. Balsfjorden flowing (negative values) streams are often strong immediately after it start flowing toward Balsfjorden. It does, however, not maintain the strength for long, and weaken significantly close to high tide. It can even *flow away* from Balsfjorden for short periods before turning back at Balsfjorden again. The northerly flow (positive values) is strongest close to low tide.

Modelled vs. observed features:
The AOTIM experiment (Figure 5.2) stream is progressive at spring tide, but not on neap tide. The double-peak is prominent at spring tide but not on neap tide. The flow can change direction for brief periods, but not in a similar manner as the observed flow.
The TPXO experiment (Figure 5.3) model a double-peak the entire tidal cycle and the stream is progressive the entire tidal cycle. The stream can turn direction but not as often as the observed flow.

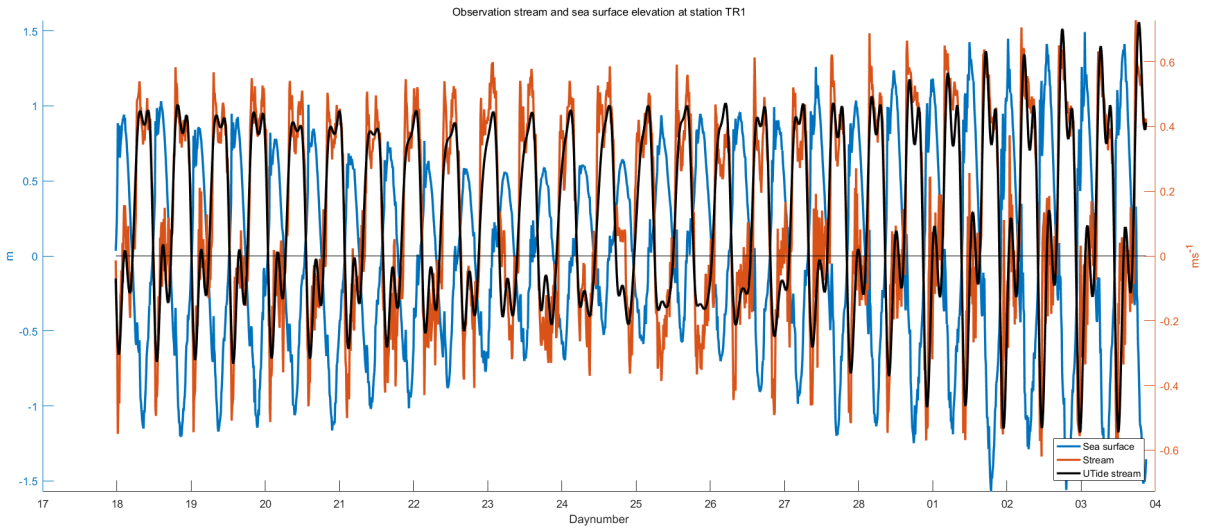

Figure 5.1: *Observed along channel current and sea surface elevation for half of a neap-spring period at TR1. The red line is the observed stream along the channel and the black line is the tidal stream (estimated by UTide). The blue line is the measured sea surface elevation.*

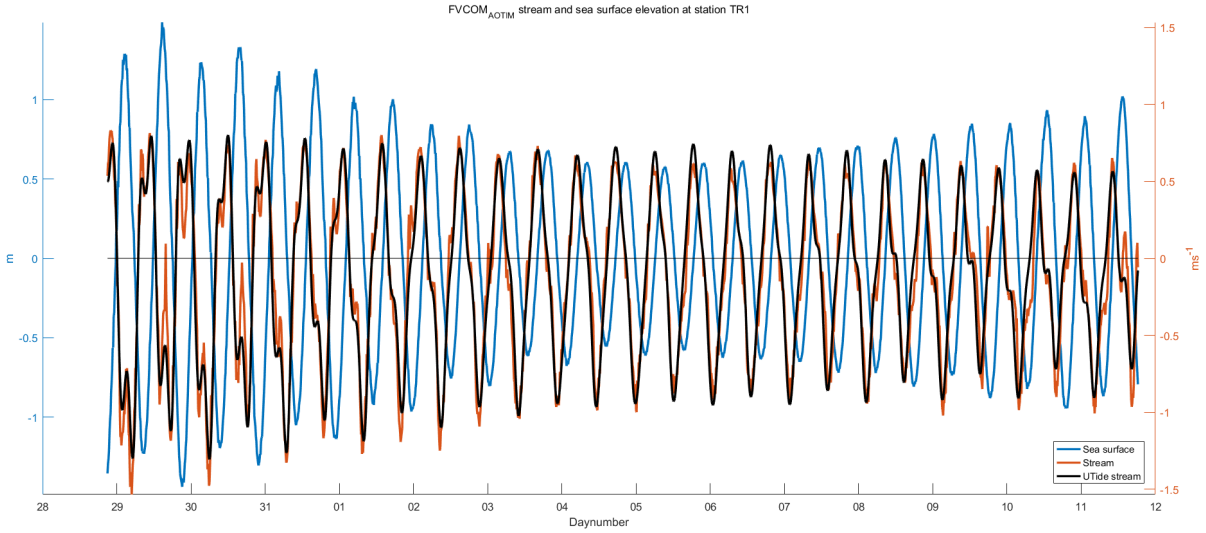

Figure 5.2: *AOTIM current and sea surface at TR1. The red line is the modelled stream, the black line is the UTide interpretation of the stream and the blue line is the modelled sea surface. Plotted for half a spring-neap period.*

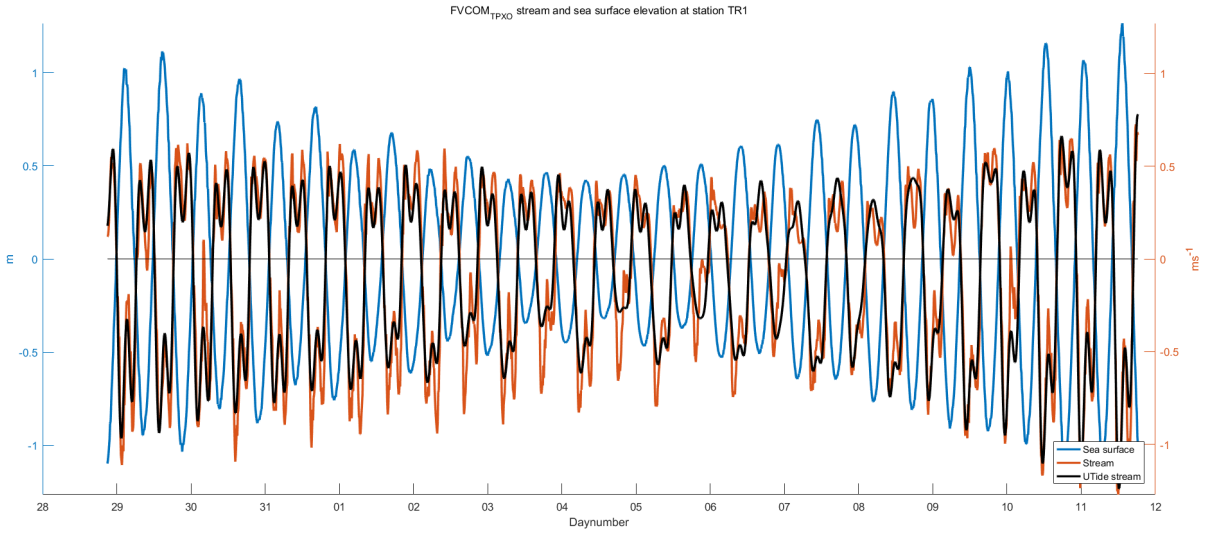

Figure 5.3: *TPXO current and sea surface at TR1. Same layout as in Figure 5.2.*

Phase difference between tidal stream and sea surface elevation

Table 5.3 show how progressive the modelled M2 stream is relative to the observed M2 stream. The AOTIM experiment gave a M2 wave which is close to standing at many of the stations in Tromsøysund. The TPXO experiment gave a more progressive M2 tide than observed at many stations. It is in general closer to the observations than the AOTIM experiment, see Table 5.3. Figure 5.4 illustrate the phase difference at TRdin1, TRdin3 and TR1 for the M2, S2 and N2 constituents. We see that TPXO modelled M2 differences are similar to the observation, while AOTIM tend to model a standing wave. AOTIM compare best with the observed S2 and N2 differences.

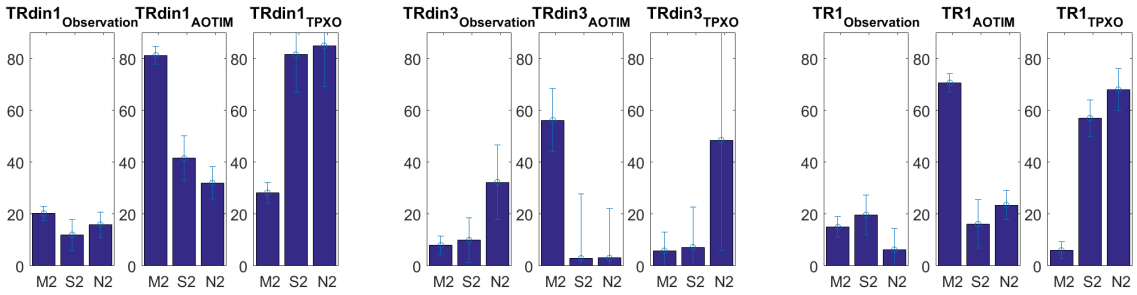

Figure 5.4: *Phase difference for some selected stations. The sum of surface and current 95% confidence intervals is indicated in brackets. The phase difference is given in degrees.*

Table 5.3: M2 sea surface elevation- vs stream phase, $g_{seasurface}$-g_{stream}. "Max 95%" is the sum of the 95% confidence intervals of the sea surface and current estimates.

	Observations		AOTIM		TPXO	
Station	$\|\delta g\|$	Max 95%	$\|\delta g\|$	Max 95%	$\|\delta g\|$	Max 95%
OU1	40.7	4.7	58.3	2.4	62.6	1.8
OU2	84.7	5.9	80.6	2.1	81.0	2.4
OU3	14.6	25.3	81.0	3.1	11.4	2.6
OU4	32.5	2.9	36.3	1.3	63.8	1.2
BL1	80.4	2.6	89.7	1.0	89.9	0.9
BL2	75.9	2.5	87.9	1.1	87.6	0.8
BL3	72.1	1.9	89.5	1.0	89.6	1.0
TR1	15.0	2.1	70.7	1.7	6.0	1.5
TR2	9.5	4.3	39.4	21.3	20.6	4.8
TR3	41.5	3.5	80.0	5.4	16.4	4.0
TRdin1	20.2	1.9	85.1	2.6	28.2	2.4
TRdin2	37.7	1.5	61.2	8.6	4.0	4.5
TRdin3	8.0	3.0	56.4	7.8	5.8	5.7
TRN1	33.9	1.6	81.4	2.3	20.6	1.6
TRN2	88.8	4.8	47.8	9.3	24.7	3.2
TRN3	17.5	1.7	44.4	5.0	6.0	7.5

5.3 Essential differences

There are three important differences between the numerical experiments;

1. AOTIM results give the best representation of the M2 sea surface amplitude, TPXO underestimates it more.

2. AOTIM creates equally large N2 and S2 constituents, while TPXO captured their ratio better.

3. TPXO produced a progressive M2 wave in Tromsøysund with double peaks during the entire spring-neap cycle. AOTIM M2 streams are closer to a standing wave without double peaks for much of the spring-neap cycle. AOTIM does, however, give progressive S2 and N2 streams, TPXO gives them as nearly standing waves.

Neither of the experiments agree perfectly with the observations, but they are not too far off. Both experiments found that the northern side of Tromsøysund is much noisier than the streams on the southern side (AOTIM not shown, TPXO results will be presented later on in the thesis). There is room for improvement, yet it is interesting to note that the *features* are reproduced by the model. I therefore think that FVCOM does a good job, and that it is suitable for a closer study of the observed phenomena since it seem to be on to something with respect to the physical mechanisms driving the flow. I will investigate these flow features in the remainder of this thesis using results from the TPXO forced experiment.

Chapter 6

Model results

I will show charts of the M2 and S2 sea surface amplitude and phases (Section 6.1) and study the modelled stream. I will thereafter show the volume transport through the straits directed toward Balsfjord to identify which channel is most important. Thereafter I look at the shallow water constituents in Tromsøysund and finish off the chapter by looking at high frequency oscillations in Tromsøysund and Rystraumen.

6.1 Amplitudes and phases

The M2 tide

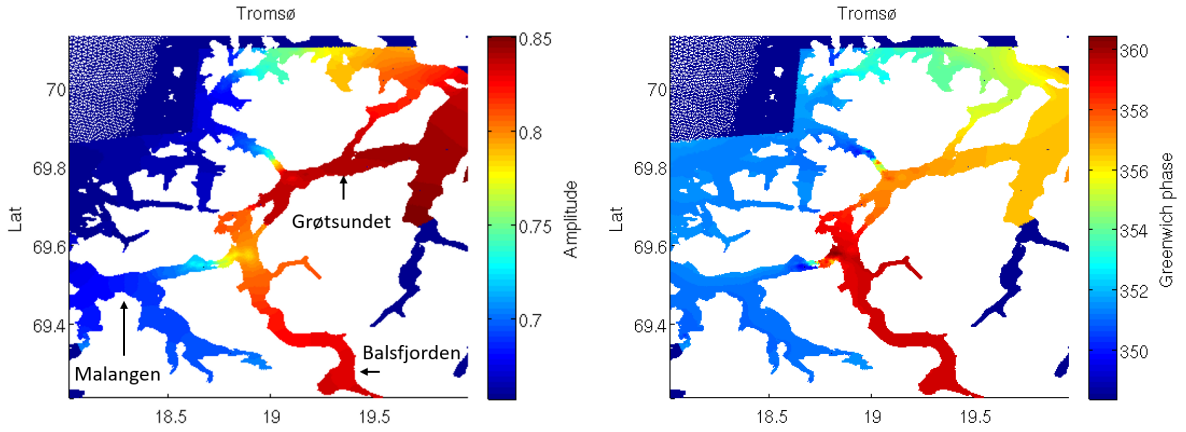

(a) Amplitude

(b) Phase

Figure 6.1: *The amplitude is given in meters, the phase in GMT degrees, and the domain in latitude (y-axis) and longitude (x-axis). The interruptions of the harmonic analysis on the sides and on top of the figures is deliberate. (less computational cost)*

Figure 6.1a shows a spatial picture of the M2 amplitude and phase. As the observations suggested, the southern side of Tromsøysundet and Sandnessundet have slightly smaller amplitudes than on the Grøtsundet side. The amplitude near the mouth of Balsfjorden is roughly $5cm$ smaller that elsewhere in the inner fjord system. Balsfjorden amplitudes

are about $10cm$ larger than in Malangen, with a transition zone near both sides of Rystraumen. Balsfjorden lags Malangen by about 10° (20 minutes). The Balsfjorden phase lag slightly behind Grøtsundet - the difference is just roughly 1° (Figure 6.1b). In short, the figures show that Balsfjorden harmonic constants are closely related to Grøtsundet and not similar to Malangen.

The S2 tide

Figure 6.2a shows that the S2 sea surface amplitude behaves similarly to the M2 tide. It has a local minimum at the mouth of Balsfjorden. The TPXO S2 tide in Balsfjorden is in phase with Grøtsundet and lag Malangen by 20° (about 40 minutes).

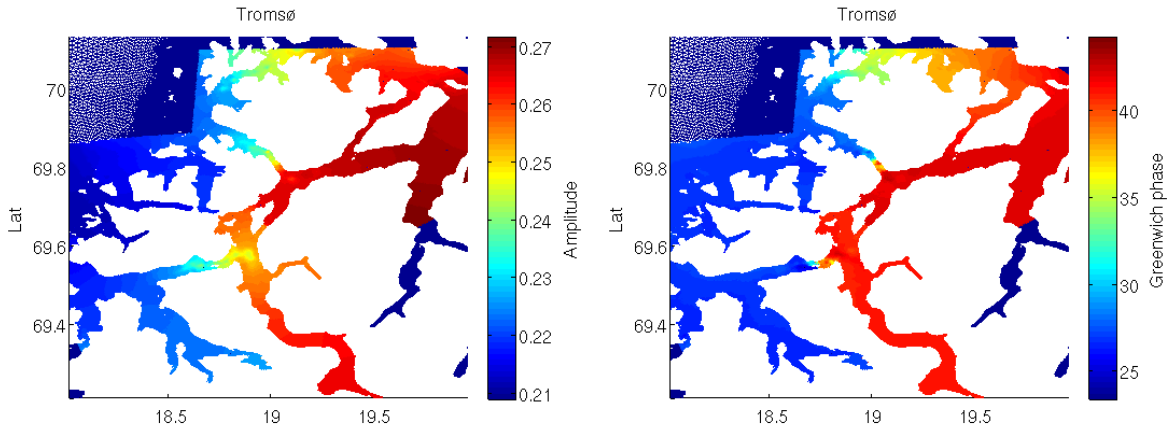

(a) Amplitude (b) Phase

Figure 6.2: *S2 constituent*

These large scale features of the tide agree well with a kelvin wave propagating northward along the coast, as one should expect, but also show small scale features such as the "dip" in amplitude near the mouth of Balsfjorden. Small scale variations are also visible near the constrictions.

Close look at the constrictions

Amplitude: The along channel difference between Grøtsundet and Balsfjorden is bigger in Tromsøysundet than in Sandnessundet ($-6cm$ vs $-3cm$). The difference across Rystraumen is $8cm$. Notice the amplitude (and phase) deviations shaped in circular patches close to constrictions, for example the blue patch indicated by "1" in Tromsøysundet (Figure 6.3b, upper panel).
Greenwich phase: The along strait M2 phase difference in Rya is about 10°, and 2° in Tromsøysundet/Sandnessundet. The phase change less across Tromsøysundet and Sandnessund than over Rya, (just roughly 1°). The S2 tide south of the Tromsøysund and Sandnessund constrictions lag Grøtsundet slightly. Two patches of dark colour in Tromsøysundet (delayed tide) on the northern side of the constriction coincide with an area I will soon introduce as the "TRdipole" where two eddies reside on northerly flow.

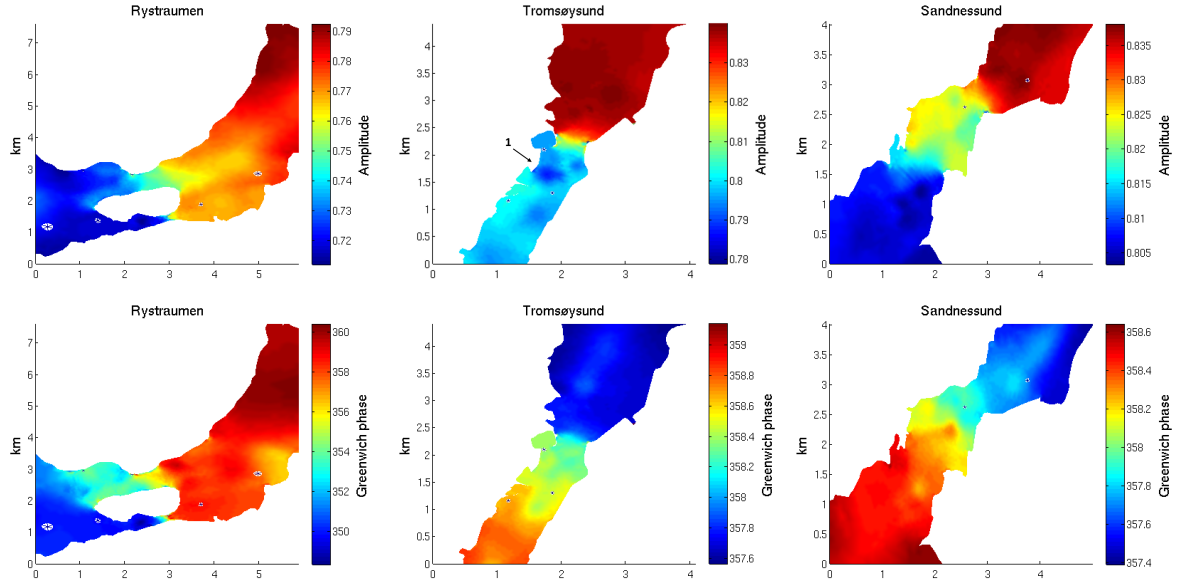

(a) Rystraumen (b) Tromsøysund (c) Sandnessund

Figure 6.3: *M2 sea surface harmonic constants. Amplitudes (upper panel) are in meters, phases (lower panel) are in degrees relative to GMT*

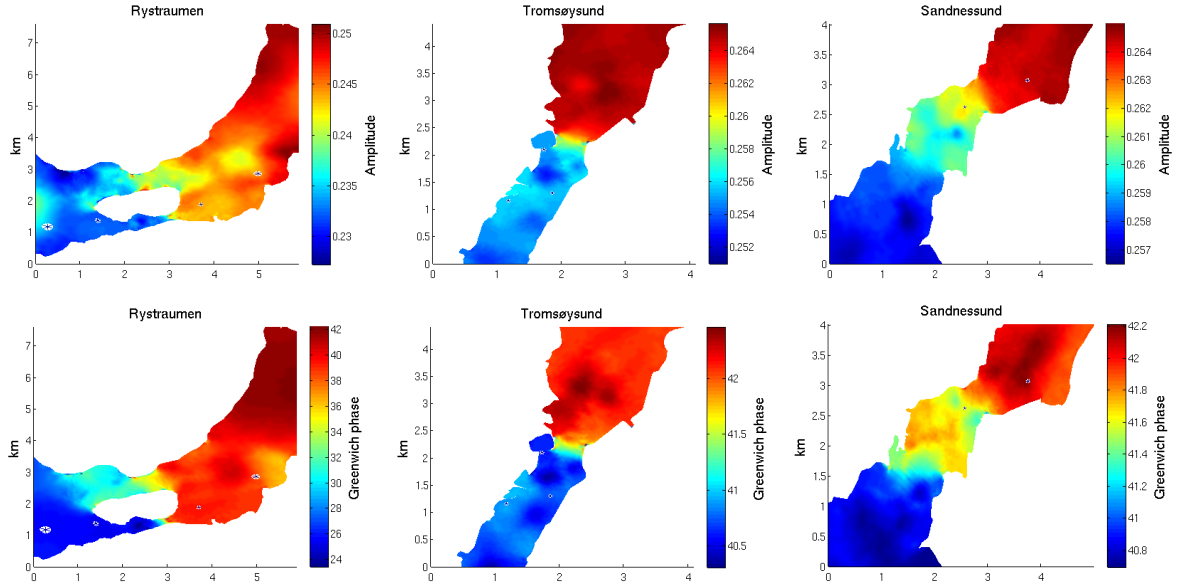

(a) Rystraumen (b) Tromsøysund (c) Sandnessund

Figure 6.4: *Same as in Figure 6.3, but for the S2 tide*

The small-scale features where amplitudes can change by one centimetre in circular patches over short distances near the straits (Figure 6.3 and 6.4) can not be forced by the M2 or S2 waves themselves. I therefore think that such significant local differences are evidence of the importance of small-scale dynamics.

6.2 Volume transport toward Balsfjorden

I want to show where the water forcing the tidal sea surface elevation in Balsfjorden originate, before going into the tidal stream and its small scale features. Figure 6.5 shows the volume transport directed toward Balsfjorden through the Tromsøysundet, Sandnessundet, Rystraumen, and Litjestraumen constrictions as well as their net transport. The Rystraumen transport dominate.

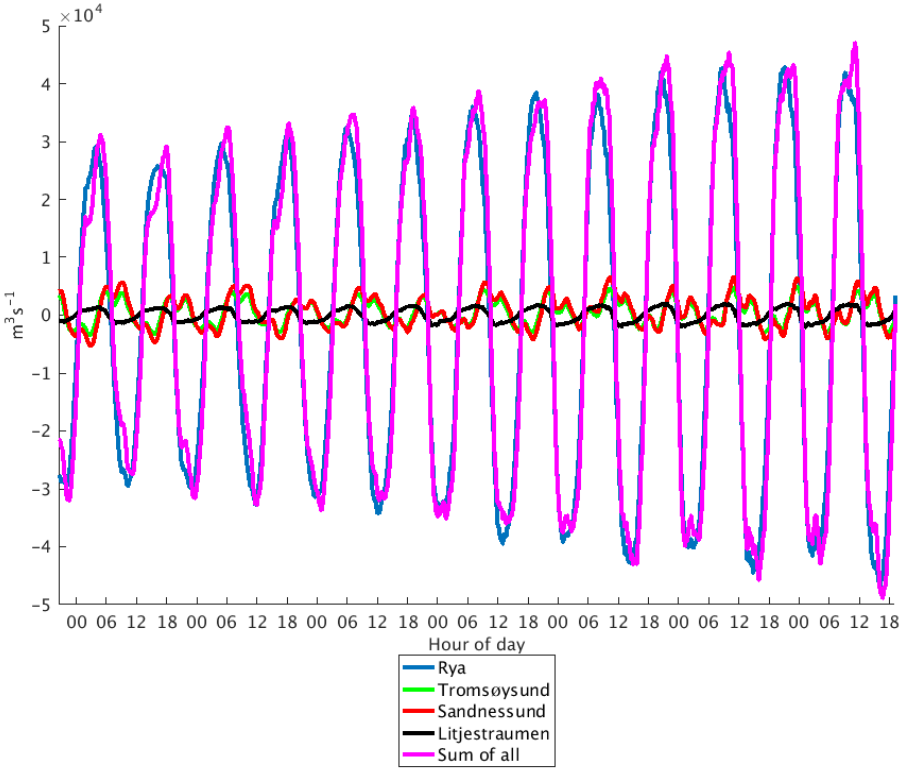

Figure 6.5: *Volume transport through the constrictions toward Balsfjorden. Negative values is a transport away (lowering the sea surface), positive values are into the fjord (rising the sea surface). The Tromsøysundet and Sandnessundet curves are difficult to distinguish since they are very similar.*

The sea surface variation in Balsfjorden should look more like that in Malangen than in Balsfjorden since the sea surface variation in Balsfjorden is dominated by Rystraumen (the southern wave). The most notable feature of the flow in Tromsøysundet and Sandnessundet is therefore not to increase the Balsfjorden tidal range, but to respond to the sea surface difference forced by the northern wave (Grøtsundet) and the southern wave (Malangen/Balsfjorden). The Tromsøysundet and Sandnessundet streams are in a sense not due to tidal waves propagating through a strait, but to the interaction of waves with *different* characteristics, as I will investigate further in the next section.

6.3 Shallow water tidal streams

The sea surface variability is dominated by the linear tides at both sides of the constrictions, but the stream in Tromsøysund and Sandnessund is nevertheless significantly influenced by shallow water harmonics. FVCOM reproduced the feature as shown in Chapter 5. FVCOM results should therefore be suitable for an in-depth study of the phenomena.

Figure 6.6 show UTide estimates of the tidal sea surface elevation at TR1 and TRdin1 plotted together. Panel 6.6a shows the sea surface elevation forced by the M2, S2, N2, K1, O1 and Q1 constituents. The maximum along channel sea surface gradient should, according to the figure, occur at high tide if non-linear harmonics are negligible. Figure 6.6b reconstruct the sea surface north and south of the constriction with all harmonics that UTide included in the analysis. The gradient is altered and shifted in time. Seemingly unimportant shallow water constituents - if one consider them at each side separately - are essential for the flow since they shift the maximum sea surface difference between TRdin1 and TR1 earlier than if shallow water effects had been negligible, and introduce several new local maxima during each tidal cycle.

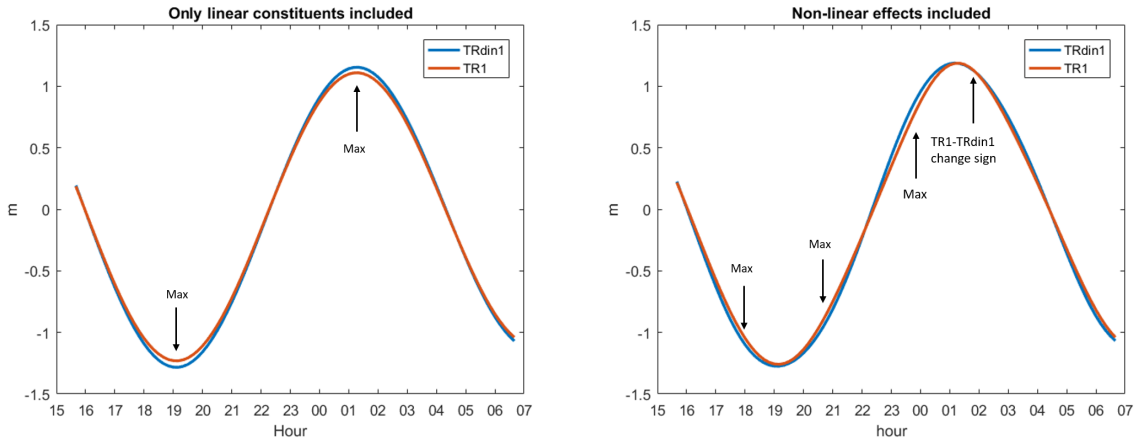

(a) Only linear constituents

(b) Including the non-linear constituents

Figure 6.6: *The tidal sea surface elevation at Tromsøysund stations TR1 and TRdin1 extracted by UTide. The time interval correspond to the first cycle in Figure 6.7. The left panel shows the sea surfaces forced solely by the linear tides, the right hand panel shows the tidal sea surface forced by all constituents. The maximum (absolute values) differences are shifted in time by the shallow water harmonics. The figures are made from FVCOM data.*

Figure 6.7a show the difference in sea surface elevation between station TR1 and TRdin1 when only including the linear harmonics. The difference is dominated by semi diurnal frequencies. Panel 6.7b show the same time-interval as Panel 6.7a and it include all higher harmonics of the sea surface (blue line). I plotted the v-component at TR1 (red line) to visualize how the stream in Tromsøysund responds to the difference in sea surface elevation. The v-component at TR1 and sea surface difference across the strait correlate well. The sea surface difference explains 75% of the variance of the current ($r^2 \approx 0.75$).

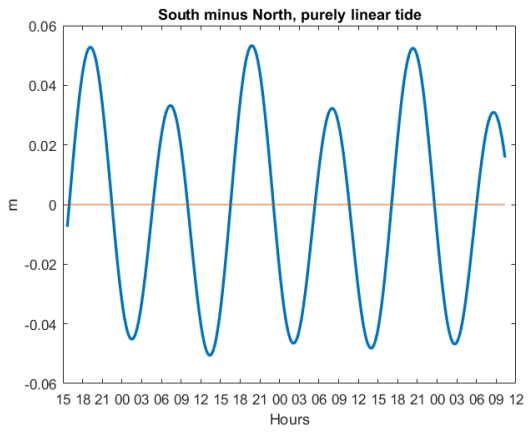

(a) *Only linear constituents.*

(b) Non-linear constituents and TR1 v-component

Figure 6.7: *Sea surface elevation at TR1 minus the elevation at TRdin1 (blue line), in panel (b) the northerly component of the velocity field at TR1 is also shown (red curve).*

Table 6.1 show the potential energy distribution for the difference in along the constriction including both the linear and non-linear constituents. The M2 constituent and its over- and compound tides dominate. The 2MS6 compound tide, for example, contribute about 3 times as much potential energy as the S2 constituent.

Table 6.1: *Potential energy associated with the sea surface elevation difference across the constriction, given in % of the total tidal wave energy*

Linear constituents					**Non-linear constituents**					
M2	S2	N2	K1	O1	M4	M6	M8	2MS6	2MN6	MS4
54.98	3.91	3.84	4.43	0.04	1.17	12.07	0.43	11.21	2.22	0.33

I believe that the different shape of the tidal waves on the northern and southern side of the constriction can be understood in terms of the fjord-system geometry. Consider two initially identical waves which separate and propagate in regions with different geometries. They do not experience the same forcing, are distorted differently, and will therefore develop different shapes with time due to the shallow water distortion. The waves near Tromsø therefore have different shapes by the time they reach the constriction even though they are related to the same Kelvin wave propagating northward. This does not mean that higher harmonics must be very important for the sea surface elevation at each side, respectively. In fact, the linear tides dominate on both sides of the Tromsøysund constriction. But the small differences in their shapes is significant for the along channel pressure gradient, as shown herein, and we therefore see the strange tidal streams in Tromsøysundet and Sandnessundet.

6.4 High frequency oscillations

The observed stream at TRdin1 is strongest in conjunction with high frequency oscillations occurring on northerly flow. FVCOM results look similar to the observed stream, see Figure 6.8. These oscillations are too frequent to be explained with shallow water harmonics, and can not relate to the large scale distortion of the tide.

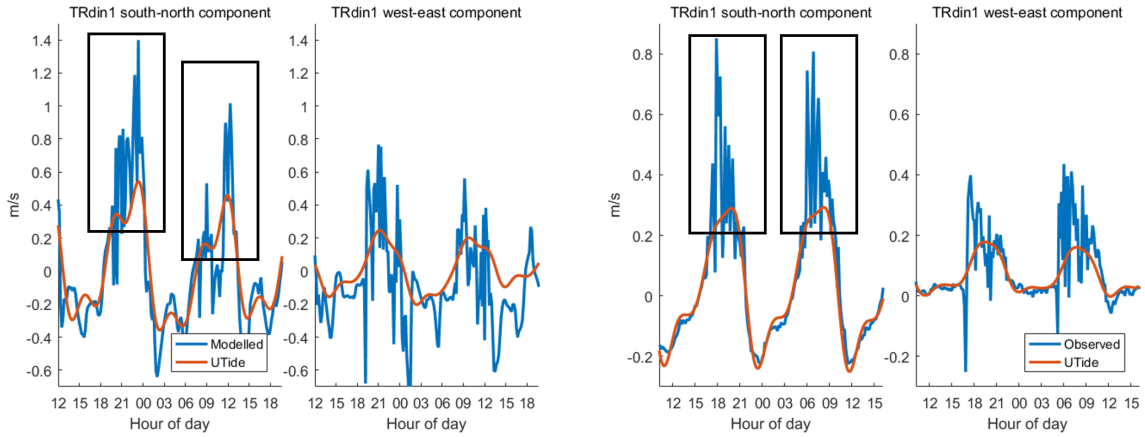

(a) Modelled (b) Observed

Figure 6.8: *Current components at TRdin1 near spring tide. Note that the speed is scaled differently at each figure. Black boxes indicate the high frequency maxima. The red curve is the tidal current determined by UTide. The blue curve is the (a) modelled or (b) observed current components.*

FVCOM create a strikingly similar phenomenon near Rystraumen (see Figure 6.9), which suggests that these oscillations are not unique to northern Tromsøysund.

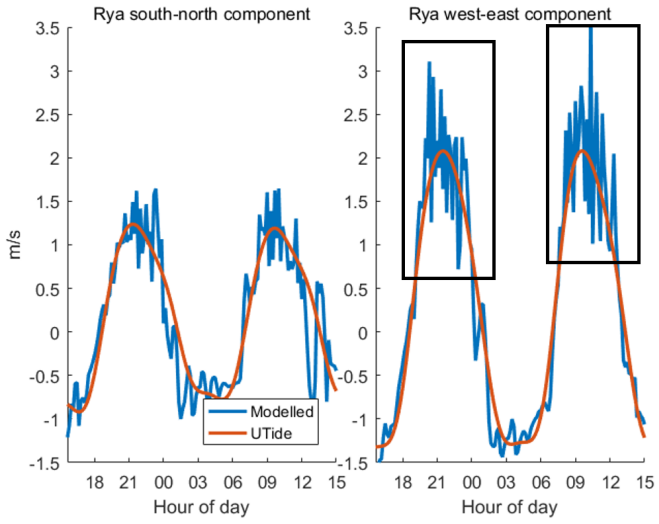

Figure 6.9: *Modelled current components in Rystraumen about* 1*km downstream from the constriction. Black boxes indicate the high frequency maxima.*

Figure 6.10 shows the maximum modelled stream at each cell near the channels after the model was spun up. I will show that the high frequency maxima on the northern side of Tromsøysundet and on the eastern side of Rystraumen are related to dipoles which form at the constriction by having a closer look at the flow in the straits. I will show the average flow in the domain near the channels, I thereafter look at how snapshots of the flow deviate from the average during flood/ebb. I will begin with northern Tromsøysund since the observations there were very similar to the model results. Eastern Rystraumen is also interesting since that is where the strongest streams in the domain occur, so I will have a look at the stream there as well. I will not consider Sandnessund or southern Tromsøysund in depth to keep the thesis short(er).
Figure 6.10b shows that the stream roughly 1 km downstream of the constriction is about $0.5m/s$ stronger than within the constriction. I will (in Section 6.4.2) show that the speed at that location regularly exceeds the speed at the constriction, which is odd given that it is located far away from the constricion (where the channel cross section is smallest).

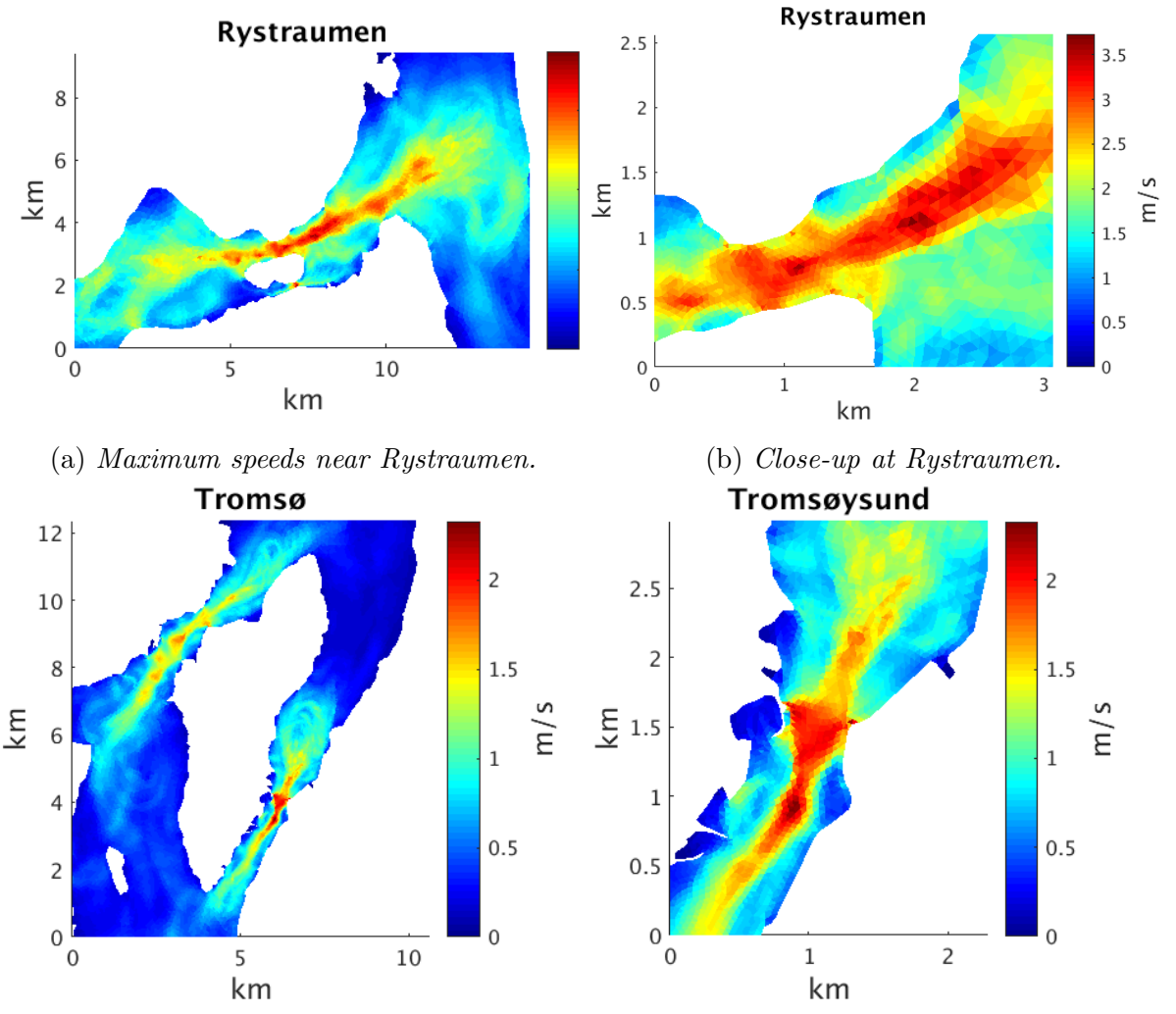

(a) *Maximum speeds near Rystraumen.*

(b) *Close-up at Rystraumen.*

(c) *Maximum speeds near Tromsø.*

(d) *Maximum speeds in Tromsøysund*

Figure 6.10: *Maximum streams in each cell after the model reached stable oscillations. (N.b. The colours tend to be poorly resolved in printed versions of the thesis.)*

6.4.1 Tromsøysund

Averaged stream

The velocity fields in Figure 6.11a and 6.11b represent an average of the tidal stream for when the tide flow toward- and out of Balsfjorden through the centre of the Tromsøysundet constriction (see Appendix B for a description of the averaging procedure). The colour limits in Figure 6.11a and Figure 6.11b are scaled to each figure separately. The figures give a good representation of the location of the jets and the dominating eddies.

Flow away from Balsfjord:
Figure 6.11b: Two eddies are located about $1-2km$ downstream, on the northern side of the constriction. I will refer to this pair as the "TRdipole". The strongest averaged stream on northerly flow is at the constriction. The jet extend roughly $1km$ downstream.

Flow toward Balsfjord:
Figure 6.11a: Two eddies, the harbour and eastern eddies, stay close to the constriction when the flow is directed toward Balsfjord. The harbour eddy force a flow close to land moving opposite to the stream in the channel. The averaged stream in the middle of the channel, close to the harbour eddy, is comparable to the constriction speed, but the maximum stream is near the eddy (see Figure 6.10d).

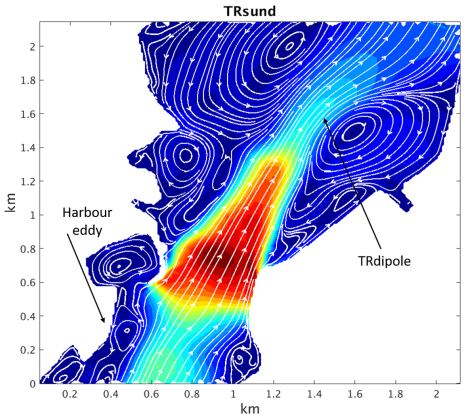

(a) *Flowing away from Balsfjorden stream*

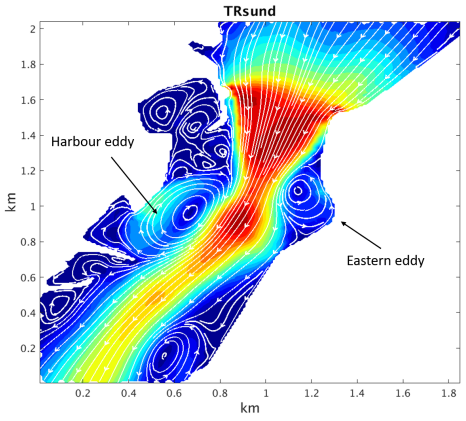

(b) *Mean flow toward Balsfjorden*

Figure 6.11: *Estimate of typical northerly and southerly stream*

Figure 6.11a is not a mirror image of 6.11b. The northern side jet decrease in strength downstream, while the strongest averaged southerly flow occurs near the harbour eddy and at the constriction. The eddies on the southern side do not move downstream, they are seemingly trapped by the channel geometry. They create a strong current far downstream of the constriction as Figure 6.11b and 6.10d show. The flow on the northern side is not so steady, being very influenced by high-frequency oscillations on northerly flow - see Figure 6.8. The remainder of this thesis will study the dipoles forcing such maxima.

Transient spatial patterns

Figure 6.12 show four situations where the current is unusually strong at station TRdin1 (the star). There is one eddy on either side of TRdin1 (forming a dipole) at these maxima. Note that dipoles can create higher speeds than at the constriction (Figure 6.12b).

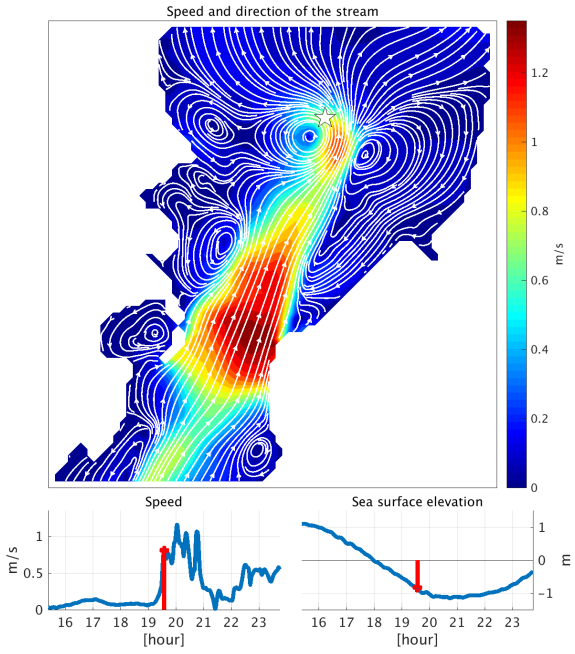

(a) *First maxima at TRdin1.*

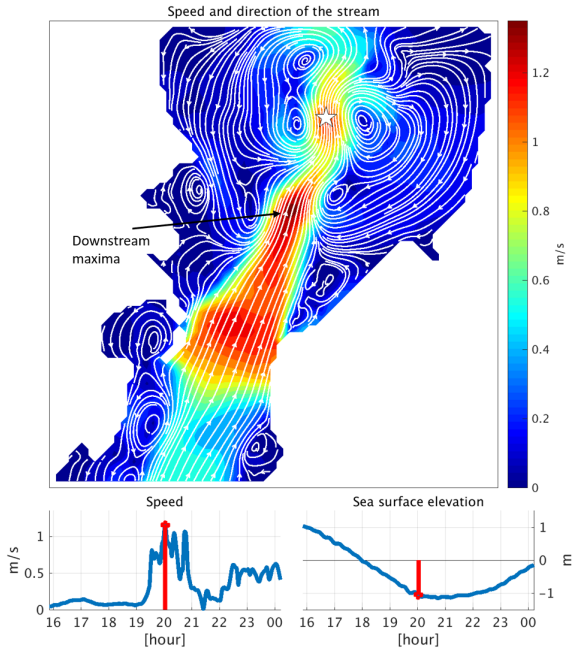

(b) *Second maxima at TRdin1.*

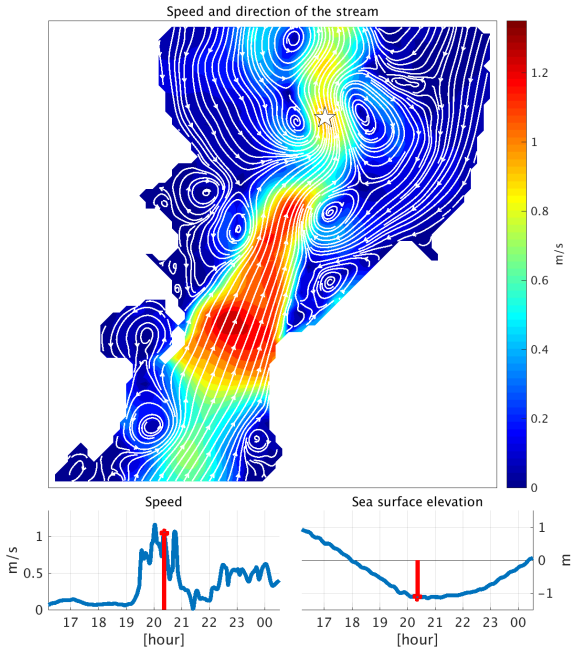

(c) *Third maxima at TRdin1.*

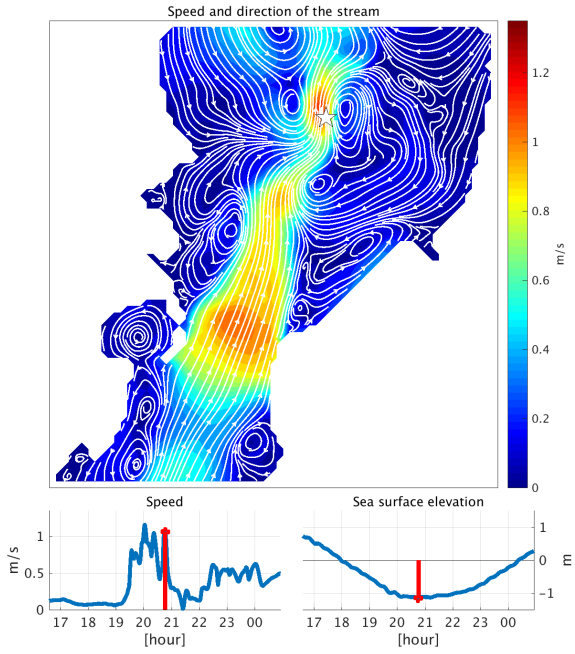

(d) *Fourth maxima at TRdin1.*

Figure 6.12: *Upper panel: Stream speed and direction. TRdin1 is indicated by a star. Bottom panels: Transient evolution and instantaneous speed- and sea surface at TRdin1. The x-axis is time (hour of day).*

Figure 6.13 and 6.14 show the evolution prior to Figure 6.12d. The boxes indicate the areas I describe. Figure 6.13a show a small eddy close to the constriction on the left side of the channel. Most of the streamlines disperse downstream of the constriction and follow the side walls. The flow follow the walls at the right hand side too, but a eddy reside to the left of the wall. The two eddies have grown five minutes later, see Figure 6.13b.

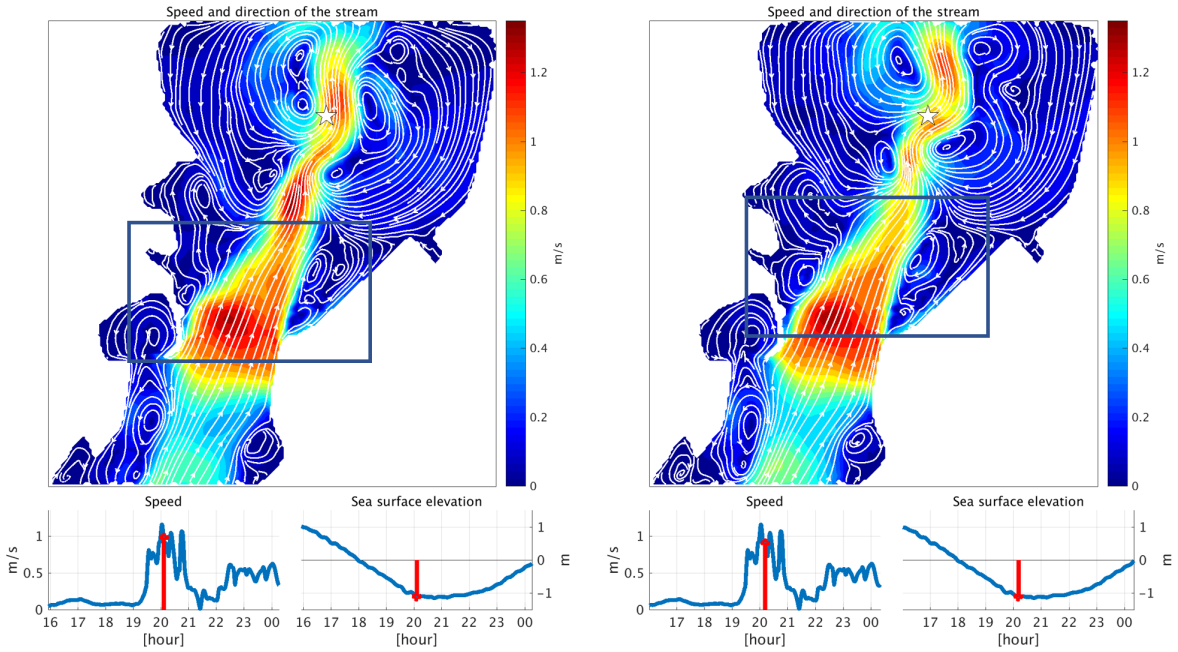

(a) *40min prior*

(b) *35 min prior*

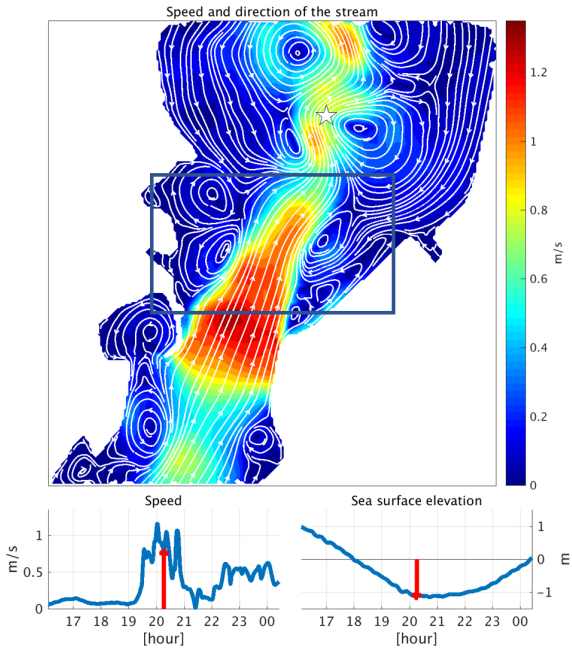

(c) *30min prior*

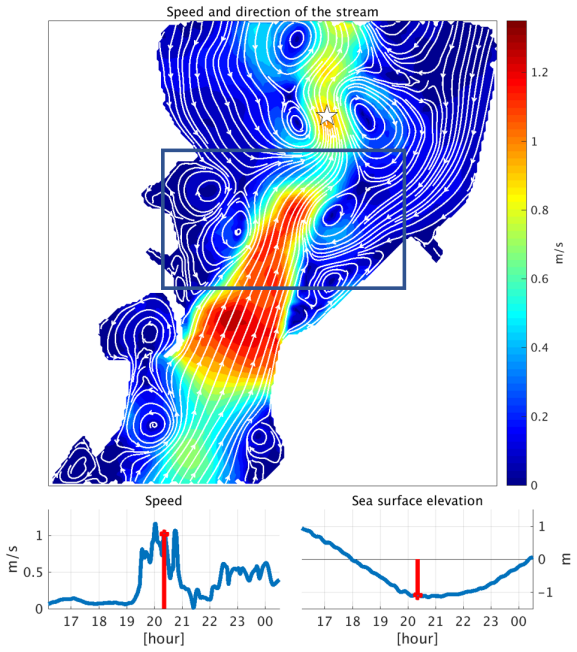

(d) *25min prior*

Figure 6.13: *Same layout as Figure 6.12. The boxes indicate areas I present in the text.*

The two eddies stay close to the constriction (Figure 6.13b, 6.13c) and expand. The jet extend downstream from the constriction to the dipole. Figure 6.13d show that the jet extend to an area which was weaker than the constriction stream 15 minutes earlier, but the speed is comparable now. Figure 6.14a and 6.14b show that the jet split in two, one near the constriction and one near the dipole as the dipole move downstream.

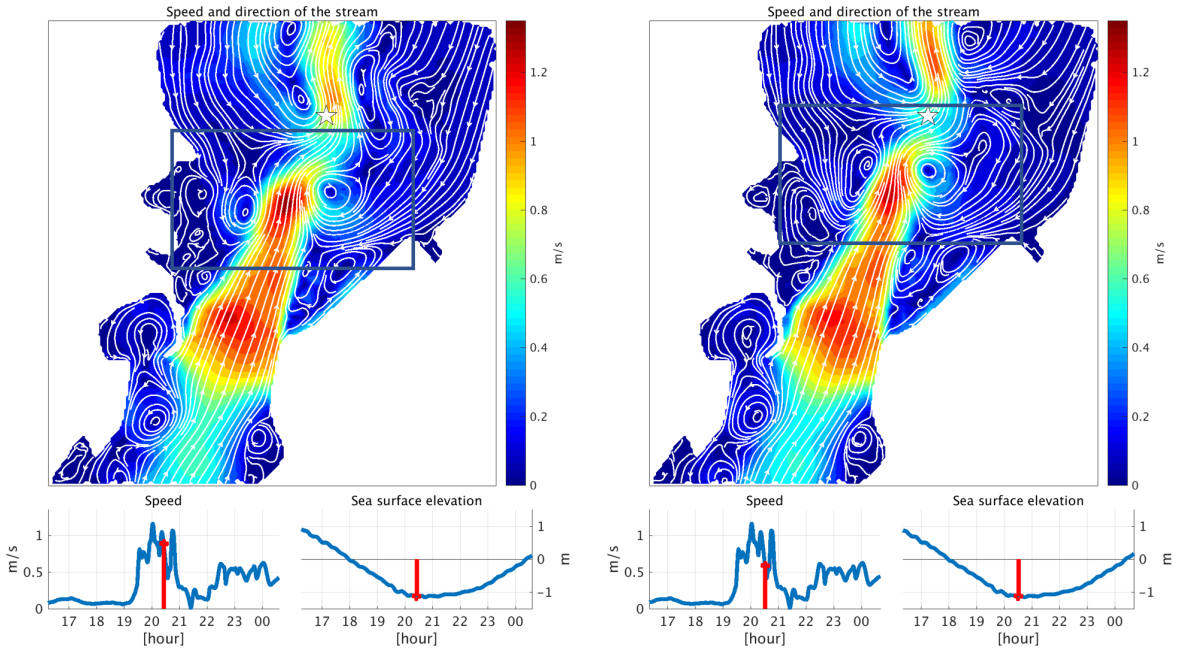

(a) *20min prior*

(b) *15min prior*

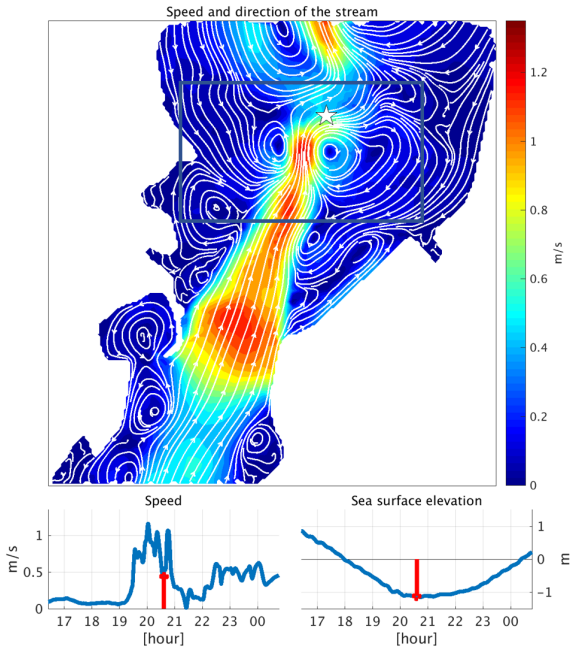

(c) *10min prior*

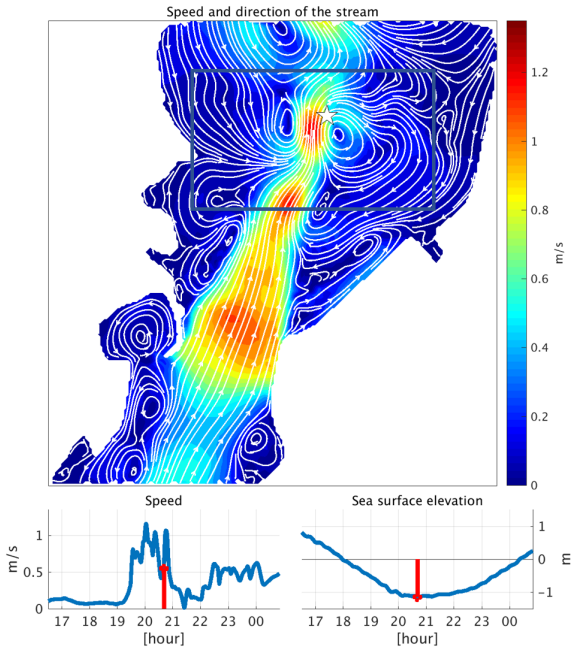

(d) *5min prior*

Figure 6.14: *Same layout as in Figure 6.13*

The dipole-jet remain in-between the eddies, in fact the only stream stronger than roughly $1m/s$ at Figure 6.15 is in between the eddies. The other patches with strong speeds have diminished. Figure 6.15 show the second-to strongest stream at TRdin1 during the tidal cycle.

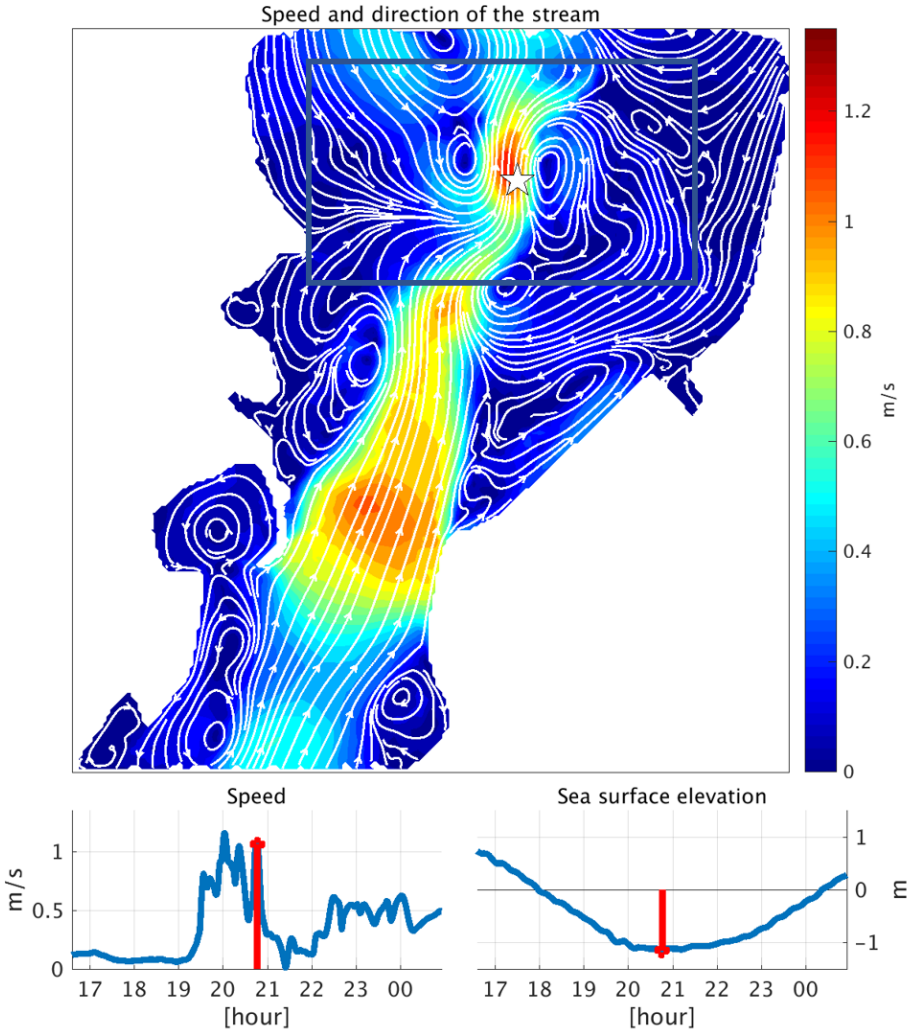

Figure 6.15: *The same layout as in Figure 6.13. At the maxima.*

Summarized; It took 35-40 minutes from two counter rotating eddies started to grow at the constriction until they forced the second-to-strongest current at TRdin1 during that tidal cycle. Figure 6.12 show that the other abnormally strong speeds at TRdin1 during this tidal cycle was forced by dipoles. Dipoles such as these occur frequently, and always originate at the constriction. Strong dipoles such as those I presented in this section occur every $20/30min$ north of the constriction during spring tide. They occur less frequently at neap tide, and with weaker extrema.

6.4.2 Rystraumen

This section show dipoles in Rystraumen causing high-frequency downstream velocity maxima, similar to the dipoles in Tromsøysund.

Averaged currents

Figure 6.16 show the average stream flowing in and out of Balsfjorden through Rystraumen made using the procedure outlined in Appendix B. The flowing in/out stream in Rystraumen is so to say in phase with flood and ebb, so I will refer to them as ebb and flood currents.

Ebb: The jet is the area not shaded in blue colours. Following that definition, one can say that the core of the ebb jet (red shading) is confined to the channel adjacent to Ryøya. An eddy on the eastern side of the constriction - the Balsnes eddy, between Ryøya and Balsnes - force the flow *away* from Little Rya along the shore toward Balsnes.

Flood: The jet downstream of the Hella headland is narrower on flood than ebb, see Figure 6.16b. The jet extend far downstream from the constriction, and is strongest at the constriction. The strength decreases toward Balsfjord, most likely since the constriction is the narrowest point of the channel. Eddies emerge downstream of obstacles close to the jet. One can, for example, see two eddies directly downstream of Rya - the Vikran and Skavberg eddies (see Figure 6.16 and 6.17). The Skavberg eddy is located just downstream of Hella, the headland in Rya. It is barely visible in Figure 6.16b, but very easy to spot in Figure 6.17. The Vikran eddy is located where the Balsnes eddy was during ebb, but is slightly deformed due to the Little Rya related flow.

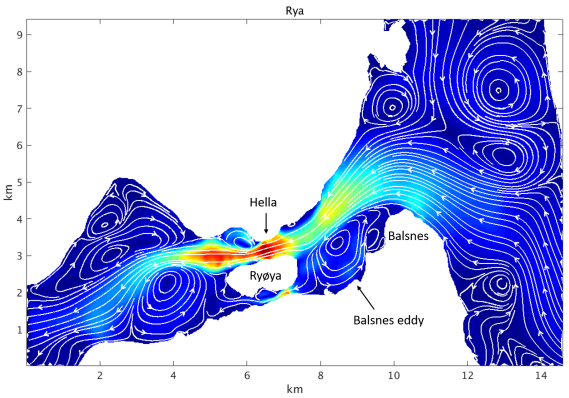

(a) Ebb currents

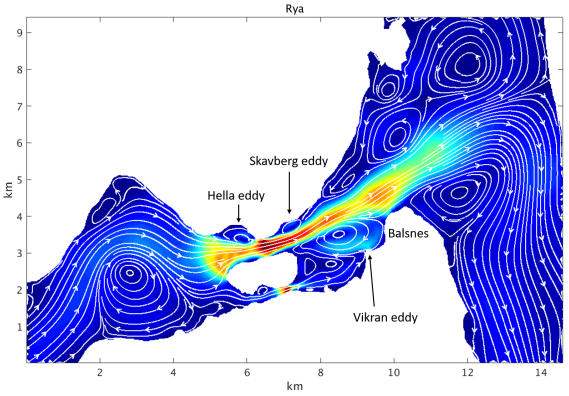

(b) Flood currents

Figure 6.16: *Mean currents direction (streamline) and magnitude during flood and ebb. The colour scale is the same at both figures, blue is weak red is strong stream.*

The large scale averaged stream in Rystraumen thus show that the eastern side of the channel distinguish itself from the western by having a more pronounced downstream extension. A closer look at the constriction reveal more details about the Skavberg and Vikran eddies.

Close to eastern Rystraumen

The Skavberg and Vikran eddies form downstream of Hella and Ryøya. They are not stationary but move around and change the velocity field. The average give a good indication on where to expect to find eddies occurring frequently. Flow separation occur close to the constriction, as indicated on Figure 6.17. The Vikran eddy shown in the figure has a long arm (squash racket shaped streamline) stretching toward Ryøya. The arm is not the "steady state" shape of the Vikran eddy, but a region where eddies formed downstream of Ryøya propagate downstream and merge with it, as I will show later on.

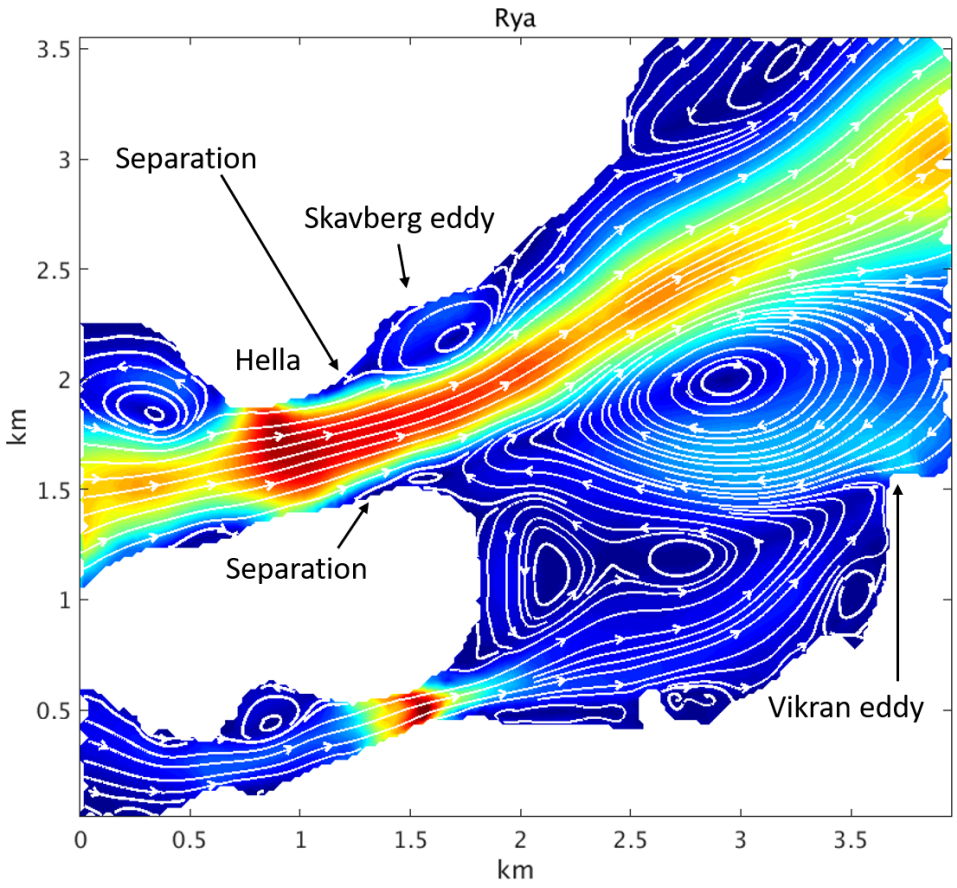

Figure 6.17: *Close-up at flood currents in eastern Rya.*

Transient spatial flow patterns

Figure 6.10b show that the strongest modelled currents in the Tromsø region occur east of Rystraumen. The stream can exceed $3.7m/s$, almost $0.5m/s$ faster than the peak current at places close to the constriction at some locations downstream. Strong currents downstream of the constriction are common in the area east of Rystraumen - not just of specific cells - suggesting that the feature is not due to model noise. The strongest maxima near Rystraumen occur about $1km$ downstream (see Figure 6.10b). Comparably strong currents to those at the constriction occur up to $5km$ downstream on the eastern side near Balsnes.

Figure 6.18b show the tidal stream at two locations in Rya, one at the centre of the constriction and one at the stream-maxima location. The flow oscillates quite smoothly at the constriction, but is noisier downstream. Higher harmonics of the stream are not important in Rystraumen, in contrast to Tromsøysundet. The tidal stream at the maximum velocity cell is slightly weaker than at the centre (as Figure 6.17, p. 50 indicates). The high frequency oscillations regularly exceed the centre stream - in fact Figure 6.10 (p. 43) suggest that the strongest streams occur downstream of the constriction, Figure 6.18b suggest that it occur frequently. Figure 6.18 shows data from two locations, but the statement is true for the spatial flow pattern as I will show later.

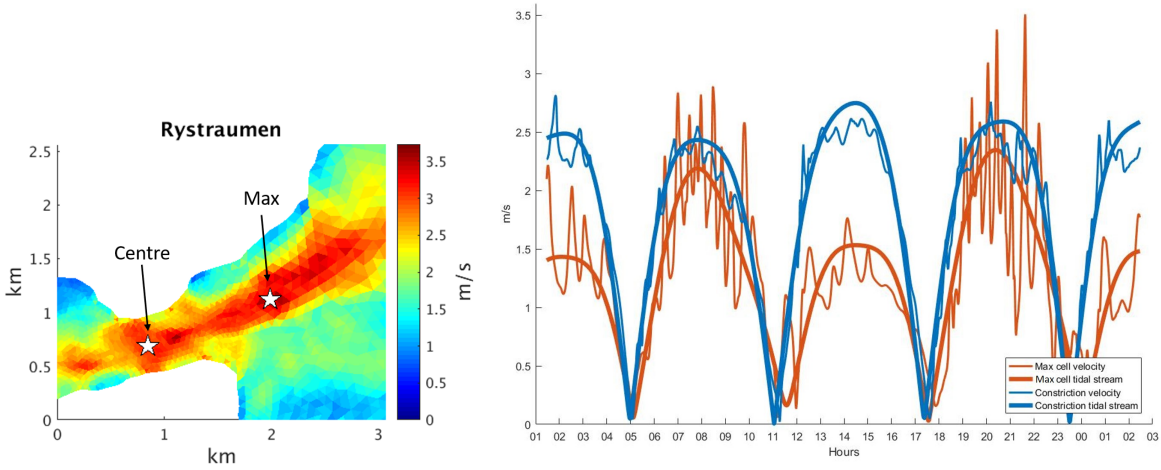

(a) *Locations*

(b) *Instantaneous tidal stream at the "Centre" (blue color) and "Max" (orange) cell. The speed at the maxima cell exceed the centre cell during rising tide.*

Figure 6.18: *The tidal stream speed in Rystraumen during spring tide for two locations - the centre and max cells (see left panel). The thick lines is the tidal stream (determined with UTide), the thin lines are the instantaneous velocities*

The figures I will show on the next pages shows the flow at some specific time steps. The flow often looks like the averaged flood stream (Figure 6.16a, p. 49). The Vikran eddy is located downstream of Ryøya, and the Skavberg eddy is often located directly downstream of Hella. The flow deviate from the average state in a systematic manner. Velocity extrema downstream of Rya, for example, occurs in conjunction with dipoles forming near the constriction, as they did in Tromsøysund. Such dipoles consists of the Skavberg eddy and an eddy formed at the tip of Ryøya - the Ryøya eddy. Figure 6.19 and 6.20 shows the evolution of an event where such dipoles created strong currents at the maxima cell (indicated by a star, same as the maxima-cell in Figure 6.18a). The figures in Tromsøysund were spaced five minutes apart, but these figures are separated in intervals of three minutes. I have made boxes in Figure 6.19 and 6.20 to highlight where the features I discuss in the text occur.

Figure 6.19a: The Skavberg eddy is downstream of Hella and the stream follows the tip of Ryøya toward Balsfjorden. The stream is strongest at the constriction. **Figure 6.19b:** The jet extends further downstream and the Hella eddy has grown in size. A small eddy has formed at the tip of Ryøya. **Figure 6.19c:** The eddies have grown bigger, and the jet continue to expand downstream. Both eddies have "arms" stretching toward the constriction. **Figure 6.19d:** The eddies are bigger and the jet extend even further downstream. This is the time-step with weakest stream at the star-cell.

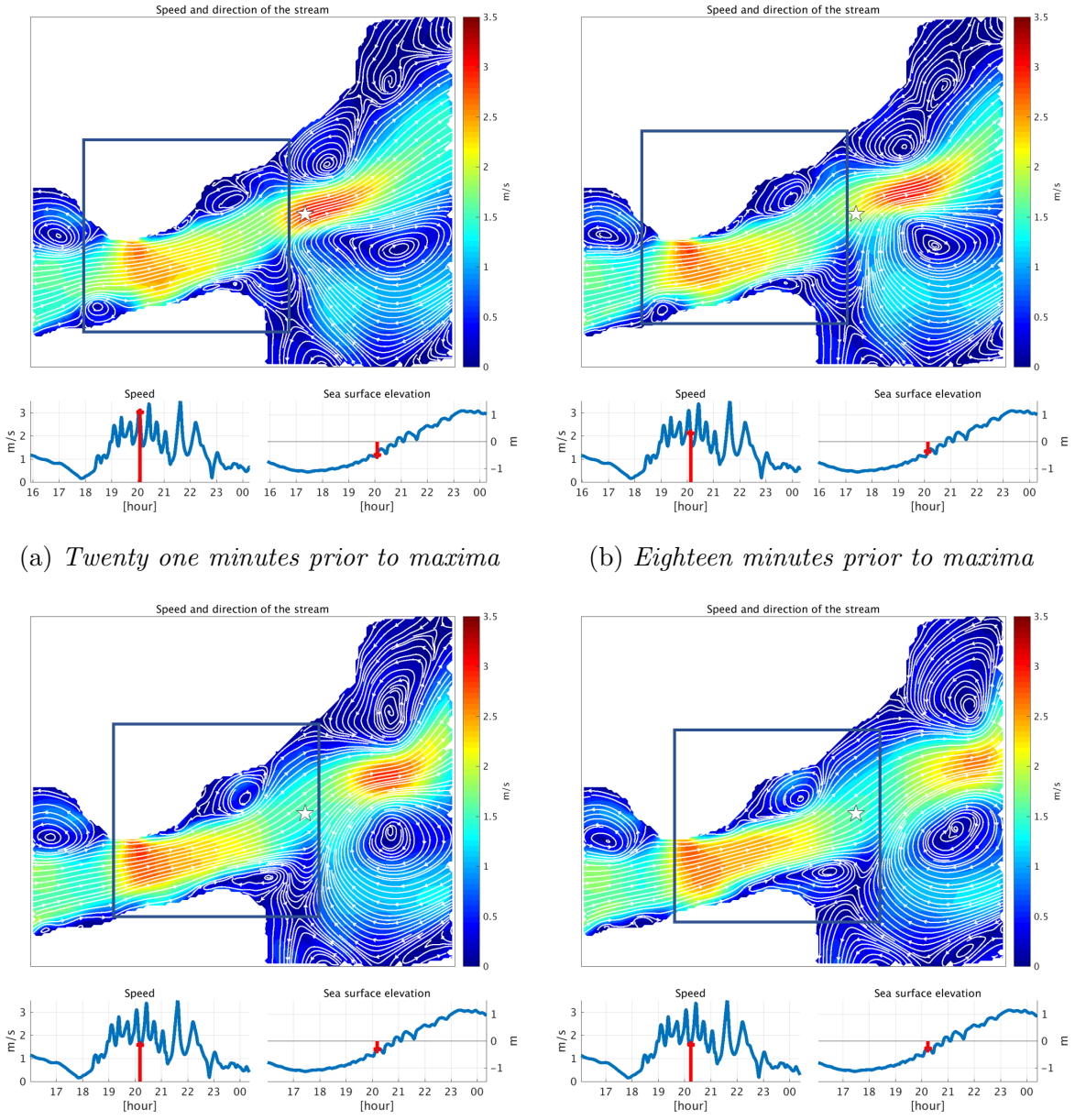

(a) *Twenty one minutes prior to maxima*

(b) *Eighteen minutes prior to maxima*

(c) *Fifteen minutes prior to maxima*

(d) *Twelve minutes prior to maxima*

Figure 6.19: *Same layout as in Figure 6.12. These figures do not represent the same time interval or tidal cycle as the dipoles in Tromsøysund.*

Figure 6.20a: The jet splits in half - one part at the constriction, and one near the eddies. **Figure 6.20b:** The eddies and their jet move downstream. They lose the arms stretching to the constriction, the eddies are now circular. The strongest stream in the domain is between the eddies for the first time since the eddies started to grow. **Figure 6.20c:** Some of the streamlines flushing out of the constriction follow land and trail the dipole, seemingly pushing it away. **Figure 6.20d:** The stream between the eddies is stronger than it was at the constriction during the build-up of the dipole. Time series in the lower left panel show that such strong streams occur frequently at the location in conjunction with sea surface depressions, see the lower right panel and Figure 6.21.

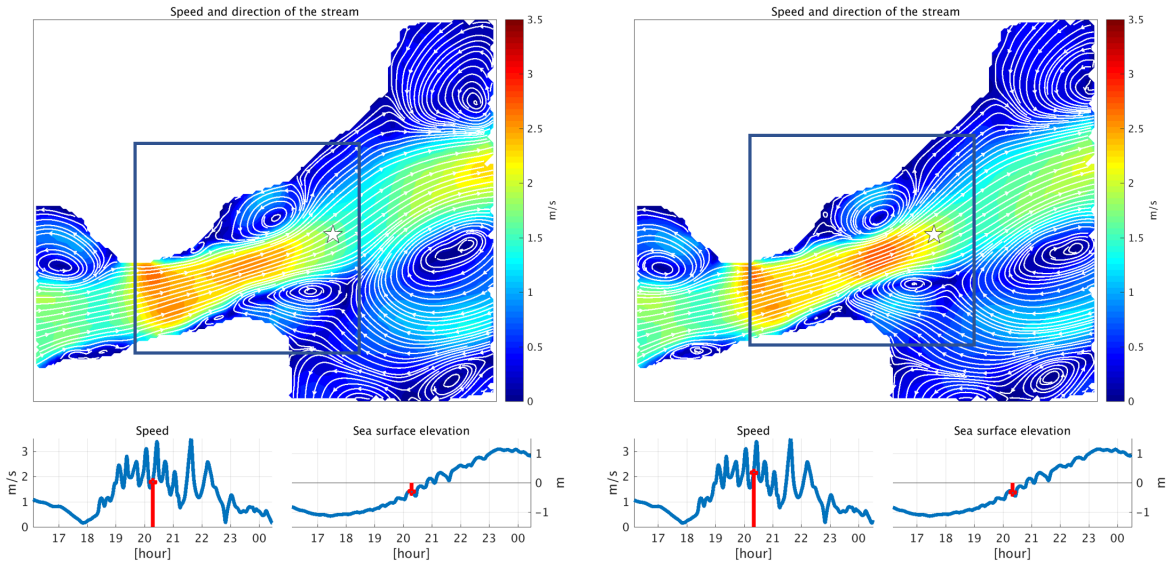

(a) *Nine minutes prior to maxima*

(b) *Six minutes prior to maxima*

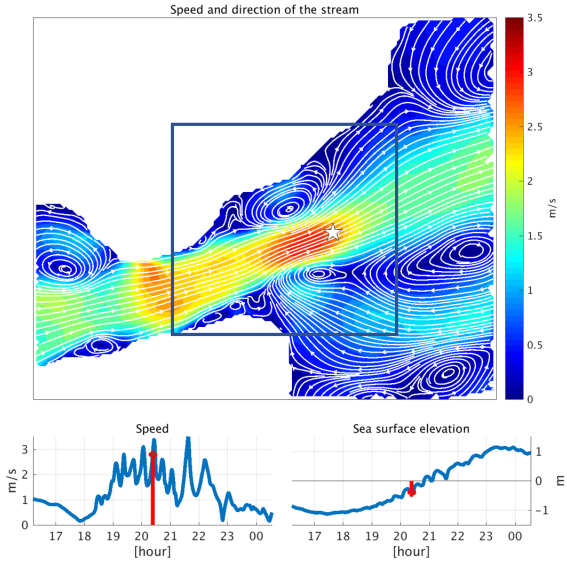

(c) *Three minutes prior to maxima*

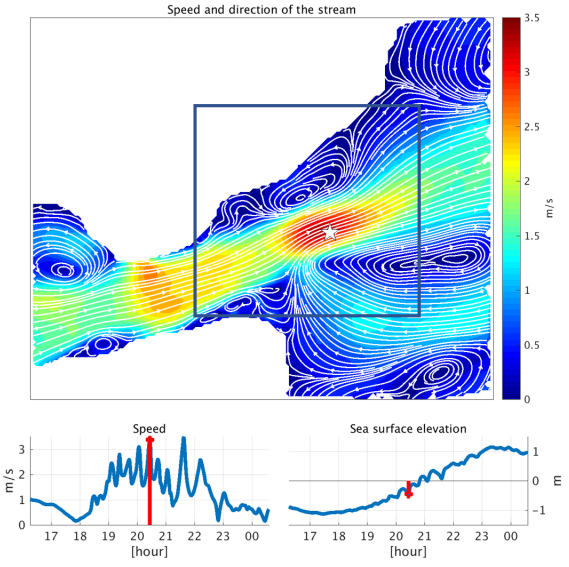

(d) *Maxima*

Figure 6.20: *Same as in Figure 6.19*

The evolution of the dipoles I just presented is typical for eastern Rystraumen, just as they were for northern Tromsøysund. Figure 6.21 shows four other examples. The figures do not look identical, but each and every one of them show that the Skavberg eddy has moved downstream and that the stream near the constriction expand (weak/no headland eddies). The Vikran eddy has merged with the Ryøya eddy in some of the figures, but the maxima are nevertheless clearly visible near a region where they coalesce.

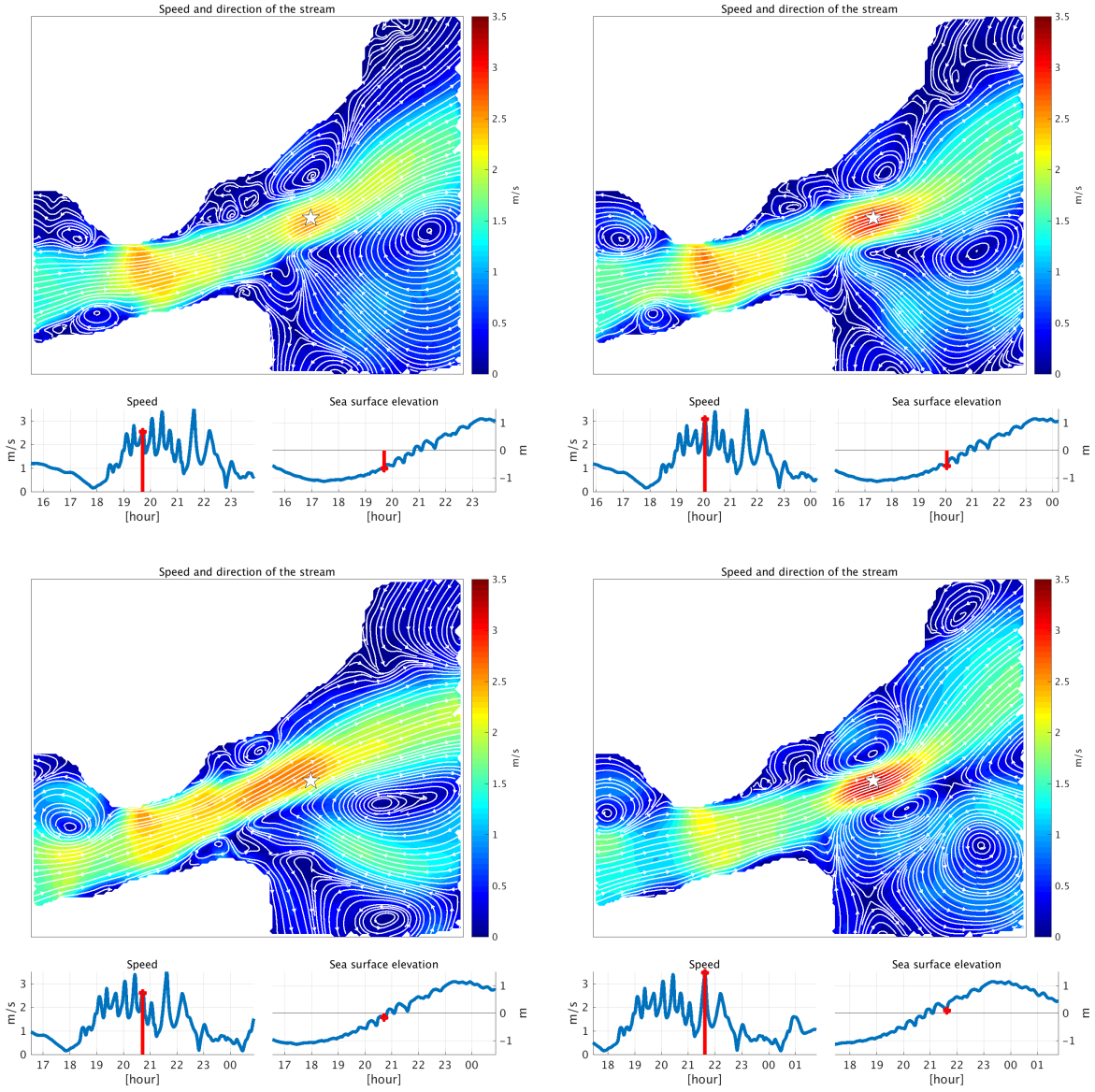

Figure 6.21: *Examples of velocity maxima. Same layout as in Figure 6.19*

The stream and eddies can of course be modified by bathymetry effects. In the next section I check if extrema such as these can occur near a strait without variation in bathymetry downstream of the constriction.

6.5 Idealized strait

Results showing strong streams downstream of Rystraumen and Tromsøysund such as those I have presented can perhaps be related to geometry of the downstream region (e.g. shallow bathymetry in the downstream area). Studying an idealized strait will give a clearer view of whether one should expect to find the highest speeds far downstream of a constriction if the domain has a flat bottom and no side walls downstream of it. The idealized strait I used, and its entire domain, is shown in Figure 6.22. Its bathymetry is a flat, 100m deep sea floor in the entire domain except near solid boundaries in the channel where it shoals abruptly. The domain is 500km long in the y-direction and 250km wide in the x-direction. Outer boundaries are forced by a M2 tide with 0.5m amplitude.

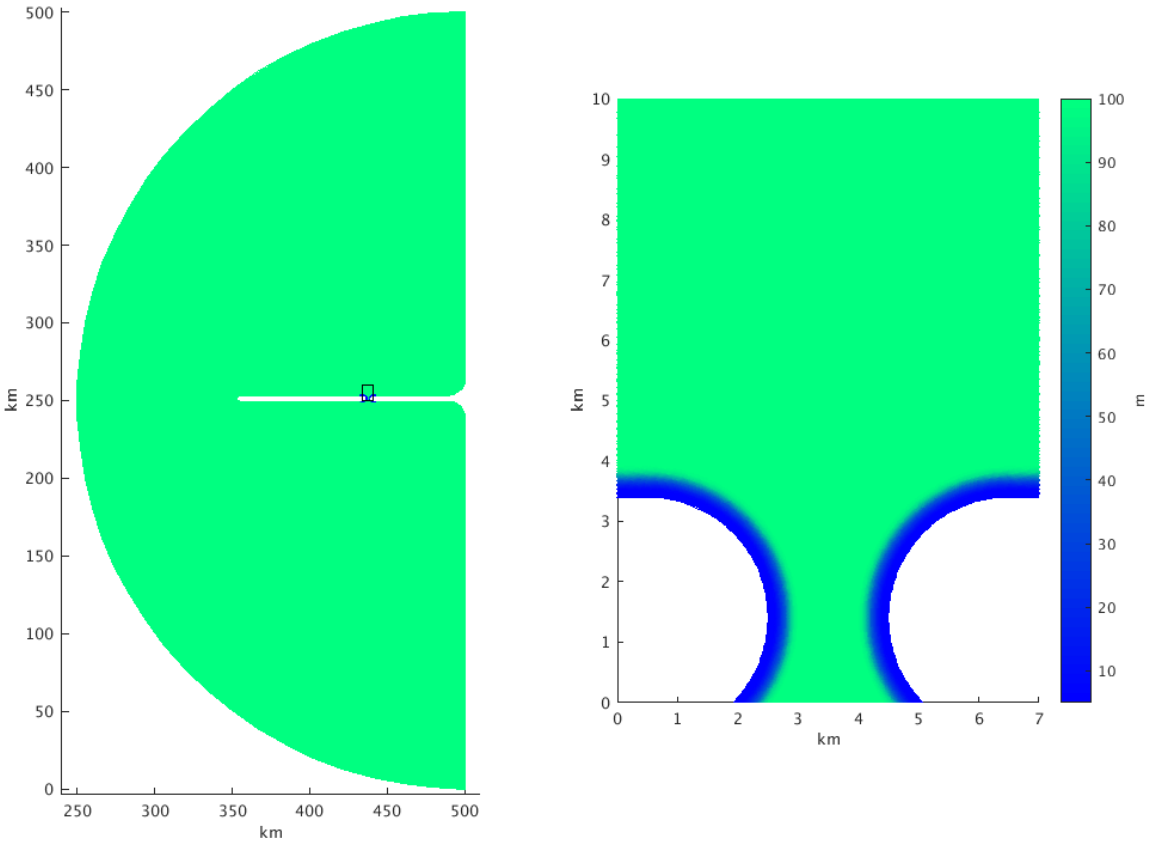

Figure 6.22: *This figure shows the entire domain. The half-circle is the open boundary, all other boundaries are land. There is a small black box in the left hand panel. This is the northern part of the channel shown in the panel to the right.*

The channel is 2km wide (4 times wider than Rystraumen and Tromsøysund). It does not have a sill. Figure 6.23 show the maximum velocities modelled near the channel, and a situation where the current downstream of the constriction is stronger than at it. Many cells downstream of the constriction have recorded streams stronger than 4m/s. The downstream region exceed the stream at the channel centre by about 1.5m/s. This topic deserves a more in-depth study than presented herein, but it nevertheless indicate that

one should expect the tidally forced streams downstream of a constriction to be stronger than elsewhere due to dipoles. A noteworthy difference between this open channel (no sidewalls downstream) and eastern Rystraumen/northern Tromsøysund, is that only a few dipoles form each tidal cycle, normally forcing two or three downstream maxima each tidal half-cycle in contrast to the much more frequent dipoles in eastern Rystraumen typically occurring 2-3 times an hour on flood. I will come back to this at the end of the discussion.

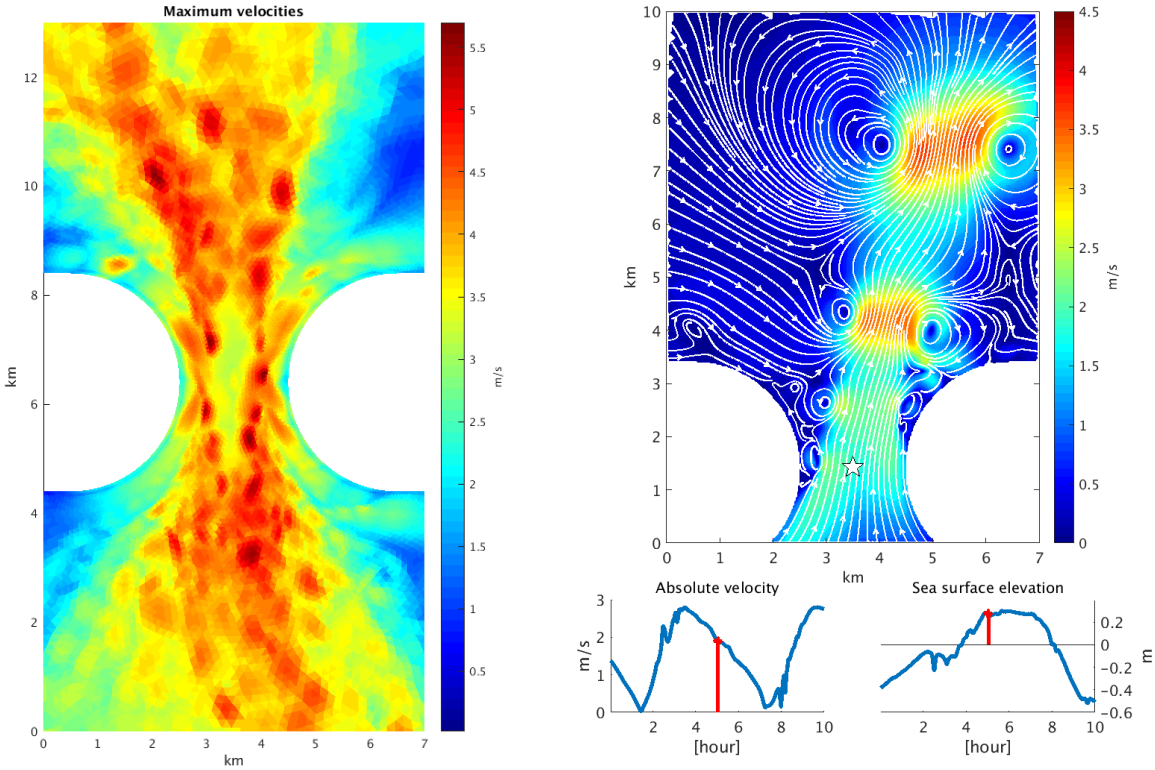

(a) Maximum modelled streams

(b) Eddy induced downstream maxima

Figure 6.23: *Idealized experiment*

Chapter 7

Discussion

The dipoles I introduced in Chapter 6 explained the high frequency velocity maxima in Tromsøysund. I will now look at the streamwise momentum balance to understand why dipoles grow strong enough to create downstream maxima. I begin by presenting my interpretation of the momentum balances and thereafter show estimates of the balances based on the model output. At the end of the chapter I discuss dipoles, transport by dipoles, and finally shallow water tides.

7.1 Downstream maxima: Eddies and Dipoles

Stable eddies exist due to a pressure gradient force and inertia balance acting perpendicular to the fluid parcels movement, see Figure 7.1a. It is called a cyclostrophic balance (Markowski and Richardson, 2011).

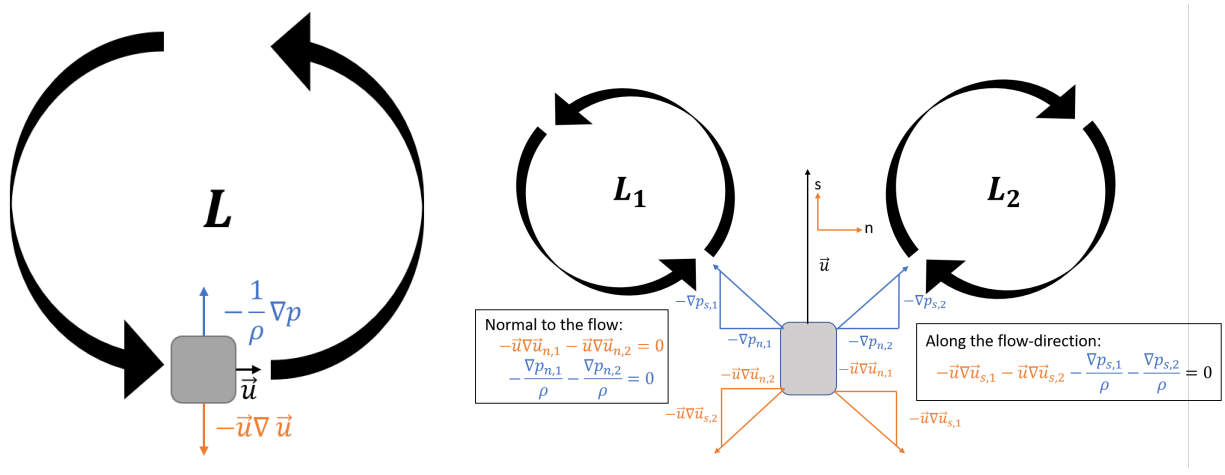

(a) (b)

Figure 7.1: *Forced experienced by a parcel in (a) equilibrium with one eddy, (b) equilibrium with each eddy. Dipoles move, and local acceleration may therefore also be important (not sketched). The s-n in orange color above "$\vec{u}$" indicates the direction of the s-n coordinate system. "L" indicates local minimum pressure, and the black arrows indicate the direction of rotation.*

The force balance in Figure 7.1a is not possible when there are two eddies in the domain. Both will introduce a pressure gradient force toward their respective centres. Let a parcel be in cyclostrophic balance with both, the situation is illustrated in Figure 7.1b. Forces normal to the flow cancel, but the component along the flow prevail. The net force is between the pressure gradient pointing toward the centre of the dipole and an inertial force opposing the flow, which is equivalent to the force balance at a constriction. I also found it interesting to investigate the momentum balance near the dipole developed when they started to grow, this sub-chapter present my interpretation of this development.

7.1.1 Dipole forming at constrictions

The flow will follow land downstream of the constriction before headland eddies start growing. The pressure-gradient is favourable (working in the flow-direction) on the upstream of the constriction and adverse (working against the flow) downstream of it. Friction and the pressure-gradient force will work together to attenuate the flow downstream of the constriction. Friction, working more effectively in shallow areas and close top shores, will attenuate the flow close to the boundaries more effectively than within the interior. The point where friction and pressure-gradient force has turned the flow back toward the constriction is known as the point of flow separation (Cohen and Kundu, 2007). Separation can only occur if there is an adverse pressure gradient in the domain (Signell and Geyer (1991), Cohen and Kundu (2007)), so an adverse gradient is a necessary criteria for flow separation. Figure 7.2 show a conceptual illustration of the process described above.

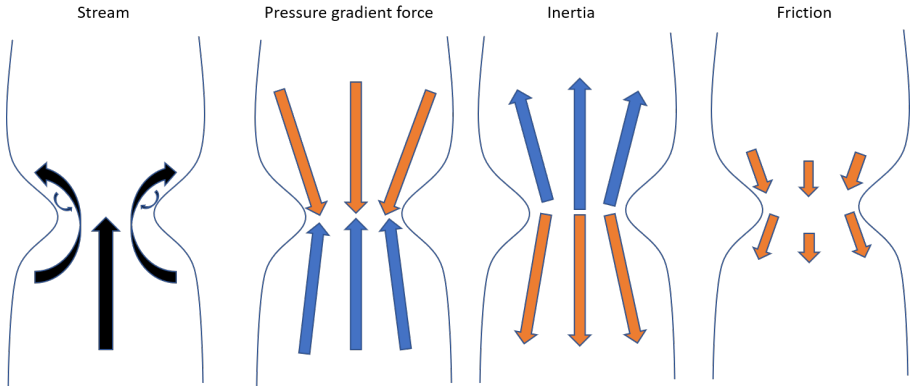

Figure 7.2: *Pressure gradient force and friction creating flow separation, and advection of momentum (intertial acceleration). The length of the arrows in the friction panel represent the relative strength of the friction.*

Two eddies develop downstream of a constriction, one on either side of the jet. Model results suggest that they are not circular when they grow but has an arm stretching to the point of flow separation with a "squash racket" shape. They create a sea surface depression at their respective centres and depress the sea surface between them, thus introducing low pressure zones downstream of the constriction as they spin up. These low pressures alter the conditions which lead to flow separation by diminishing the adverse pressure gradient close to the constriction, see Figure 7.3. Notice that the region of strongest adverse pressure gradient is shifted further downstream.

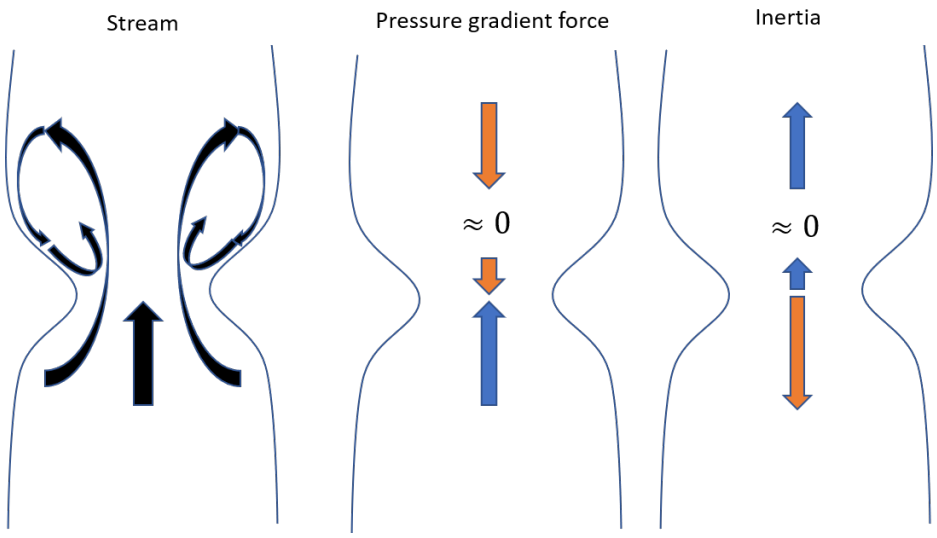

Figure 7.3: *Headland eddies form downstream due to flow separation. They decrease the downstream pressure gradient adjacent to the constriction, and shift the maximum gradient downstream. The pressure-gradient is weaker now that there are eddies downstream.*

The eddies spin faster as time pass by, create a stronger low pressure, and induce a favourable pressure gradient which become comparable to the adverse pressure-gradient directed toward the constriction, as illustrated in Figure 7.4. The net streamwise pressure gradient becomes zero. Without an adverse pressure gradient there can not be flow separation near the constriction hence the fluid in the eddies is no longer attracted to the constriction, but instead toward the dipole centre. The dipole now exists independently of the forcing from the constriction.

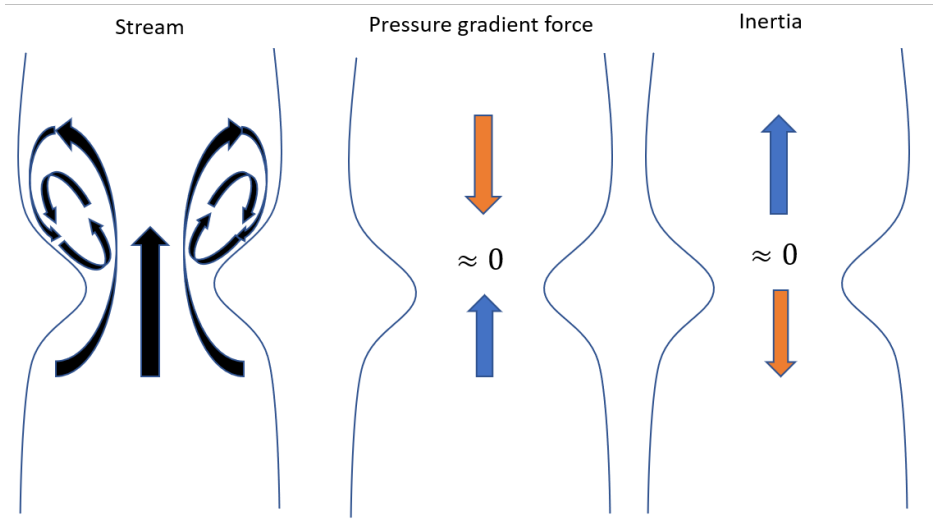

Figure 7.4: *The eddies spin faster and diminish the attenuating pressure gradient directly downstream of the constriction. Flow separation can no longer occur. The jet extends further downstream from the constriction, which means that the adverse pressure gradient is shifted downstream. The dipole in a sense extend the constrictions downstream.*

The stream flowing out of the constriction will no longer separate (due to the favourable streamwise pressure gradient). It flows out and follow the solid boundaries downstream of the constriction, just as it did prior to when the eddies started to grow. The dipole moves away and the adverse pressure gradient rebuilds downstream of the constriction, illustrated in Figure 7.5. The entire process can build up again several times during each tidal cycle in Tromsøysund and Rystraumen.
I noted that the stream near the constrictions had an arm stretching toward it such that the eddies looked like a squash-rackets. Normally an eddy would be circular, as they are after the dipole pinch off the constriction. I believe the squash racket shape is due to the pressure gradient toward the constriction. It influence the water in the eddies to move toward the constriction, therefore deforming the eddies to make the squash racket shapes. The eddies will loose their racket shape when the dipole form a sufficiently strong pressure gradient to force the water toward the dipole rather than toward the constriction.

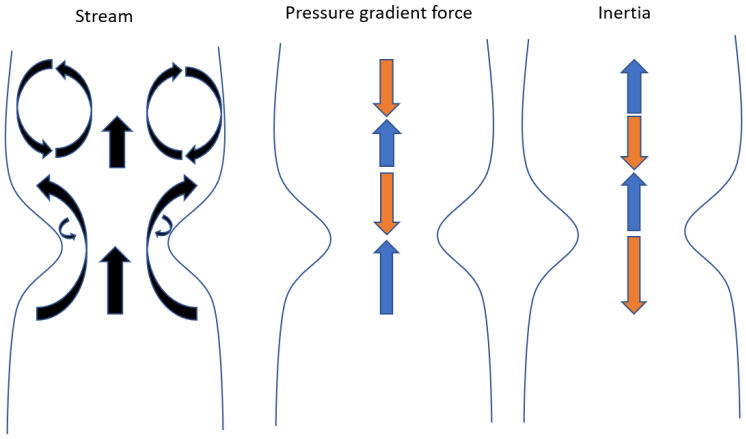

Figure 7.5: *The dipole moves away from the constriction, and the process begins from scratch.*

Shortly summarized; The dipoles builds up a strong low-pressure downstream of the constriction. This low pressure intensify as the eddies grows, and they grow since the flow separates near the constriction. When the eddies create the downstream-low, they also alter the pressure gradient close to the constriction. Flow separation require that there is an adverse pressure gradient. If the eddies create a strong enough favourable pressure gradient to nullify the adverse, then flow separation can no longer occur. I have spoken about "an arm" stretching toward the constriction, and a "squash racket"-shape. This shape require that the water in the eddy is influenced by- and attracted to the constriction. When it is not, the water in the eddy will rather flow toward the eddy centre and create a more circular shape. The flow flushing out of the constriction will "fill the void" left by the dipole, and push it downstream. The conditions for flow separation are satisfied once the dipole has moved downstream, and the process will start over again. Since dipoles have comparable favourable pressure gradients as in the constriction, and have a translation velocity downtream, they should create a stream at least as fast as at the constriction. I arrived at this interpretation of how the dipoles grow after looking at the streamwise momentum balance based on the FVCOM data, which I will show in the next subsection.

7.1.2 Rystraumen

I want to stress that the code estimating the momentum balances use a different scheme than FVCOM and the local acceleration is based on velocity data spaced $60s$ apart rather than the $5s$ in the FVCOM calculations. Additionally, these figures present data close to grid scales and the smallest scales are likely influenced by model noise - such as the "chess board" on the right hand side of Figure 7.6 where the advection term fluctuate strongly (blue colors)

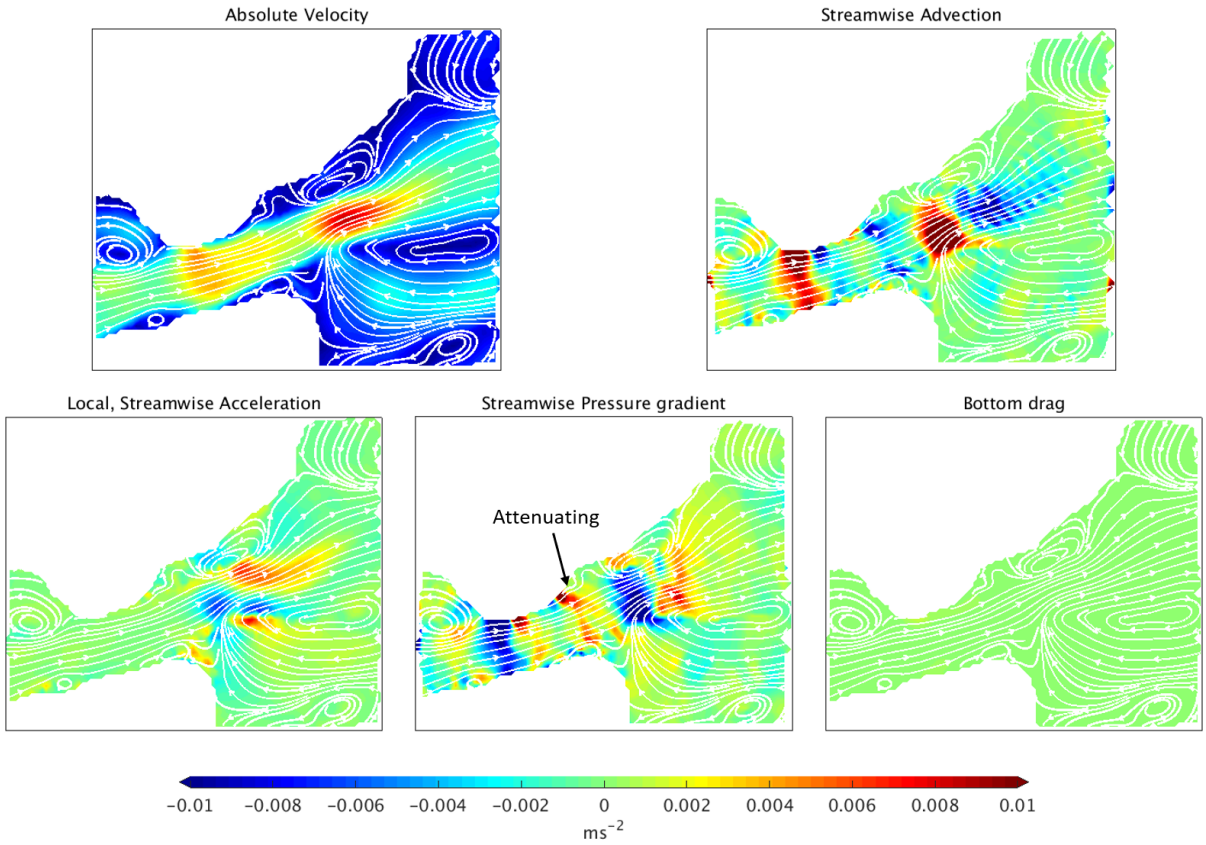

Figure 7.6: *Momentum balance in Rystraumen corresponding to the velocity field in Figure 6.20d on page 53. The colorbar does not apply for the velocity figure.*

Figures 7.6 show the stream (upper left panel), advection of momentum, local acceleration (lower left panel), streamwise pressure gradient, and friction corresponding to Figure 6.20d on page 53. Advection and the pressure-gradient dominate at the Rystraumen constriction, as is to be expected close to a constriction. Local acceleration and friction is negligible in comparison, and headland eddies are therefore likely to form. The balance between the eddies is dominated by the pressure-gradient, advection and local acceleration. The sketches in Figure 7.1b correspond to the balance within the dipole. I believe that Figure 7.6 show a good example of that eddy dipoles can be interpreted as propagating constrictions in terms of the force balance. Notice that the streamwise pressure gradient (and advection) near the dipole are comparably strong to the forces near the constriction. I have noticed that that is a general feature. I therefore made

Figure 7.7 to 7.13 to see the temporal development of the force balance in a growing dipole.

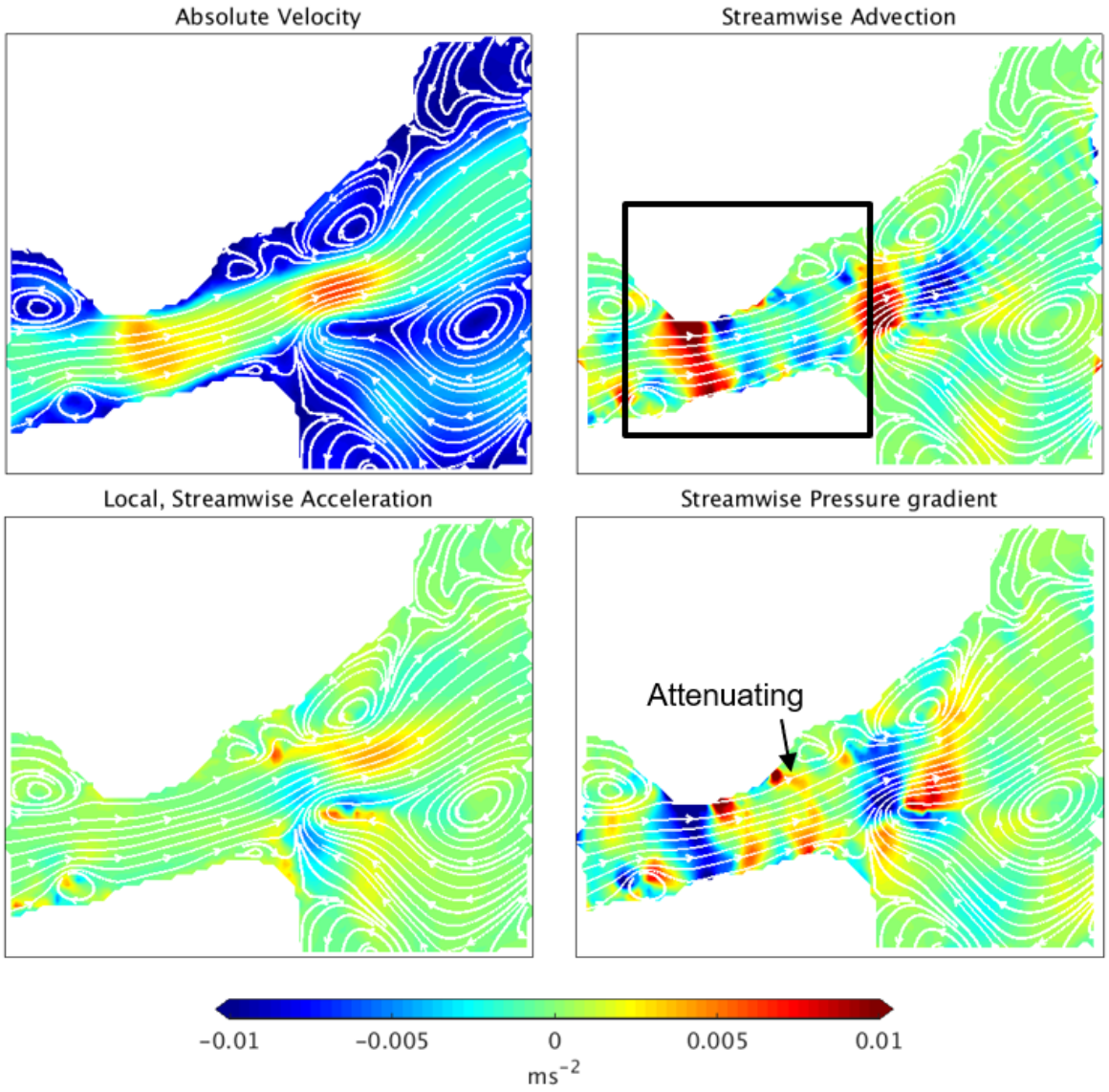

Figure 7.7: *Situation when a dipole leave the constriction, 9 minutes prior to Figure 7.8. The arrow on the lower right panel indicate that the pressure gradient where the channel expand attenuates the flow. The box on the upper right panel indicate the region I discuss in the text.*

The black box in the streamwise advection plot highlight the constriction and where dipoles form downstream of it. The pressure-gradient is balanced by advection upstream- and downstream of the constriction. The flow downstream of the constriction where the channel expands is decelerated by an adverse streamwise pressure-gradient (indicated with an arrow). Local streamwise acceleration is insignificant in the domain, except near the dipole a distance further downstream of the constriction. This situation resemble the sketch in Figures 7.3 and 7.5.

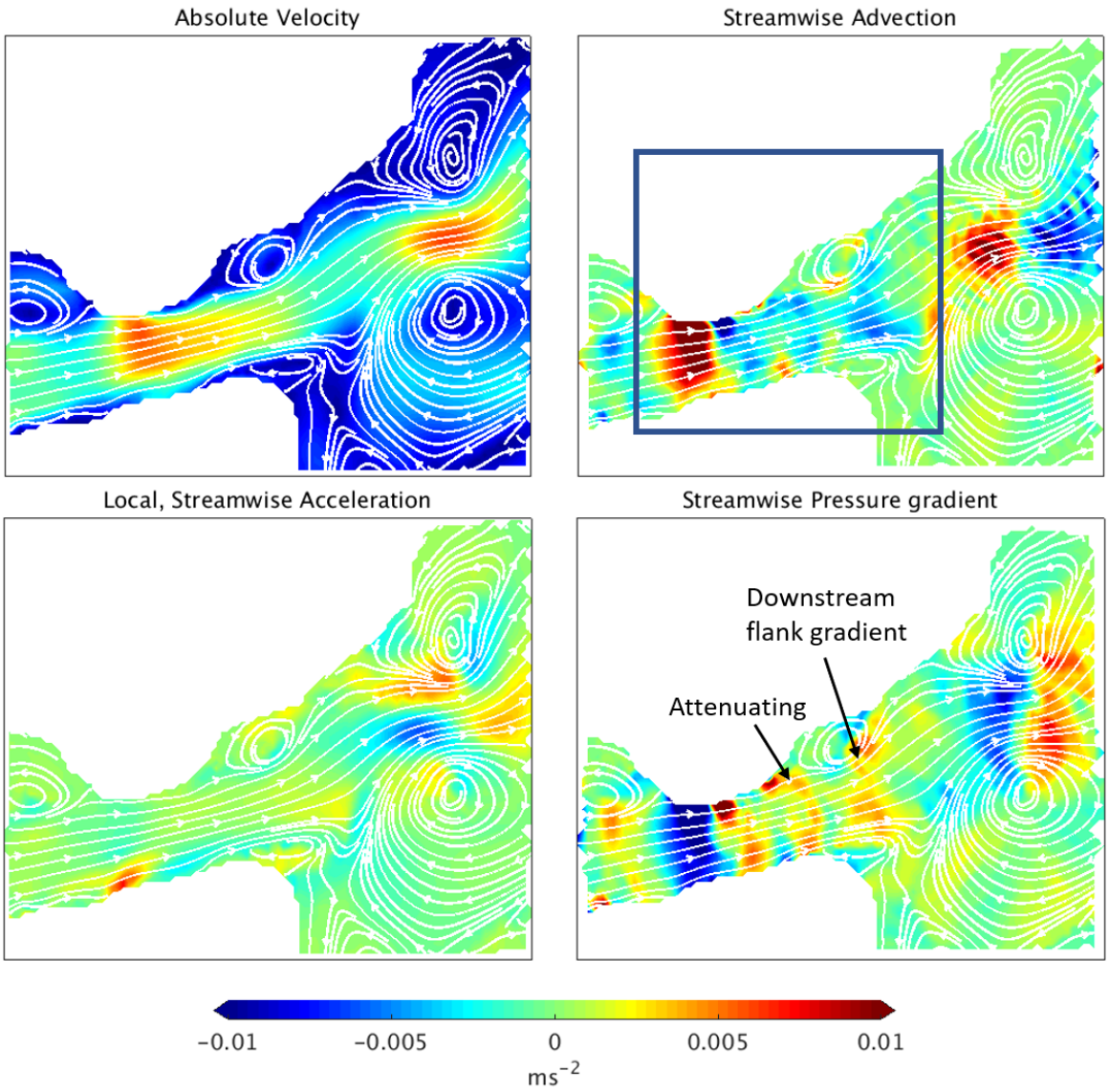

Figure 7.8: *Transient evolution prior to velocity maxima, corresponding to Figure 6.19c. The colorbar apply for the forces, not the stream - it is scaled by the same colorscale as Figure 6.19c. This figure is 15 minutes prior to a dowstream maxima formed by the dipole at the constriction.*

Figure 7.8: Two weak eddies reside directly downstream of the constriction, one on either side of the jet. There is still a pressure-gradient to advection balance upstream- and downstream of the constriction. Note that there is a strong attenuating pressure gradient on the downstream flank of the dipole near the constriction, this situation also resemble the sketch in Figure 7.3. Local streamwise acceleration is significant near the dipole far downstream of the constriction (near the downstream velocity maxima), but not near the dipole close to the constriction.

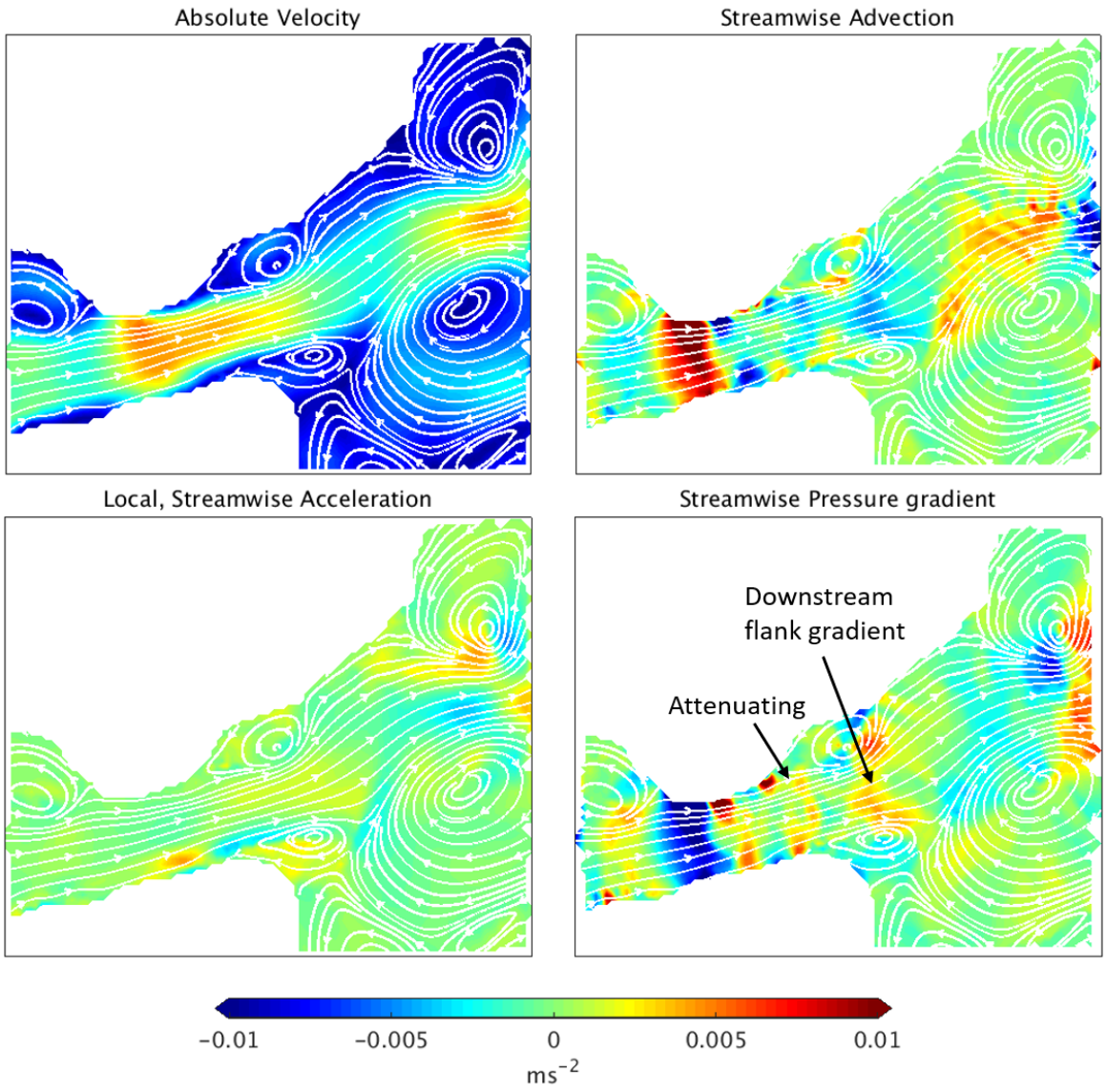

Figure 7.9: *12 minutes prior to maxima*

Three minutes later, the pressure-gradient in Figure 7.9 is weaker, but still work to attenuate the flow where the channel expand (compare Figure 7.8 and 7.9). Local acceleration close to the eddies at the constriction is insignificant, and the balance near the channel is still dominated by inertia and the pressure gradient. The attenuating pressure gradient at the dipoles downstream flank is now slightly stronger and more widespread than at the upstream flank (opposite side) of the dipole - the situation still look like the sketch in Figure 7.3

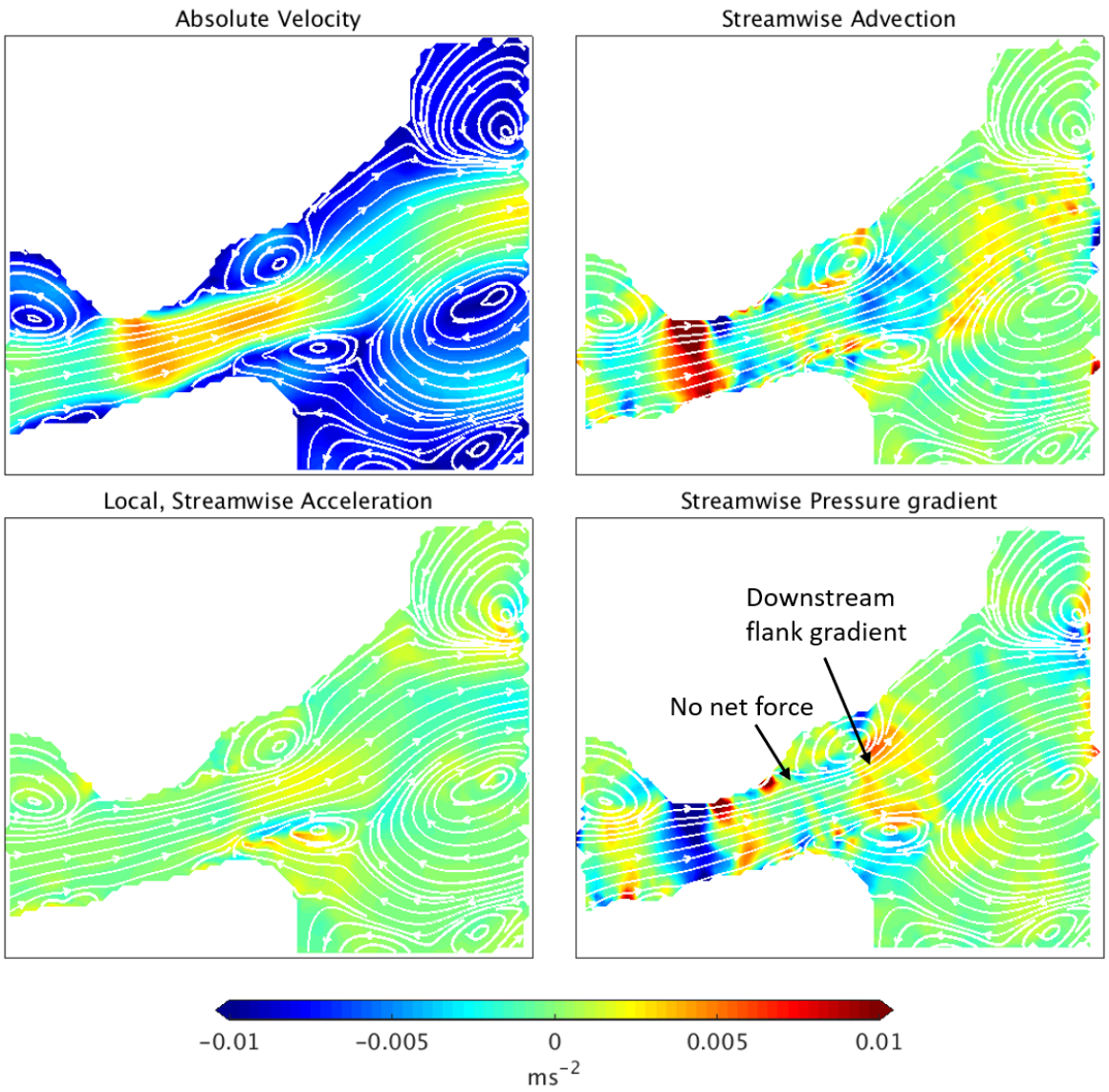

Figure 7.10: *9 minutes prior to maxima*

Another three minutes later (Figure 7.10): The attenuating pressure-gradient on the upstream flank of the dipole is close to zero which suggests that the dipole has grown strong enough to force a favourable pressure being equally strong as the attenuating force due to the constriction flow. The flow "feel" a strong attenuating force on the downstream flank of the dipole. In short, there are now two regions of attenuating pressure forces, one at the constriction where there are no eddies, and one downstream of the dipole which consist of headland eddies downstream of where the channel expands. The dipole can be said to have extended the channel further downstream, and we therefore find a strong jet far downstream of the constriction. The balance is still primarily between advection and pressure, but local acceleration is becoming increasingly important. Hence this situation looks like the sketch in Figure 7.4.

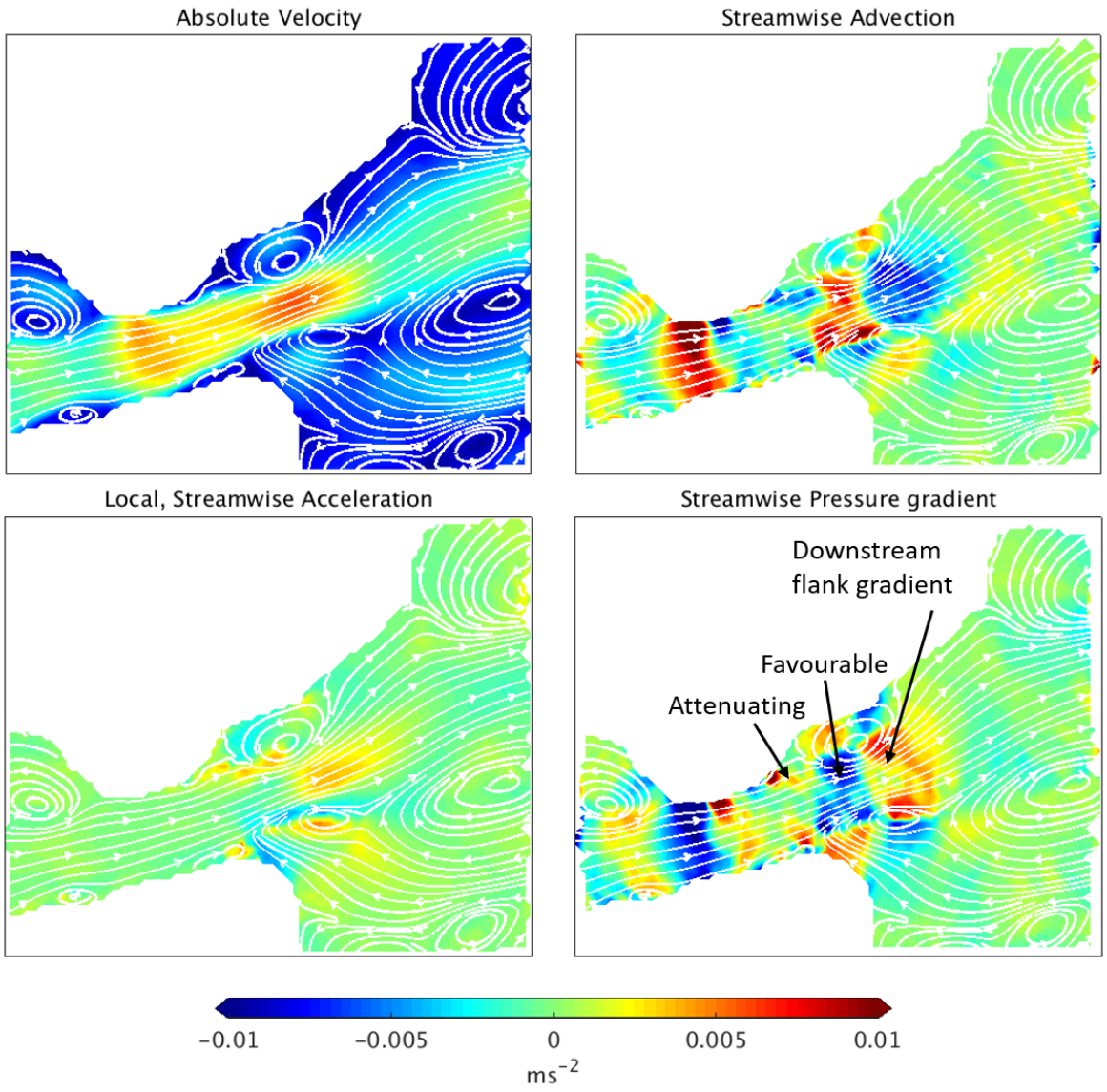

Figure 7.11: *6 minutes prior to maxima*

Thereafter the jet splits in two very distinct parts, one at the constriction and one near the eddies. The jet close to the eddies has the highest speed. The dipole has detached from the constriction, and the area where the pressure gradient was close to zero in the previous figure has now grown a weak attenuating pressure gradient. The dipole has a favourable pressure gradient on the upstream flank, and attenuating on the downstream flank. Local acceleration is important on the downstream flank, but the balance is still dominated by advection and pressure. This situation therefore look like the sketch in Figure 7.5.

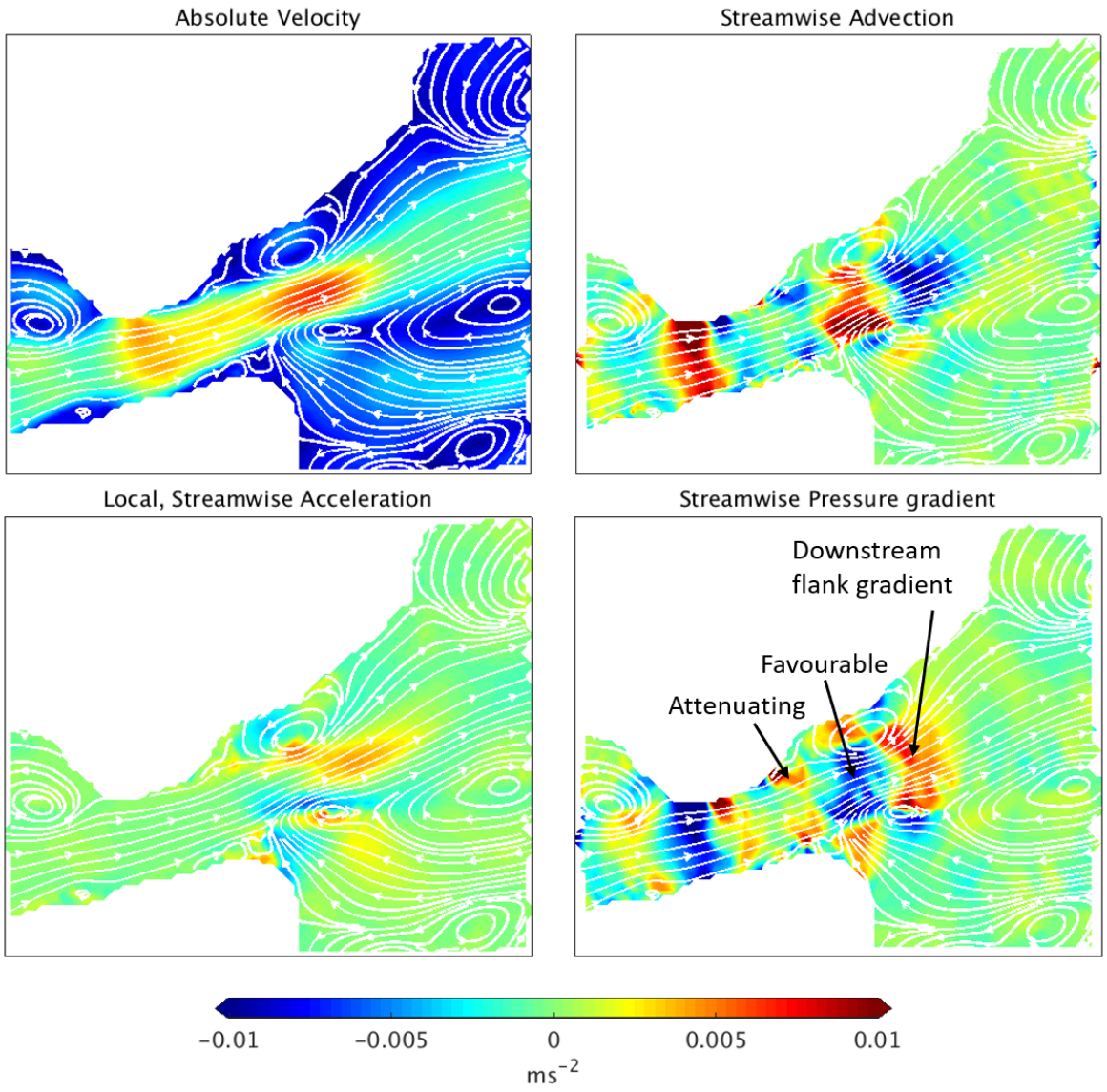

Figure 7.12: *3 minutes prior to maxima*

Figure 7.12 shows much the same as Figure 7.11. The pressure gradient attenuate the flow where the channel expand downstream of the constriction. The balance near the dipole resemble that at the constriction, except for local acceleration which once again is important downstream of the constriction. The situation still look like the sketch in Figure 7.5.

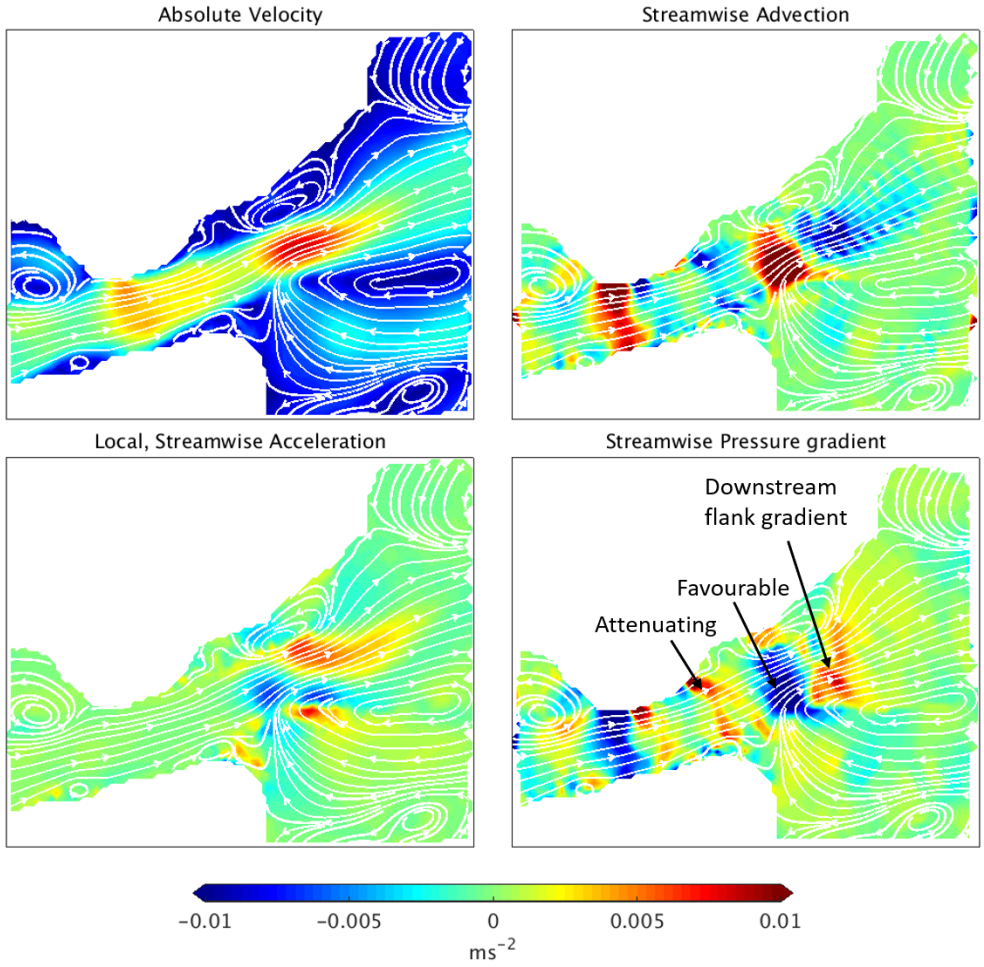

Figure 7.13: *Time-step corresponding to Figure 6.20d.*

Figure 7.13 show the situation at maximum speed flow at the maxima-cell in Rystraumen (the time step correspond to Figure 6.20d). The eddy on the right-hand side of the jet has merged with the Vikran eddy but the streamwise momentum balance near the downstream velocity maxima is nevertheless the same as previously. The figure look like the sketch in Figure 7.5, and the area near the constriction looks like the sketch in Figure 7.3

Summarized; Eddies forming on each side downstream of the constriction (a dipole) first act to decrease the attenuating pressure gradient directed toward the constriction and therefore allow the jet to extend from the constriction far downstream. The dipole detach in conjunction with the streamwise pressure gradient upstream of the eddies turning from adverse to favourable. The stream downstream of the constriction no longer "feel" the presence of the constriction, in contrast to previously where parcels in the eddies were forced away from the dipole centre to the constriction. The dipole now seem to be free to move downstream. Thus dipoles will support a similarly strong pressure gradient as the constriction forces, and they will have a downstream propagation velocity which in sum explains why the stream far downstream of a constriction can be stronger than at it.

7.1.3 Tromsøysund

The eddies in Tromsøysund are similar to those in Rystraumen, and dipoles forces the strong streams far downstream of the constriction there as well. Figure 7.14 show that the force balance within the dipole is very similar to the ones I presented in Rystraumen. The flow in the constriction is balanced by advection and pressure. Advection, pressure and local acceleration dominate near the eddies. Local acceleration is in general not important, so the force balance is not dominated by the tidal wave (which would force a local acceleration to pressure gradient balance), but by secondary effects forced by the tide - the dipoles and the choking. Tromsøysund and Rystraumen looks very similar, but bottom friction in Tromsøysund is stronger relative to the other forces than it was in Rystraumen (compare Figure 7.14 to Figure 7.6). It does, however, not reach the similarly strong values as the pressure-gradient, advection, and local acceleration.

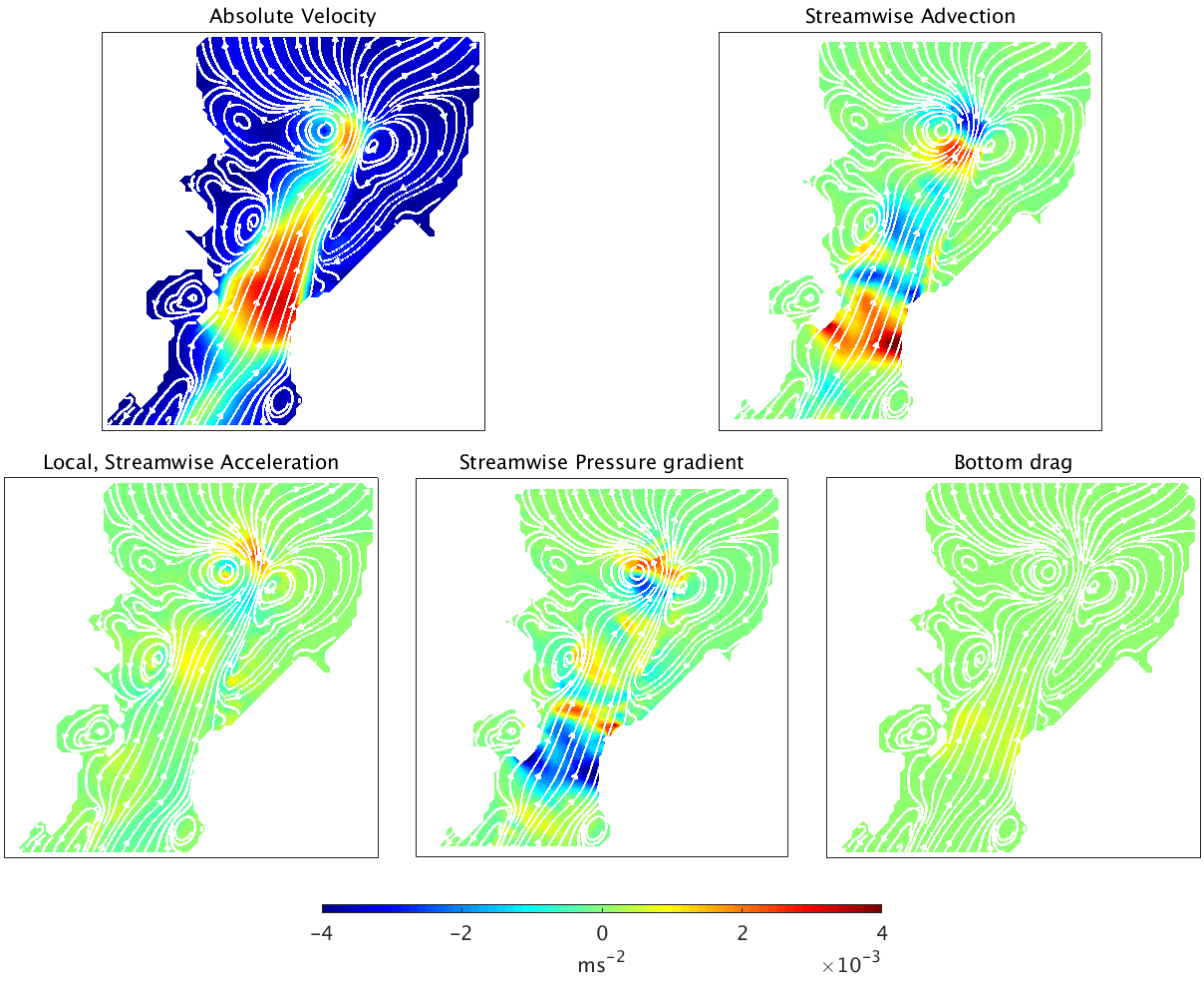

Figure 7.14: *Dominating forces at Tromsøysund for the situation in Figure 6.12a*

Figure 7.15 shows two other maxima at TRdin1. The maxima in Figure 7.14 is "cleaner" than the others, in terms of having far less eddies in the domain so that the force balance is easier to read. The other plots nevertheless give the same picture, with enhanced inertia and pressure gradients near closed streamlines.

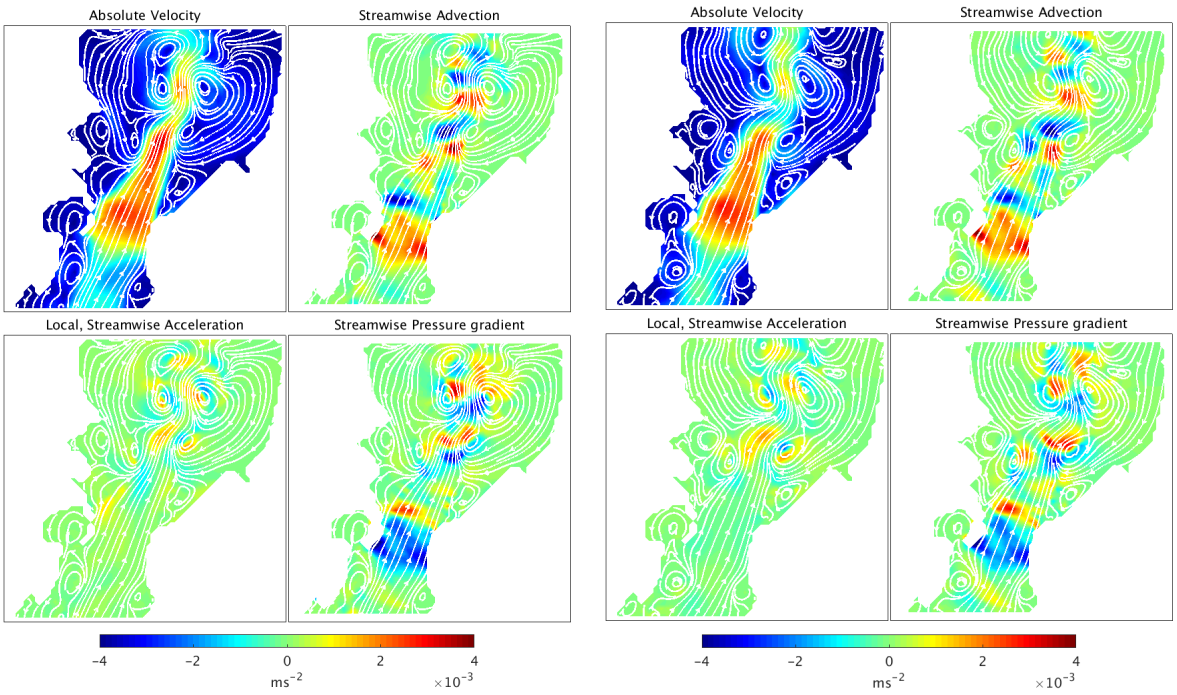

(a) *Same situation as Figure 6.12b*

(b) Same situation as Figure 6.12c

Figure 7.15: *Force balances in situations with strong TRdin1 currents*

A small side note (Figure 7.16); The stream on the southern side did not show similar high-frequency oscillations as the northern side, apparently due to the harbour eddy being trapped by a quay south of it. The stream was very strong downstream of the constriction on the southern side as well, and it turns out that the process accelerating the flow on the southern side is similar - namely downstream low pressures due to a headland eddy. The jet flows through the eddy so that the stream is accelerated when it flows into areas where the eddy forces a depression and it is decelerated when it flows out of such areas. The position where the maxima is located moves a little during the tidal cycle, probably since the eddy interact with the jet. The weak local acceleration indicates that the maxima does not move near this snapshot, and this maximum is located at the same position as the averaged stream (Figure 6.11b) suggested it should be.

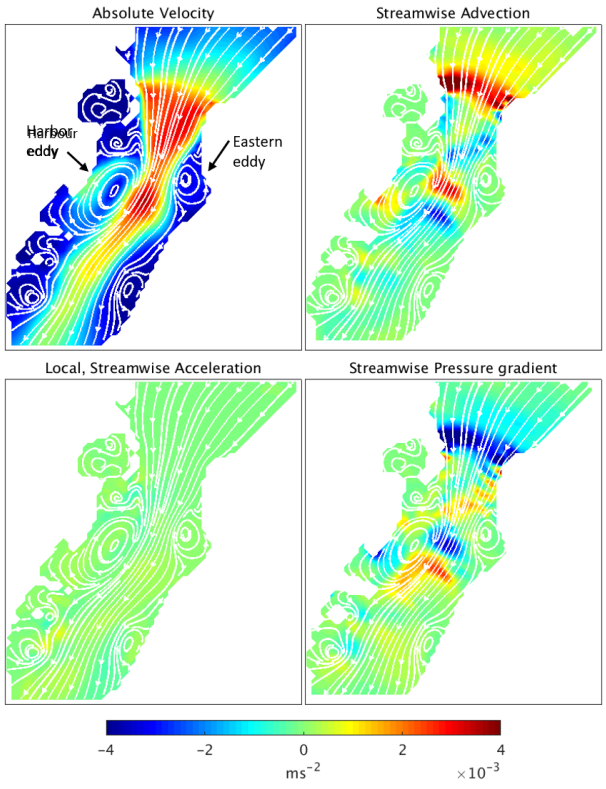

Figure 7.16: *Streamwise balance south of the Tromsøysund constriction.*

7.1.4 Idealized strait

Figure 7.17 shows the force balance during the event shown in Figure 6.23b.

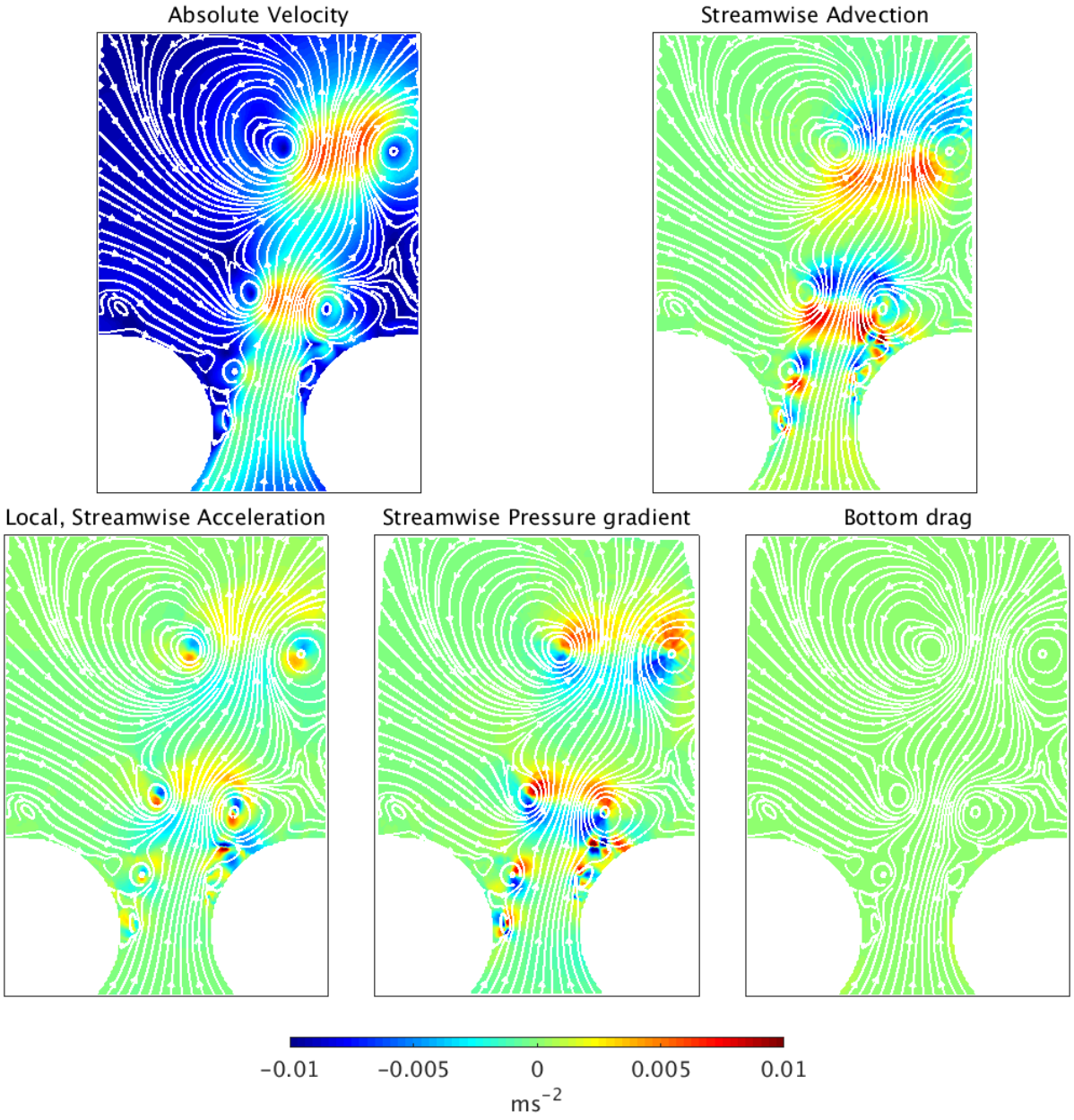

Figure 7.17: *Force balance corresponding to Figure 6.23b*

The snapshot shows two unique dipoles. The force balance in these dipoles is mainly between the pressure gradient, advection and local acceleration. Bottom friction is insignificant compared to those terms, the balance is therefore similar to what we saw in Tromsøysund and Rystraumen.

7.1.5 Some thoughts about dipoles near constrictions

The dipoles in eastern Rystraumen and in Tromsøysund occur frequently, about $2 dipoles/h$, the idealized experiment in contrast produced two/three dipoles pr. flood, which is roughly $0.5 dipoles/h$. Dipoles moved away from the constriction on the western Rystraumen side two or three times during each tidal cycle, so with similar frequencies as the idealized strait. The frequency of dipole generation can depend on the coastline geometry adjacent to the channel. I believe that it may be understood by looking at the downstream pressure-gradient. Consider a growing eddy. It will expand in size, and there will be a minima pressure in the centre of the eddy. If the downstream region is very wide, then the eddy may expand without meeting a side-wall. On the other hand, if the downstream region is narrow, then the eddy will expand until meeting the side wall, and any further expansion must be into the jet instead. The lowest pressure associated with a circular eddy is in its centre. If the eddy expand into the jet, then the centre of the eddy should also move toward the centre and the expansion will introduce a strong streamwise pressure gradient much earlier than if the downstream region was wide. I believe that the dipoles destroy the adverse pressure gradient earlier in such cases, such that they move downstream much faster than if the channel was wide.

Afanasyev (2006) studied dipoles in a laboratory to identify the formation of vortex dipoles, and among other things attempted to estimate the time from it started to grow until it moved away from the constriction, the so-called startup time. He found that the dipole startup time could be approximated by looking at the growth of the dipole. He propose that the reason to why the dipole stay close to the constriction, is that it does not move faster downstream than it expand upstream. Even though it move downstream while growing, it increase its radius such that it still stay connected to the constriction. My model and his thus agree that the eddies have to grow to a "sufficient" size before they can move downstream, but the approach to identify why they move is different.

7.2 Transport by complex streams

Dipoles can move over great distances and carry water-borne stuff with them. Callendar et al. (2011) studied a dipole which propagated away from the coast off British Columbia. They propose that it can be an important source of nutrient loss from coastal areas. Wells and van Heijst (2003) performed a laboratory experiment and found that the net transport through a strait was significantly increased when strong dipoles formed and moved away from the constriction. It may therefore be important that numerical models must resolve dipoles forming on either side of Rystraumen or Tromsøysund if one wish to study the net transport of water-borne particles in this fjord system. Dipoles can be important in areas with islands creating narrow passages as well, which is quite common along - for example - the Norwegian coast. Dipoles should be able to form essentially everywhere where vorticity of negative and positive sign is generated adjacent to each other. I would not be surprised if dipoles such as those presented herein play a role in the transport of salmon lice and pollutants/properties associated by a water-mass. Dipoles generated by the tide occur very frequently, in contrast to processes such as Ekman-pumping along the coast which depend on large scale wind systems (Klinck et al., 1981), the integrated

effect of dipoles over time may therefore be important even if each single dipole force a relatively minor transport compared to the Ekman-pumping.

Shallow water tides can also influence the net transport. Pugh and Woodworth (2014) state that shallow water constituents can be essential for transport of sedimented material. Such particles must be put into motion, and a simple model to understand the phenomena depend on the strength of the stream since those particles will only move once the stream exceed a threshold value. Particles may therefore move in only one direction if the stream just exceed the threshold on, for example, flood.

7.3 Amplified shallow water tides

The results in Chapter 6 gave a thorough description, and a short discussion, of why I found strong shallow water tides in Tromsøysundet and Sandnessundet. In short, it is due to the channel being forced by two tidal waves which have been distorted differently by the non-linear processes generating shallow water harmonics which meet at the Tromsøysundet and Sandnessundet constrictions. They meet there since the sea surface within Balsfjorden is primarilly forced by the Malangen tide (the southern wave).

I have not seen significant shallow water harmonics in Rystraumen since the volume transport through Rya is significantly bigger than through Tromsøysundet and Sandnessundet. The sea surface oscillation on either side of Rystraumen therefore behave similarly, such that most of the pressure difference is caused by the tidal wave phase shift across the constriction. If someone reduced the flow through Rystraumen by increasing the drag (e.g. tidal turbines), decreased its cross section, or increased the cross section of Tromsøysundet and Sandnessundet, we should see that the wave in Grøtsundet would influence Balsfjorden more and that the shallow water harmonics in Tromsøysundet/Sandnessundet would become less significant. We should also see more pronounced shallow water harmonics in Rystraumen.

I made an assumption when I proposed that the shallow water tides altering the pressure gradient across the constriction will result in an altered stream, namely that the pressure-gradient is directly linked to the speed of the flow through the constriction. It worked well, the speed and the pressure gradient correlated nicely. But that may not always be the case. I listed two processes which alter the speed at a constriction;

1. The along channel pressure gradient $\frac{\partial p}{\partial L}$ (L being a coordinate following the channel).
2. Conservation of mass such that the flow intensify in narrow sections. This process can also be thought of as an inertial effect. The speed is gained by a local pressure gradient ∇p near the constriction which add to $\frac{\partial p}{\partial L}$

There exist an analytical expression for a steady flow balanced by advection ($\vec{u}\nabla\vec{u}$) and the pressure gradient force ($-\nabla p/\rho$) caused by the dip in the sea surface due to conservation of mass. This balance is steady state given a constant mass flux toward and away from the channel and negligible friction in what is known as a sub-critical flow (e.g. Chapter 1 in Pratt and Whitehead (2007)). $\frac{\partial p}{\partial L}$ alter the stream by *accelerating* the

flow through the constriction in a channel where friction is negligible, hence $\frac{\partial p}{\partial L}$ is not *directly* linked to the instantaneous speed. The speed should not decay if $\frac{\partial p}{\partial L}$ weaken - just when it switch sign, since that will decelerate the flow. The flow in channels where friction is significant respond in a different way to changes in $\frac{\partial p}{\partial L}$. Stigebrandt (1980) discuss a momentum balance at a constriction where friction is significant. The along channel pressure gradient there balance the bed stress, so the speed through the channel is directly linked to the strength of the pressure gradient - which is more or less what I assumed in Tromsøysund. So the pressure gradient do two things. It accelerate the flow and force a volume transport through the constriction, and it compete with friction within the channel. In a channel which is very influenced by friction, any change in the pressure gradient should either increase or decrease the speed. In a channel where friction is insignificant, one should expect that any change in the pressure gradient will influence the acceleration. The speed will only decrease if the pressure gradient turns negative and start competing with the intertia of the flow. I therefore expect the currents following shallow water harmonics due to along channel pressure gradient to be more pronounced in shallow and narrow channels (where friction is significant) than in deep channels (where inertia balance the pressure gradient and friction is insignificant). Both shallow and deep channels will correlate to the along channel pressure gradient, but shallow channels will correlate best since friction work to remove the momentum. Tromsøysund is influenced by friction (e.g. Figure 7.15), while Rystraumen was not (Figure 7.6). Rystraumen may therefore respond differently to how the shallow water harmonics alter the pressure gradient than Tromsøysund. Little Rystraumen, the subsidiary channel on the other side of Ryøya, is very shallow and may respond to changes in the pressure gradient in a similar manner as Tromsøysund. A more in-depth study of shallow water harmonics may therefore benefit from comparing how the two Rya-constrictions respond to the along channel pressure gradient.

Chapter 8

Summary and Conclusions

The tide in Tromsø propagates in an area with complex bathymetry and topography. An inner fjord system with a $280km^2$ large surface area is connected to the open ocean on both the northern and southern sides on the domain. The tide propagates from south to north along the outer boundary, hence forcing the northern openings of the fjord system later than the southern. Gjevik et al. (1994) explained that the tide amplifies on the northern side of the domain due to co-oscillations over the Finnmark/Barents sea shelves which is in agreement with results from observations and numerical experiments presented in this thesis. The tide on northern side of the fjord system is therefore "taller" than on the southern side.

Maximum along-channel forced M2 and S2 sea surface differences in Tromsøysundet (and Sandnessundet) occur on high- and low tide. The maximum along channel pressure gradient does, however, not follow the M2 and S2 tides. It is altered by shallow water harmonics. The tidal stream in Tromsøysundet and Sandnessundet is thus not strongest at high/low tide, in fact it has several extrema during the tidal cycle - even though the sea surface variability at both the northern and southern sides are dominated by linear harmonics. It turns out that large scale modifications of the tide as it propagates around the islands separating the inner fjord system from the open ocean modify the tide sufficiently to create a clear difference between the tide entering the fjord system from the southern and the northern sides. The difference is sufficient to create strong streams following the shallow water harmonics in the Tromsøysundet and Sandnessundet channels. Shallow water tides are important for the stream in Tromsøysundet, but they are not the only process excited by the M2 and S2 tides.

Observed time series from the Tromsøysundet constriction reveal that the northern side is significantly different from the southern. Strong high frequency oscillations occur at the northern- but not on the southern side. Model results show a similar relationship, and the spatial flow pattern reveal that the oscillations are related to eddy dipoles which initially form at the constriction and move downstream after some time. The same feature is apparent in Rystraumen, where the dipoles create much stronger streams downstream of the constriction than at it. These dipoles originate at the constriction, where they are generated due to flow separation. The force balances show that dipoles create very strong streamwise pressure gradients as they move downstream.

I propose that the phenomena can be understood as follows: Dipoles exist due to flow separation, a process occurring due to an adverse pressure gradient pointing toward the constriction. The flow separation and the eddies are indistinguishable. The flow can not be separated if the pressure gradient accelerates the flow in any other direction than toward the constriction. Dipoles seem to destroy the conditions working to separate the flow when they create a sufficiently strong favourable pressure gradient at their upstream flank. It renders the dipoles independent of the constriction, and they are free to move downstream since they no longer exist due to flow separation, but rather due to the vorticity they generated when the flow was separated. Thus they have a comparable streamwise pressure gradient as the gradient which forced the flow separation when they detach, and they also have a velocity relating to their movement downstream. Streams excited by dipoles moving away from constrictions should therefore be stronger than at the constriction where they gained their momentum unless their rotation rate is stalled by frictional effects. An idealized numerical simulation has revealed that the downstream maxima can occur for domains with flat bathymetry as well. Downstream maxima should therefore be a phenomenon which can be found in many areas where dipoles are generated - and it is therefore not unique to the Tromsø tidal system.

In short, this thesis has shown that the tidally forced flows in Tromsø can be explained by three mechanisms working over very different horizontal scales.

1. The large scale pressure gradient forced by the gravitation of the moon and sun.

2. Modifications of the large scale pressure gradient due to shallow water effects working on the scale of this system impose strong shallow tide-gradients across Tromsøysund and Sandnessund.

3. Introduction of local low pressures due to flow separation near the constrictions.

FVCOM modelled the first process since it was forced by tides at the open boundaries. The second scale is resolved since the model cover a domain covering the path the tide moves between the southern and northern opening of the fjord system. And the third process is resolved since the model capture fine-scale processes in the narrow straits. It is therefore imperative to model a large domain to resolve the processes distorting the tide, as well as resolving the straits with fine scales to capture the headland eddies. The characteristics of these vortices depend on the headland geometry, and it is therefore important to use a mesh which follow the shape of headlands in the domain (Signell and Geyer, 1991).

Chapter 9

Future perspectives

This thesis provided possible explanations for the horizontal 2D dynamics of the Tromsø tidal system. FVCOM is in general in good agreement with the observations, reproducing similar phenomena. I hope that future attempts to better understand the system first and foremost try to measure the downstream maxima to verify if the maxima speeds actually occur far downstream of the constrictions. A more extensive fieldwork can measure many constrictions to see if it is common for fjords with strong tidal streams to have their maximum stream far downstream of their tightest cross sections. Rystraumen may be a nice real world laboratory for such studies. Additionally, future modelling studies of this region should use a mesh which resolve the adjacent areas of the channel with equally high resolution as within the channel, since the channels create dipoles moving away from the constriction and in such propagate information from the constriction downstream. One risk loosing this information when using a mesh with coarser resolution downstream, which is unfortunate when for example looking at the dipole-forced transport.

I did not study the net transport of water-borne and sedimented pollutants in this fjord system. I would like to stress that the wind driven transport should be included in such studies. It is possible to compare the transport between experiments including and neglecting wind driven effects to assess how important these purely tidally driven effects are for dispersal of water-borne particles. I believe that the goal of such a study should be to understand if it is necessary to model dipoles to understand dispersal in fjords, or if dipoles are significantly less important than estuarine and wind-driven effects.

My thesis assumed that 2D dynamics dominate 3D effects which implicitly leads to an assumption that the eddies are mainly attenuated by bottom- and horizontal friction. In reality, they are also affected by a 3D, barotropic effect due to the bottom boundary layer of the eddy. There will be a radial transport of mass toward the centre of the eddy in the boundary layer, which will attenuate the rotation rate. Future studies can include that effect, to see if these eddies are attenuated sufficiently to hinder them from creating downstream maxima. A 2D simulation of the stream should give weaker streams than the 3D simulation, and it can be interesting to investigate where the 3D stream is strongest in the domain. The results herein can therefore be interpreted as "downstream volume-transport maxima" rather than true stream maxima. One can expect the modelled maximum stream to be stronger in a 3D simulation.

Appendix A

The streamwise momentum balance

Hench and Luettich Jr (2003) inspired me to study the momentum balances in this shallow region with narrow constriction. The momentum balance is most intuitive when expressed in a coordinate system following the flow.

A.1 Rotating the coordinate system

Figure A.1 illustrates how the cartesian and the rotated coordinate system are positioned relative to each other.

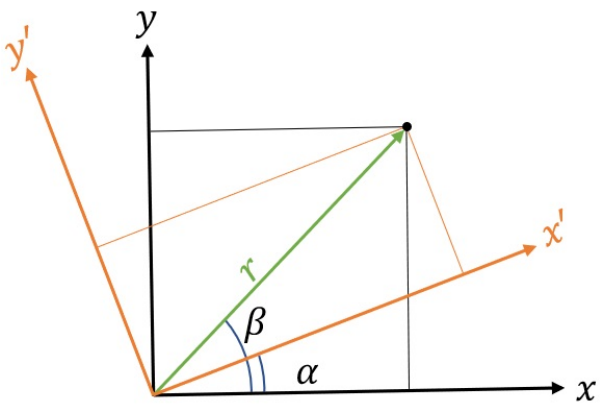

Figure A.1: *Rotation from (x,y) to (x',y') coordinates.*

One can find the coordinate transformation by noting that $x = rcos(\beta)$, $x' = rcos(\beta - \alpha)$ and $y = rsin(\beta)$, $y' = rsin(\beta - \alpha)$. The (x', y') components can be expanded to get

$$x' = rcos(\beta)cos(\alpha) + rsin(\beta)sin(\alpha) \tag{A.1}$$

and

$$y' = -rsin(\alpha)cos(\beta) + rsin(\beta)cos(\alpha) \tag{A.2}$$

which is equivalent to

$$x' = xcos(\alpha) + ysin(\alpha) \tag{A.3}$$

$$y' = -xsin(\alpha) + ycos(\alpha) \tag{A.4}$$

A.2 Rotating the Cartesian momentum balance

Starting from the FVCOM depth integrated equations, but ignoring viscosity.
x-momentum

$$M_x = \frac{\partial U}{\partial t} + U\frac{\partial U}{\partial x} + V\frac{\partial U}{\partial y} - fV + g\frac{\partial \eta}{\partial x} + C_d\sqrt{U^2+V^2}U = 0 \tag{A.5}$$

y-momentum

$$M_y = \frac{\partial V}{\partial t} + U\frac{\partial V}{\partial x} + V\frac{\partial V}{\partial y} + fU + g\frac{\partial \eta}{\partial y} + C_d\sqrt{U^2+V^2}V = 0 \tag{A.6}$$

All of the terms are transformed to the streamwise coordinate system through the transformation $M_s = M_x cos\alpha + M_y sin\alpha$ and normal $M_n = -M_x sin\alpha + M_y cos\alpha$. The velocity of a parcel U_s is related to its x and y components through $U = U_s cos\alpha$ and $V = U_s sin\alpha$.
Streamwise acceleration

$$M_{s-acc} = \frac{\partial U}{\partial t}cos\alpha + \frac{\partial V}{\partial t}sin\alpha \tag{A.7}$$

$$M_{s-acc} = \frac{\partial U_s cos\alpha}{\partial t}cos\alpha + \frac{\partial U_s sin\alpha}{\partial t}sin\alpha \tag{A.8}$$

Derivatives of angles cancel and the only remaining term is

$$M_{s-acc} = \frac{\partial Us}{\partial t}(cos^2\alpha + sin^2\alpha) = \frac{\partial U_s}{\partial t} \tag{A.9}$$

Streamwise advection:

$$M_{s-adv} = (U\frac{\partial U}{\partial x} + V\frac{\partial U}{\partial y})cos\alpha + (U\frac{\partial V}{\partial x} + V\frac{\partial V}{\partial y})sin\alpha \tag{A.10}$$

$$M_{s-adv} = (U_s cos\alpha\frac{\partial U_s cos\alpha}{\partial x} + U_s sin\alpha\frac{\partial U_s cos\alpha}{\partial y})cos\alpha + (U_s cos\alpha\frac{\partial U_s sin\alpha}{\partial x} + U_s sin\alpha\frac{\partial U_s sin\alpha}{\partial y})sin\alpha \tag{A.11}$$

Derivatives of angles cancel, and we are left with

$$M_{s-adv} = U_s cos\alpha(cos^2\alpha\frac{\partial U_s}{\partial x} + sin^2\alpha\frac{\partial U_s}{\partial x}) + U_s sin\alpha(cos^2\alpha\frac{\partial U_s}{\partial y} + sin^2\alpha\frac{\partial U_s}{\partial y}) \tag{A.12}$$

$$M_{s-adv} = U_s(cos\alpha\frac{\partial U_s}{\partial x} + sin\alpha\frac{\partial U_s}{\partial y}) \tag{A.13}$$

Streamwise pressure gradient

$$M_{s-press} = g\frac{\partial \eta}{\partial x}cos\alpha + g\frac{\partial \eta}{\partial y}sin\alpha \tag{A.14}$$

Streamwise friction

$$M_{s-fric} = \frac{C_d\sqrt{U^2+V^2}}{H}Ucos\alpha + \frac{C_d\sqrt{U^2+V^2}}{H}Usin\alpha \tag{A.15}$$

$$M_{s-fric} = \frac{C_dU_s}{H}U_scos^2\alpha + \frac{C_dU_s}{H}U_ssin^2\alpha \tag{A.16}$$

$$M_{s-fric} = \frac{C_dU_s^2}{H} \tag{A.17}$$

Note that the force-terms are negative since they are on the left hand side of the equation. Friction will never *provide* momentum to the fluid, and that is why it is always positive in my streamwise momentum balances. It extracts momentum from the flow, and stores it - but friction from the (stationary) bed can not provide momentum to the fluid - hence never becomes negative.

Numerical procedure

I solved the momentum balance in (x,y) coordinates and rotated them to (s,n) using Equation A.7, A.10, A.14 and A.15.

Appendix B

Averaged flowing in/out currents: Procedure

This appendix describes the procedure I used to make the plots showing averaged streams. Let n_a be the index defining when the flow turns from positive to negative velocity component, and n_b define when the current turns negative to positive. Similarly, I define n_h to be the indices of high water, and n_l those of low water. The indices between n_a and n_b are therefore the time-period of negative currents, and n_b to n_a are those of positive currents. Defining n_a and n_b is not a trivial task, since the modelled stream at the constriction is noisy. The alternative procedure I used finds n_h and n_l. I pre-define the difference $n_a - n_h$ as a constant manually based on time-series from the constriction. I then assume that $n_a = n_h + (n_a - n_h)$ and $n_b = n_l + (n_a - n_h)$ for all tidal cycles.

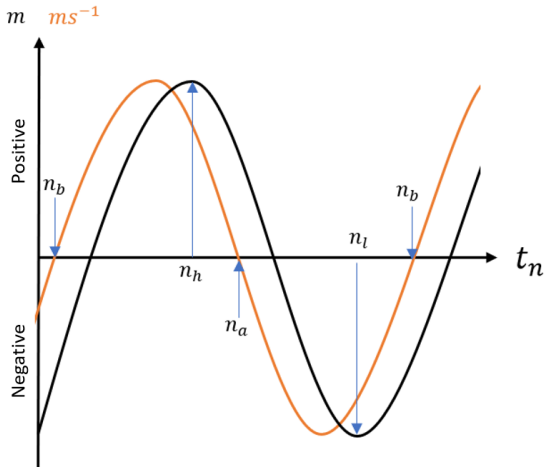

Figure B.1: *Scheme for averaging the stream (orange) and sea surface (blue).*

This procedure is only valid if the relation between stream and sea surface remain fairly constant over the tidal cycle. It would for example not hold for Figure 5.2 since the relation depends on time. Figure 5.3 suggests that it should work fine for the TPXO data.

The matlab script creating the averaged flowing in/out plots works such that I define $n_a - n_h$ in advance, and the script determines the location of n_h and n_l for as many tidal periods as I want. I then average the velocity field in the area adjacent to the constriction over 20 flowing in/out cycles.

The purpose of the procedure is to identify jets and other very pronounced streams. It should also be able to detect eddies occurring at a location for large parts of the flowing in/out periods. The figures agreed well with recurrent patterns in figures showing the transient features of the stream in both Tromsøysund and Rystraumen, but they are probably not *perfect* representations of the average stream.

Appendix C

Timeseries of measured and modelled currents

Figures C.1 to C.3 show measured and modelled currents from some stations for 13 M2 cycles at spring tide. How well UTide reproduces the measurements/model results varies with the spring-neap cycle which means that UTide does not capture the true tidal stream. I could thus have chosen a time series that fit better or worse. The model and the observations agree quite well. There are more high-frequency oscillations in the model results than in the observations. Some of the model and observation results look remarkably alike. Stations TR1 and TRdin1, for example, agree very well with the numerical results, even though the stations themselves differ significantly. Where TR1 behave very cleanly with close agreement between UTide and measured currents, TRdin1 includes intermittent velocity extrema on northerly flow.

Grøtsundet currents agree fairly well (Figure C.3 with the observations with respect to magnitudes, and while both agree that there is significant nonlinear contributions at the mouth of Grøtsundet, they do not agree on its frequency. Especially the zonal current at TRN2 differ, and the UTide interpretation of FVCOM results is significantly weaker than for the observations.

C.1 Tromsøysund

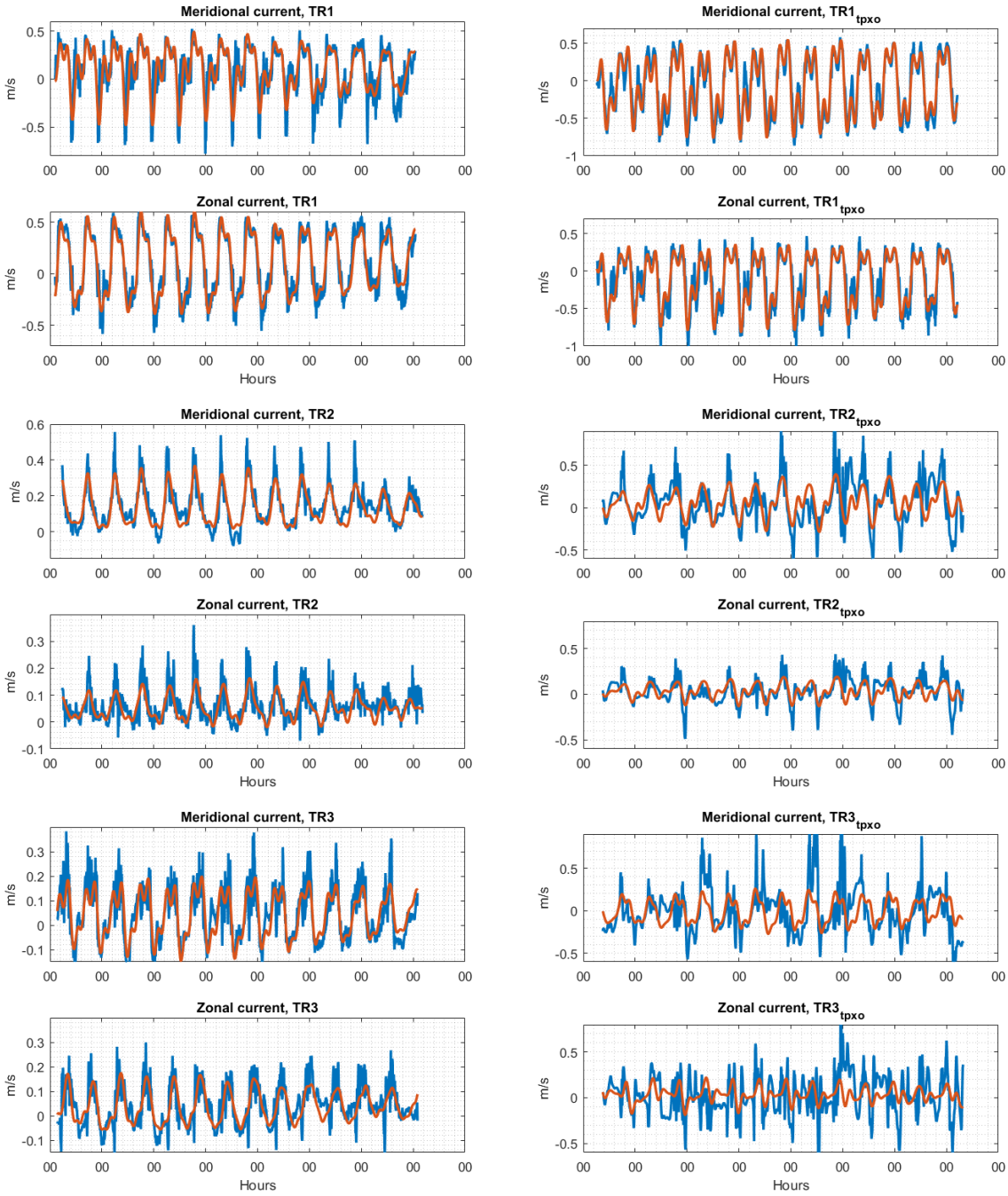

(a) Observations

(b) Model results

Figure C.1: *The orange line is the UTide interpretation of the tidal currents, while the blue is measured and/or modelled current.*

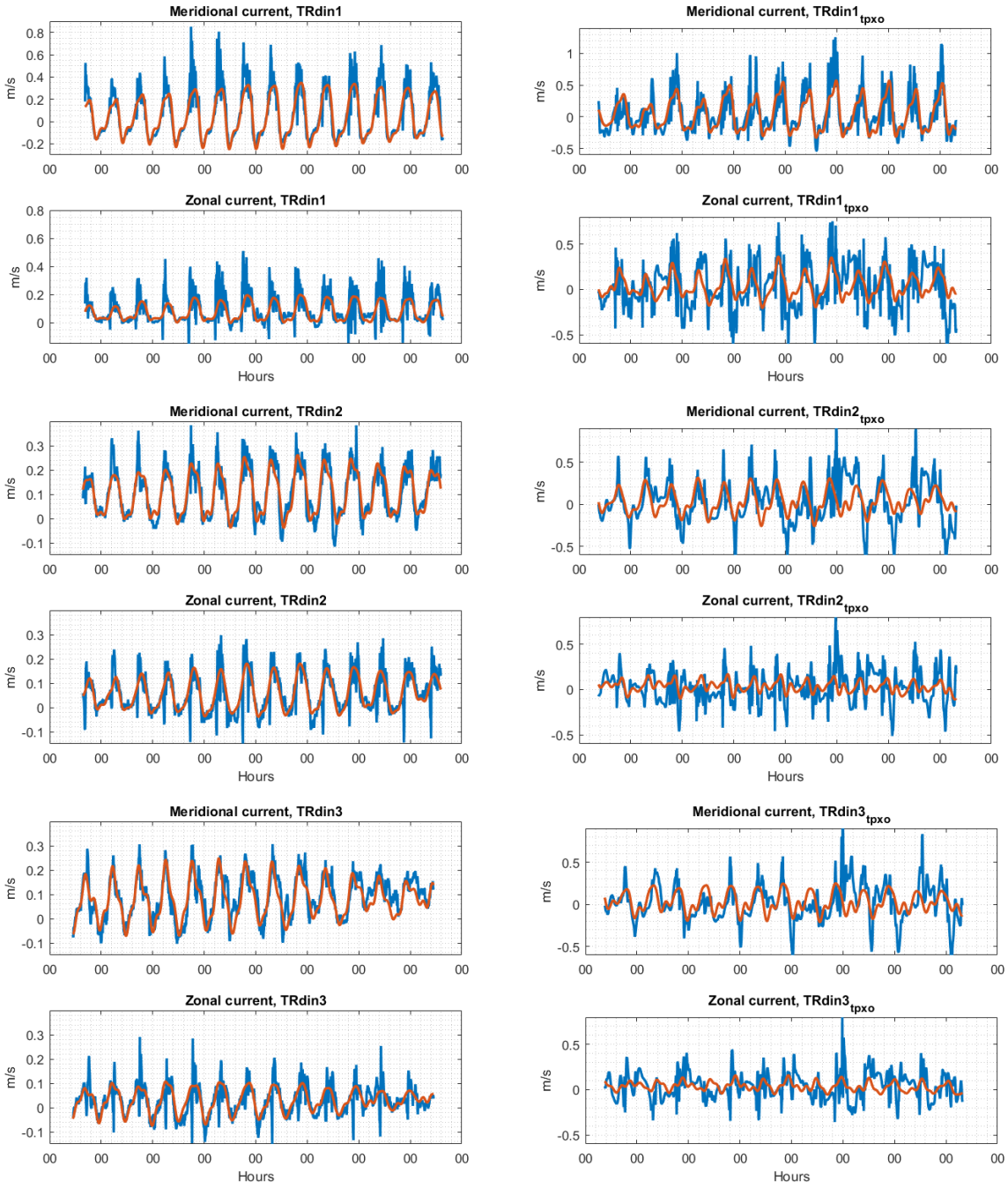

(a) Observations (b) Model results

Figure C.2: *Same layout as in Figure C.1*

C.2 Other stations

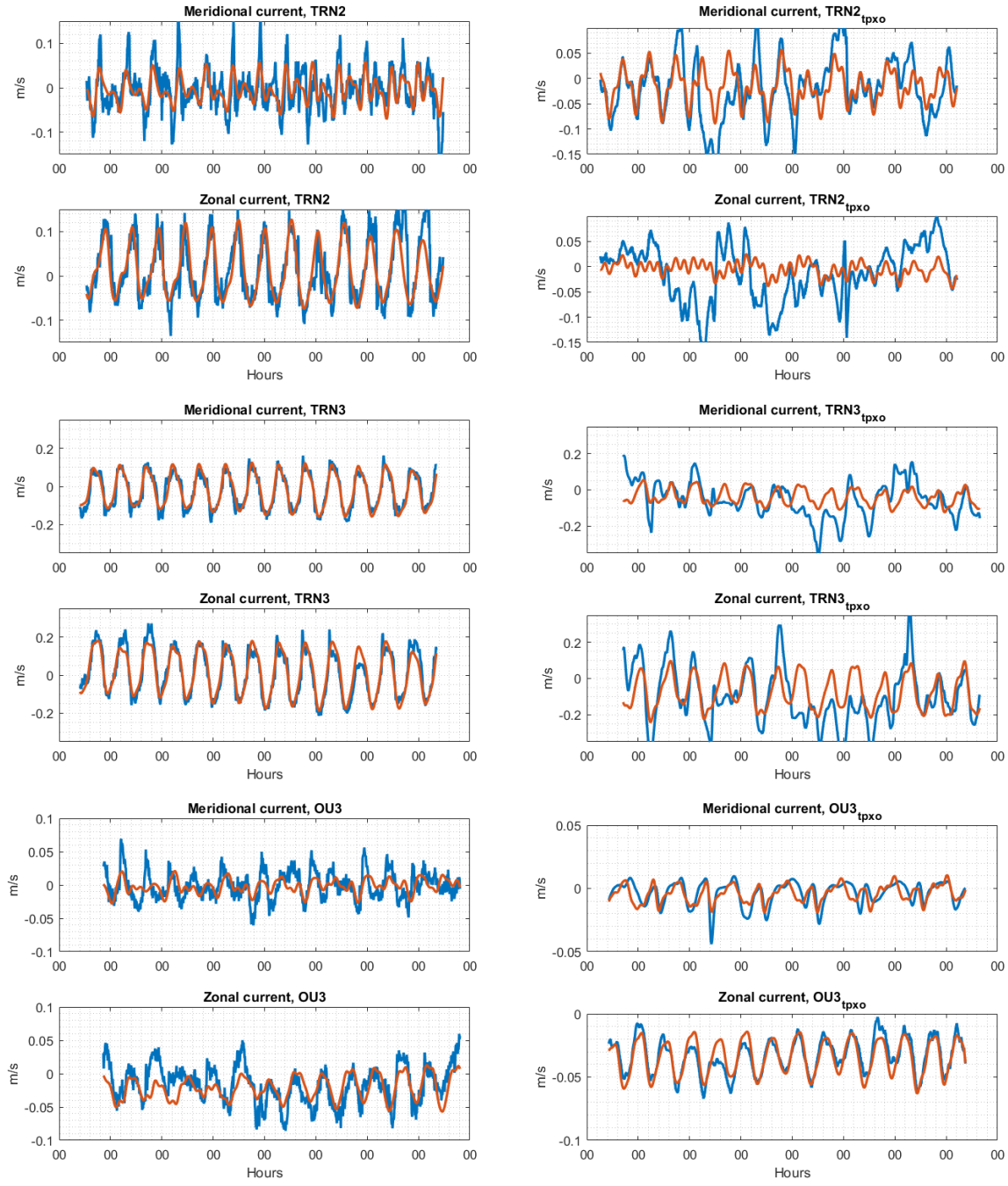

(a) Observations (b) Model results

Figure C.3: *Same layout as in Figure C.1. Stations in Grøtsundet*

Bibliography

Afanasyev, Y., 2006: Formation of vortex dipoles. *Physics of fluids*, **18 (3)**.

Andersen, O. B., G. D. Egbert, S. Y. Erofeeva, and R. D. Ray, 2006: Mapping nonlinear shallow-water tides: a look at the past and future. *Ocean Dynamics*, **56 (5-6)**, 416–429.

Callendar, W., J. Klymak, and M. Foreman, 2011: Tidal generation of large sub-mesoscale eddy dipoles. *Ocean Science*, **7 (4)**, 487.

Chen, C., H. Huang, R. C. Beardsley, H. Liu, Q. Xu, and G. Cowles, 2007: A finite volume numerical approach for coastal ocean circulation studies: Comparisons with finite difference models. *Journal of Geophysical Research: Oceans*, **112 (C3)**.

Chen, C., H. Liu, and R. C. Beardsley, 2003: An unstructured grid, finite-volume, three-dimensional, primitive equations ocean model: application to coastal ocean and estuaries. *Journal of atmospheric and oceanic technology*, **20 (1)**, 159–186.

Chen, C., et al., 2013: An unstructured grid, finite-volume community ocean model fvcom user manual, smast. Tech. rep., UMASSD Technical Report-13-0701, University of Massachusetts-Dartmouth.

Codiga, D. L., 2011: Unified tidal analysis and prediction using the utide matlab functions.

Cohen, I. and P. Kundu, 2007: *Fluid Mechanics*. Elsevier Science.

Drange, H., 2016: *Notes to GEOF331 - Tidal dynamics*. October 18, 2016 version. Accessed August 10, 2017. Available at http://folk.uib.no/ngfhd/Teaching/teaching.html.

Droniou, E., 2012: Vessel mounted adcp survey typical report. Tech. rep., Aquaterra Ltd.

Dupont, F., D. N. Straub, and C. A. Lin, 2003: Influence of a step-like coastline on the basin scale vorticity budget of mid-latitude gyre models. *Tellus A*, **55 (3)**, 255–272.

Egbert, G. D. and S. Y. Erofeeva, 2002: Efficient inverse modeling of barotropic ocean tides. *Journal of Atmospheric and Oceanic Technology*, **19 (2)**, 183–204.

Gjevik, B., E. Nøst, and T. Straume, 1994: Model simulations of the tides in the barents sea. *Journal of Geophysical Research: Oceans*, **99 (C2)**, 3337–3350.

Hench, J. L. and R. A. Luettich Jr, 2003: Transient tidal circulation and momentum balances at a shallow inlet. *Journal of Physical Oceanography*, **33 (4)**, 913–932.

Huang, H., C. Chen, G. W. Cowles, C. D. Winant, R. C. Beardsley, K. S. Hedstrom, and D. B. Haidvogel, 2008: Fvcom validation experiments: Comparisons with roms for three idealized barotropic test problems. *Journal of Geophysical Research: Oceans*, **113 (C7)**.

Jones, J. E. and A. M. Davies, 2007: On the sensitivity of tidal residuals off the west coast of britain to mesh resolution. *Continental Shelf Research*, **27 (1)**, 64–81.

Kabbaj, A. and C. Provost, 1980: Nonlinear tidal waves in channels: a perturbation method adapted to the importance of quadratic bottom friction. *Tellus*, **32 (2)**, 143–163.

Klinck, J. M., J. J. O'Brien, and H. Svendsen, 1981: A simple model of fjord and coastal circulation interaction. *Journal of Physical Oceanography*, **11 (12)**, 1612–1626.

Markowski, P. and Y. Richardson, 2011: *Mesoscale meteorology in midlatitudes*, Vol. 2. John Wiley & Sons, 366–368 pp.

Padman, L. and S. Erofeeva, 2004: A barotropic inverse tidal model for the arctic ocean. *Geophysical Research Letters*, **31 (2)**.

Parker, B. B., 1991: Tidal interactions. *Tidal hydrodynamics*, **237**.

Pratt, L. L. and J. A. Whitehead, 2007: *Rotating hydraulics: nonlinear topographic effects in the ocean and atmosphere*, Vol. 36. Springer Science & Business Media.

Pugh, D. and P. Woodworth, 2014: *Sea-level science: understanding tides, surges, tsunamis and mean sea-level changes*. Cambridge University Press.

Signell, R. P. and W. R. Geyer, 1991: Transient eddy formation around headlands. *Journal of Geophysical Research: Oceans*, **96 (C2)**, 2561–2575.

Stigebrandt, A., 1980: Some aspects of tidal interaction with fjord constrictions. *Estuarine and Coastal Marine Science*, **11 (2)**, 151–166.

Stigebrandt, A., 2012: Hydrodynamics and circulation of fjords. *Encyclopedia of lakes and reservoirs*, Springer, 327–344.

Thomson, R. E. and W. J. Emery, 2014: *Data analysis methods in physical oceanography*. Newnes.

Wan, D., J. M. Klymak, M. G. Foreman, and S. F. Cross, 2015: Barotropic tidal dynamics in a frictional subsidiary channel. *Continental Shelf Research*, **105**, 101–111.

Wells, M. G. and G.-J. F. van Heijst, 2003: A model of tidal flushing of an estuary by dipole formation. *Dynamics of atmospheres and oceans*, **37 (3)**, 223–244.

Zhao, L., C. Chen, and G. Cowles, 2006: Tidal flushing and eddy shedding in mount hope bay and narragansett bay: an application of fvcom. *Journal of Geophysical Research: Oceans*, **111 (C10)**.